AD NUMBER

AD854912

NEW LIMITATION CHANGE

TO

Approved for public release, distribution unlimited

FROM

Distribution: USGO: others to Director, Defense Atomic Support Agency, Washington, D. C. 20305.

AUTHORITY

DTRA ltr. 6 May 99

HIGH PRESSURE HUGONIOT MEASUREMENTS FOR SEVERAL NEVADA TEST SITE ROCKS

by

F.H. Shipman
W.M. Isbell
A.H. Jones

Materials & Structures Laboratory
Manufacturing Development
General Motors Corporation

DASA – 2214
MSL – 68 – 15
Copy No. 16

Final Report
On

HIGH PRESSURE HUGONIOT MEASUREMENTS FOR SEVERAL NEVADA TEST SITE ROCKS

by

F.H. Shipman
W.M. Isbell
A.H. Jones

Materials & Structures Laboratory
Manufacturing Development
General Motors Corporation

1969, March

"This work was sponsored by the Defense Atomic Support Agency under NWER Subtask SB047."

ABSTRACT

The hugoniot equations of state have been determined experimentally for the materials over the following pressure ranges: Fansteel-77 (0.3 to 5.0 Mb), OFHC copper (1.0 to 4.5 Mb), NTS Climax Stock granodiorite (0.6 to 1.9 Mb), NTS Rainier Mesa tuff - vacuum dry - (0.2 to 1.3 Mb), NTS Rainier Mesa tuff - > 95% water saturated - (0.08 to 1.33 Mb), $V44_D$ grouting material (0.11 to 1.15 Mb), schistose gneiss (0.47 to 2.5 Mb), NTS Ferris Wheel dolomite (0.63 to 1.74 Mb), NTS Banded Mountain limestone (0.15 to 1.22 Mb), NTS desert alluvium (0.15 to 0.90 Mb). Where possible, comparisons are made to previous hugoniot measurements by other workers.

FOREWORD

This report presents a description and gives the results of the experimental work performed under contract DA-49-146-XZ-429. The work was sponsored by the Strategic Structures Division of the Defense Atomic Support Agency, Washington, D. C., during the period October 1965 to December 1968. High pressure hugoniot state measurements were performed on five Nevada Test Site (NTS) rocks, a schistose gneiss and a volcanic tuff impedance-matching grout. In addition several experiments were performed on OFHC copper and Fansteel-77, a copper-nickel-tungsten alloy. These two metals were employed throughout the program as hugoniot impedance match standards. Table XIII lists the materials tested and the pressure ranges achieved.

Section I of the report describes in detail the experimental procedures and target designs employed for the hugoniot determinations. The data analysis procedure is presented in Section II, as well as a discussion of sources of experimental error. Section III presents the experimental data and descriptive interpretation of the resulting hugoniots. No attempt is made to relate the results to geophysical problems. To ascertain the accuracy and validity of the compiled results, comparisons are made with the published data of other researchers. A summary of the results is presented in Section IV and general conclusions are drawn.

TABLE OF CONTENTS

LIST OF ILLUSTRATIONS

LIST OF ILLUSTRATIONS (Continued)

LIST OF ILLUSTRATIONS (Continued)

LIST OF ILLUSTRATIONS IN APPENDIX

LIST OF TABLES

(Page x is blank)

BLANK PAGE

INTRODUCTION

The purpose of the program described herein was to experimentally obtain high pressure shock wave data to aid in the interpretation of the results of underground nuclear testing. Since the nuclear experiments are performed at NTS, the interest is mainly in the NTS geological environment. The experimental program undertaken at first by GM Defense Research Laboratories, Santa Barbara, California, and then the Materials and Structures Laboratory of Manufacturing Development, General Motors Technical Center, Warren, Michigan, have been to provide data on several selected rocks from NTS.

In the past two decades, high explosives have been the main energy sources for experimental systems used to induce high pressure shock states in materials of interest. By these techniques, pressures of about 1 Mb may be achieved in the denser rocks. For this study an accelerated-reservoir light-gas gun (ARLG gun) was employed as an impactor launching instrument.[1] The ARLG gun is capable of launching high density metal impactors at velocities of up to $\sim$ 8 km/sec. This method of experimentation offers significant advantages over the explosive techniques previously used. Shock induced pressures of over 2 Mb in many rocks are obtainable with impactors launched by the ARLG gun. By proper selection of impactor material and launch velocity, the induced shock pressure states are continuously variable over the range from $\sim$ 0.1 to 2.0 Mb.

The experimental program described here may be considered for convenience to consist of three phases, though not necessarily in the sequence presented. The first effort was to establish

the hugoniots of OFHC copper and Fansteel-77. The second phase involved the determination of the hugoniot equations of state for NTS Climax Stock granodiorite ("granite"), Rainier Mesa volcanic tuff (dry), a NTS Ferris Wheel dolomite, a NTS Banded Mountain limestone, and a schistose gneiss, not from NTS. The third phase consisted of the hugoniot determination of materials that presented peculiar experimental difficulties, including the water-saturated Rainier Mesa tuff, the grouting material, $V44_D$, and the NTS desert alluvium.

SECTION I

HUGONIOT STATE MEASUREMENTS

TECHNICAL APPROACH

Hugoniot Theory

Application of the principles of conservation of mass, momentum, and energy across a shock front have led to the well-known Rankine-Hugoniot equations. The equations may be used to relate the discontinuous changes across a shock front of the variables: Pressure, P, density, ρ, specific volume, $V = \frac{1}{\rho}$, particle velocity, u_p, and specific internal energy, E. Where the shock wave is travelling at constant velocity, U_s illustrated in Figure 1. The particle velocity ahead of the shock is zero, and subscript 1 designates conditions behind the shock.

$$\rho_o U_s = \rho_1 (U_s - u_p) \tag{1}$$

$$P_1 - P_o = \rho_o U_s u_p \tag{2}$$

$$E_1 - E_o = 1/2 (P_1 + P_o) (V_o - V_1) \tag{3}$$

A measurement of any two parameters, e.g. shock wave velocity and the particle velocity, associated with a shock wave provides sufficient information to determine the other adiabatically achieved state variables of the shocked specimen. implicit in the Rankine-Hugoniot relations is the assumption that the

material behind the shock front has reached steady-state or equilibrium conditions.

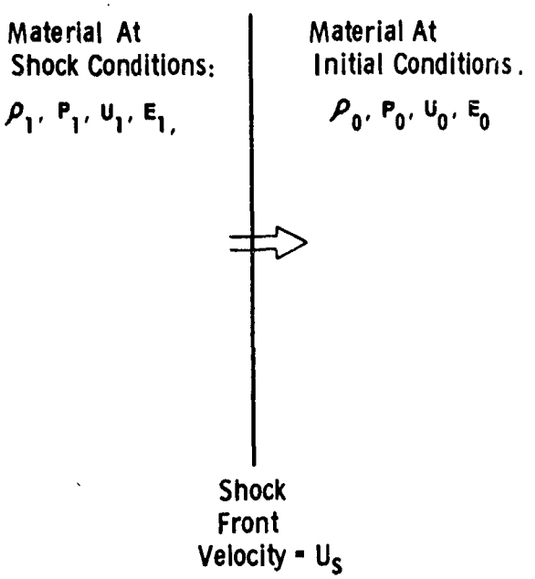

Figure 1 Schematic of a Shock Wave Propagating Into a Material

Although measurement of shock velocity is relatively straightforward, the measurement of particle velocity is more difficult experimentally. For this study an adaptation of the impedance matching technique developed by Walsh, et. al.[2] was used to calculate the particle velocity associated with a measured shock wave velocity in the specimen. A shock wave was induced in a specimen material customarily by the arrival of an impactor at its front surface. The shock wave then passed through the specimen, where the specimen shock wave transit time was recorded. The shock velocity was calculated and in the P-u_p plane a line of slope $\rho_o U_s$ established the Rayleigh line passing through $P = 0$, $u_p = 0$, as shown in Figure 2.

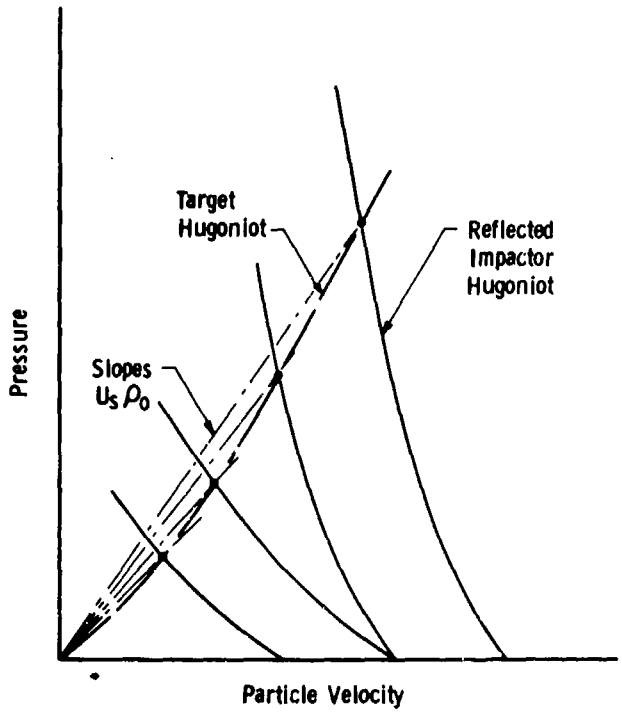

Figure 2 Schematic of Impedance Match Method Using Dissimilar Materials

The hugoniot of the impactor in the form $P = P(u_p)$ previously determined then was reflected about the vertical established by $u_p = v$ (the impact velocity). The intersection of the Rayleigh line with the reflected impactor hugoniot represents the shock state of the specimen.

An advantage of substantial importance is the possibility of impacting the specimen with a gun launched impactor of the same material. With this technique, the impedance symmetry is exact, i.e., $u_p = 1/2\ v$. The shock pressure may be determined directly from equation (2).

Figure 3 illustrates schematically the impedance symmetry approach wherein like materials are made to collide. A series of experiments on OFHC copper and Fansteel-77 were

performed over the full velocity range of the gun for each material using these symmetrical impact conditions, to determine their hugoniots. The accuracy and precision with which the impact velocity may be measured is 0.03%.

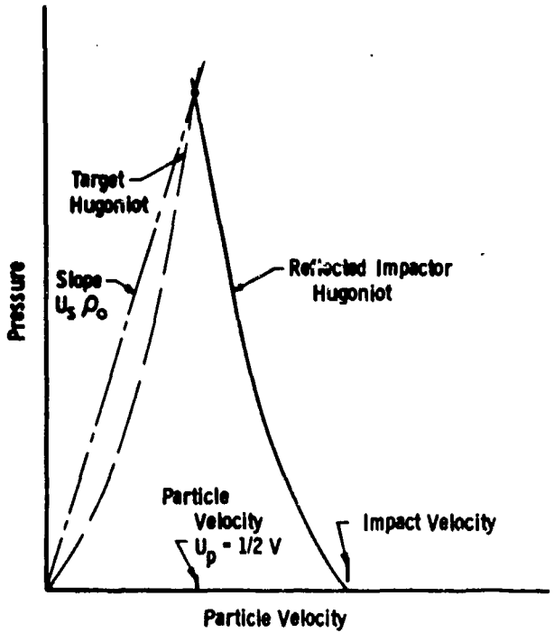

Figure 3 Schematic of Symmetrical Impedance Match Method

With the standard hugoniots established, the second phase test series began using impactors of either OFHC copper or Fansteel-77 and the dissimilar impedance approach as discussed above.

EXPERIMENTAL TECHNIQUES

During the course of the work on the program, refinements of design and instrumentation have been made. The following is a description of the experimental system as it is currently in use. The areas of significant improvement are in target design and in the instrumentation for the measurement of impact velocity. The changes will be noted in the discussion of these topics.

Launching Techniques

The gun used to accelerate the impactor is an accelerated-reservoir light-gas gun[3] with a launch tube bore diameter of either 29 mm or 64 mm. This type of gun maintains a reasonably constant pressure on the base of the projectile during the launch allowing the acceleration of a variety of unshocked impactor materials. Figure 4 shows the layout of the range.

The gun consists of the following major components:

1. Powder chamber
2. Pump tube, 87 mm inside diameter by 12 m long
3. Accelerated-reservoir high-pressure coupling
4. Launch tube, either 29 mm inside diameter by 8 m long or 64 mm inside diameter and 8 m long
5. Instrumented target chamber and flight range.

When the gun is loaded for firing, a weighted plastic-nosed piston is placed in the breech of the pump tube. Gun powder is then loaded in to the powder chamber behind the piston and the pump tube is filled to the required pressure with

hydrogen. After ignition of the gun powder, the hydrogen is compressed into the coupling by the accelerated piston. The saboted impactor is in turn accelerated by the release of the compressed hydrogen through a high pressure burst diaphragm.

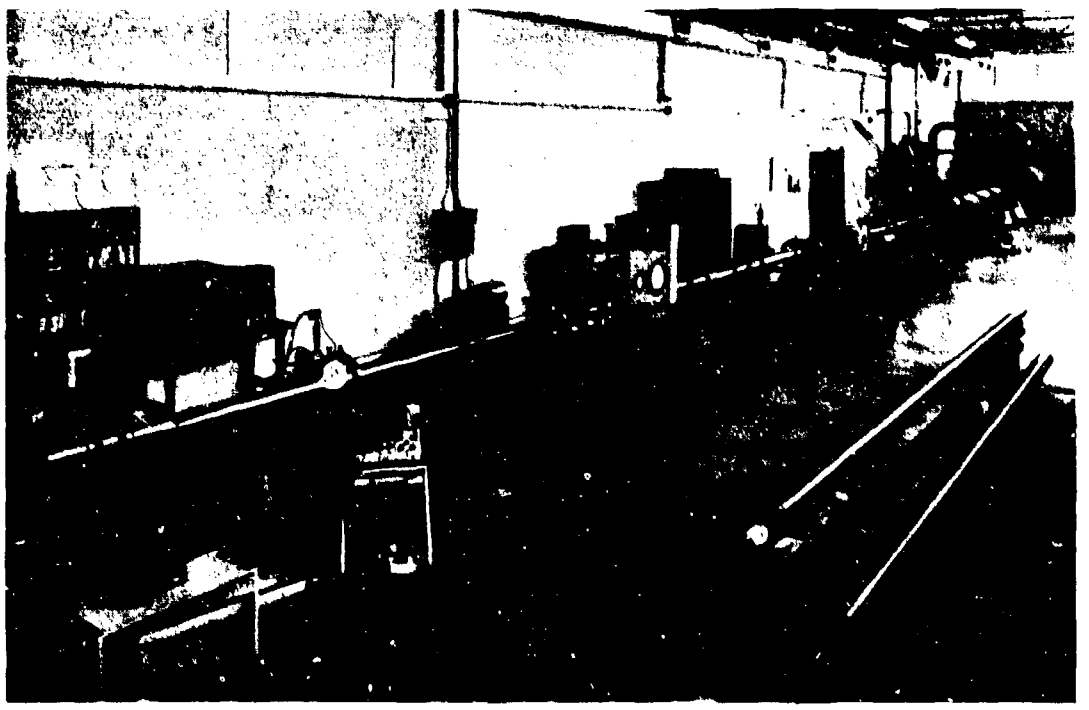

Figure 4 Layout of ARLG Gun Range

Prior to firing, the flight range and instrument chamber are evacuated and then flushed with helium to approximately 10^{-3} torr to eliminate any spurious effects of gas build-up and ionization between projectile and target. Sealing lips on the rear of the plastic sabot are pressed tightly against the inside of the launch tube bore by an interference fit and the high pressure gas, effectively eliminating blow-by.

Careful attention to the condition of the launch tube is necessary for successful firing in the high velocity ranges. Bore

linearity of better than 0.2 mm over the full 8 m length of the launch tube is maintained. The internal diameter is maintained to within 0.01 mm. Launch tubes are cleaned and honed after each firing and are removed every 15 to 20 firings for thorough reconditioning.

Figures 5 and 6 show the instrumentation chamber designed for the high pressure studies. The chamber is connected to the barrel of the gun only through an O-ring seal to allow free axial movement of the launch tube. The target chamber is shock-mounted to prevent target displacement before projectile impact. To facilitate this, several stages of mechanical isolation have been arranged in the barrel, I-beam support structure and concrete foundation.

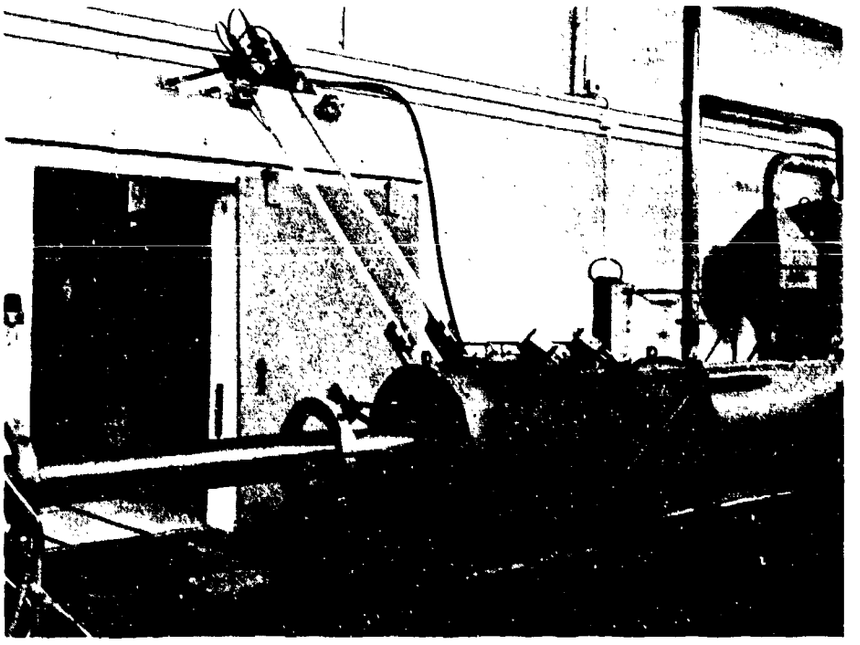

Figure 5 Target Chamber Set-up

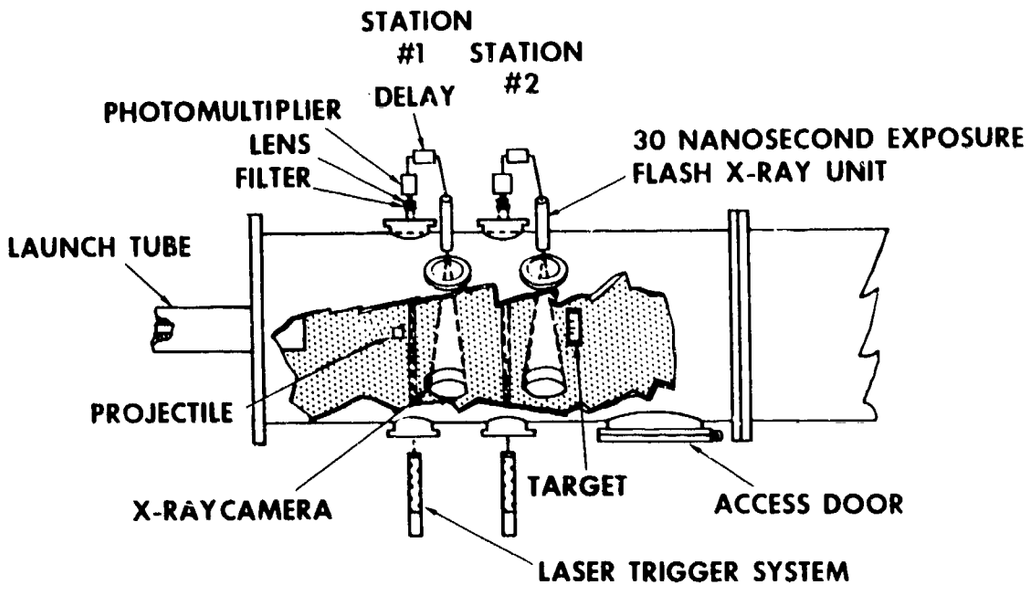

Figure 6 Schematic of Target Chamber (Top View)

The target chamber is a steel cylinder of 61 cm O.D. and 1.5 m length. Physical access and instrument ports are precisely machined in a horizontal plane and in planes 45° above horizontal.

Two sets of the ports are employed as x-ray windows and house the secondary spatial references. The references are cross wires with the separation distance between windows (nominally 30.0 cm) accurately determined by an optical comparator.

Operationally, the ports are closed against O-ring vacuum seals with Plexiglas or magnesium windows for optical and x-ray instrumentation or with steel cover plates.

Instrumentation

The impactor velocity measuring system consists of a two laser triggering system and a short duration dual flash x-ray as described by R. Lingle and A. H. Jones.[4] With such a system, impactor velocities are measured accurately to ∿ 0.03%. The triggering system consists of two sets of neon-helium gas lasers aimed at photodetectors across the impact chamber orthogonal to and intersecting the line of flight of the projectile. Photomultipliers monitor the laser outputs through circular apertures and narrow band filters. When light interruption occurs at each station because of projectile passage, a sharp change of voltage level is converted into a trigger signal of sufficient voltage to initiate a Field Emission Corporation 30 nsec dual flash x-ray unit. The x-ray flash exposes a Polaroid film plate on the opposite side of the chamber by means of a fluorescing intensifier screen.

Spacing between the two x-ray field position referenced is indicated by fiducial wires which are measured by an optical comparator to within 0.1 mm. Measurements of the impactor face position relative to the window fiducials allow determination of the projectile position and distance traveled over the time interval measured between flash exposures. Figure 7 is an example of the shadowgraphs taken at the two x-ray stations showing the projectile in free flight before impact.

Serving as a backup technique, a second method is employed to measure impactor velocity by recording the time interval between the first x-ray flash and the event of shorting of a rear surface shock velocity pin. The impactor and target

positions are measured from the x-ray shadowgraphs. Variations in measurements between the two techniques are usually less than 0.05%.

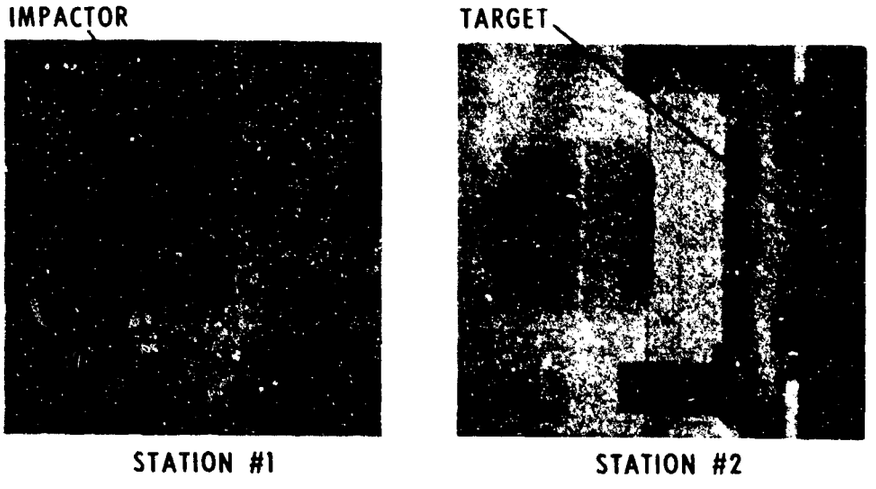

Figure 7 X-Ray Shadowgraphs of Projectile Before Impact

The early experimentation was somewhat different from that described. A single laser system was the x-ray trigger source, and the x-ray flashes then occured at preset delay times. During low and intermediate launch velocity tests, the system was ∿ 95% reliable. But in the highest velocity (7 - 8 km/sec) tests, the x-rays were nearly always pretriggered, resulting in the x-ray flashes occurring before the arrival of the projectile. The hugoniot data recorded - the shock wave transit times - are not totally invalidated, when the impact velocity is not recorded directly. Through ballistics the light gas gun muzzle velocity is well documented and cross correlated

with secondary parameters. It is posible through the use of the leading data and related cross curves of hydrogen pressure, powder load, and piston velocity history, to estimate the impact velocity to within ±2%.

The target is located approximately 60 cm from the launch tube muzzle and is included in the #2 x-ray field of view. Recordings of the shock wave transit time in the target are made using four coaxial self-shorting pins as sensors. Shorting of a pin results in a sharply rising current to ground which produces a signal across the time-interval-meter input termination resistors. The pin supply circuit is so designed that each pin signal can be seen on three output lines, free of any reflections or ringing for several hundred nanoseconds. The Individual circuits are "tuned" by the use of trimmer capacitors so that the risetime of each signal is 1.0 ± 0.1 nsec to 12 volts. The time-interval-meter trigger level is set precisely at 1 volt. Thus the combined mechanical-electronic signal system can make use of the ± 1/2 nsec resolution of the time recording instruments.

The shock wave transit time-interval-meters are Eldorado Models 793. These counters, which have a specified time resolution of ± 1/2 nsec, may be read digitally to the nearest nanosecond. They require an input signal of 1 volt minimum and a risetime of approximately 1 nsec. Although instrument stability is specified to be one part in 10^4 for long term use (∿ 24 hours) and five parts in 10^6 for short term (∿ minutes), in actual practice the instruments are calibrated prior to each shot over a period of about 30 minutes. The shot is then fired within five minutes of completion of the calibration procedure.

The coaxial self-shorting pins* employed as sensors consist of an outer sheath of brass surrounding a teflon sleeve and a copper inner conductor. The pins, connected to RG-174 50 Ω cable by soldered joints, are made self-shorting by the placement of a brass cap over the sensing end which leaves a small gap (on the order of 0.050 ± 0.015 mm) between its inner face and the flat end of the inner conductor. Pin gaps are recorded by x-ray shadowgraphy of which Figure 8 is an example, and the measurements taken from the film are employed in the shock velocity calculations for corrections as pin closure times.

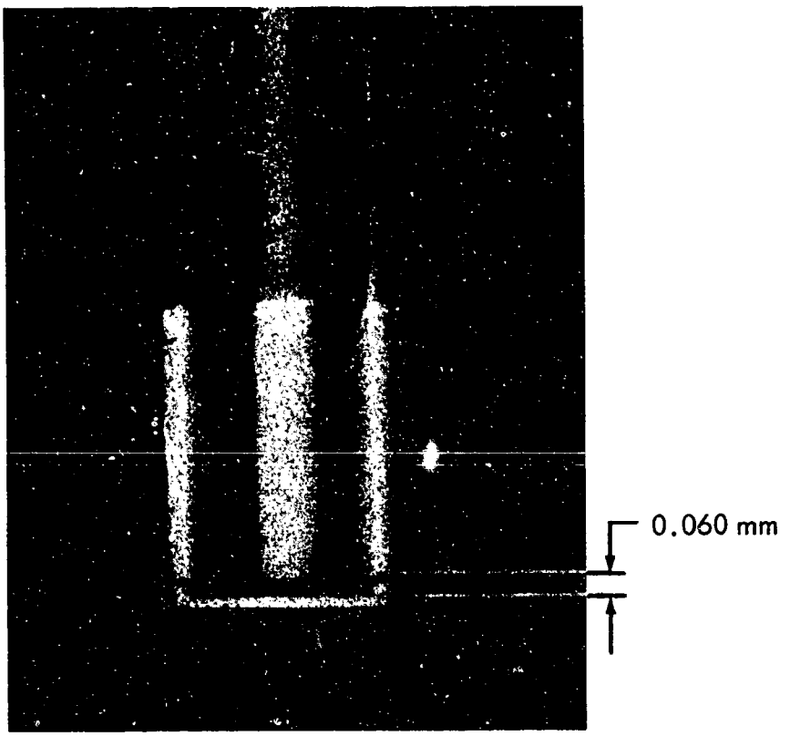

Figure 8 X-Ray Shadowgraph of Coaxial Self-Shorting Pin

* Model Ca-1039, Edgerton, Germeshausen and Grier, Santa Barbara, California

Careful attention is given to the electrical characteristics of the coaxial self shorting pins. A Tektronix 1S2 time-domain-reflectometer is used to detect slight changes in the reactance of the pins, and serve as an indicator of probable pin failure in the vacuum environment.

Impactor striking tilt is, in the present system, recorded with the Eldorado time-interval-meters. Most of the experiments reported here employed a Tektronix 519 oscilloscope as the impact tilt recorder. The 20 nsec/cm standard sweep rate was found to be nonlinear over the first centimeter of the CRT graticule. Calibration plots were periodically generated and employed to correct the recordings.

Planarity of the shock wave induced in the target is dependent on the impactor flatness at impact. The impactor surface is machine lapped and then hand polished flat to 0.5×10^{-3} mm. Tests of the effect of launching on surface flatness were performed by impacting into mirrors to optically observe the impact linearity. With impactors of 6061-T6 aluminum, the surface curvature over a 44.5 mm diameter (length/diameter - 1:45) at impact is less than the 5 nsec time resolution of the optical recorder at a launch velocity of $\sim$ 2 km/sec. Similar tests with 21 mm diameter impactors at launch velocities of $\sim$ 6 mm/sec also showed < 5 nsec curvature. The impactor diameter for equation of state experiments is nominally 21 mm and the L/D $\sim$ 1:12. The expected launch induced curvature for the copper and Fansteel-77 impactors is < 1 nsec because of the greater stiffness and the larger L/D.

Impactor tilt relative to the target specimen front surface is sensitive to launch tube linearity and sabot alignment as well as to target alignment, even though the projectile flies

free from the launch tube before impact. The capability to adjust the target position and perpendicularity relative to the launch tube centerline by an optical technique brings the average tilt at impact to approximately 0.05 radians (approximately 20 nsec of tilt at an impact velocity of 6 km/sec).

Because of the comparatively gentle acceleration of the projectile to its terminal velocity, the impactor plate is not shock stressed or shock heated. In addition, free flight in an evacuated range precludes aerodynamic heating. The estimated temperature rise during launch is of the order of 1°C. This temperature increase does not significantly affect the flatness of the impactor.

Target Design and Construction

The photograph and drawing of Figure 9 illustrates the basic features of the target design. Two coaxial self-shorting pins (stations 1 and A) are passed by the edge of the specimen with their cap faces exactly in the plane of the specimen impact surface. These pins are used to initiate the timing for the shock wave transit and to measure impactor tilt as the time interval differences between their respective closures. Two rear surface pins, stations B and C, (or B only depending upon the impactor diameter) are mounted in line with the tilt pins to record the shock wave arrival at the rear surface. All four pins are mounted in a guide fixture which assures accurate geometrical spacing. The tilt pins are fixed in position by dimensionally stable epoxy, while the rear surface pins are spring loaded against the target. The pin retainer and cable bracket lend rigidity to the assembly preventing accidental damage to the pin shafts.

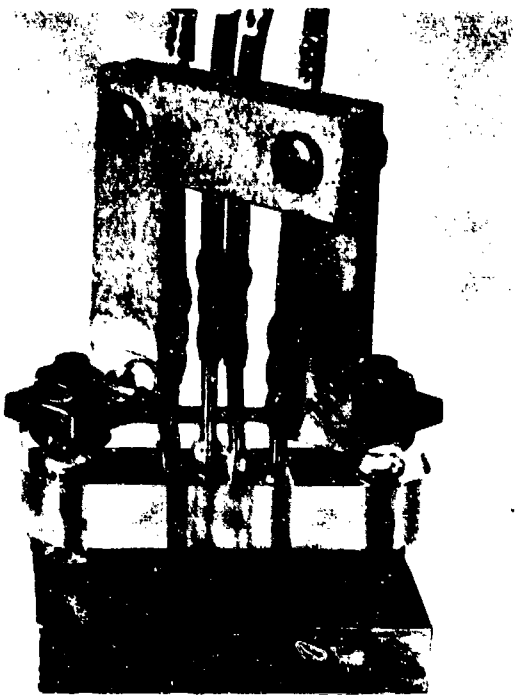

Figure 9a Photograph of Equation of State Studies Target

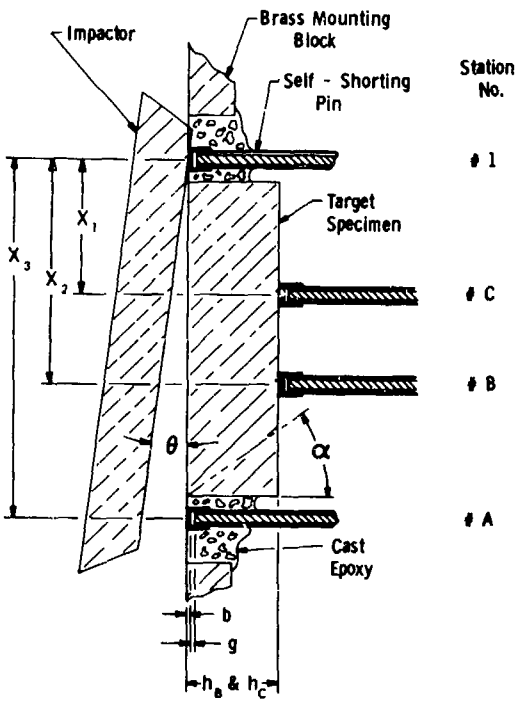

Figure 9b Schematic of Equation of State Studies Target

Two target sizes were chosen, each to be used over a given stress range. The four-pin target required a 21 mm diameter impactor which was limited to a maximum impact velocity of about 6.5 km/sec. Single-rear-surface-pin targets requiring 11.7 mm diameter impactors were used for launch velocities up to $\sim$ 8 km/sec. The four-pin targets, in conjunction with four Eldorado one-nsec time interval meters, allow the determination of two sets of measurements, yielding four values of shock wave transit time. As described in Section III, these four values are combined to calculate a single shock wave velocity in the specimen, and by a system of cross-checking, to provide an indication of the accuracy of the measurement.

Throughout the program, the edge rarefaction angle (α in Figure 9b) was assumed to remain constant at $\tan \alpha \simeq 1.0$ which is in agreement with a Poisson'a ratio of $\sim$ 0.3, typical for rocks under hydrostatic stress. Similarly, the target-impactor thickness ratios of 3.3 and 3.8 for the two target sizes were established so as to be thinner than the point at which the rear surface (forward going) elastic rarefaction overtakes the shock front.

Except for the granite and most of tuff targets, the specimens were machined into solid rectangles where the dimension along the pin array was 17.6 mm and 9.7 mm for the two target sizes. The base line (X_3 in Figure 9b) was 19.2 mm and 11.2 mm for the intermediate and the high velocity targets, respectively. The impact and rear surfaces were machine lapped and, where possible, hand polished to as fine a finish as the material would take. The lapping procedure also served to enhance the surface flatness and parallelism. These specimen surfaces were generally flat and parallel to within $5 \cdot 10^{-3}$ mm.

Target specimen thicknesses at the pin stations were measured with a Zeiss light-section microscope employed as a comparator. The references were precision laboratory-grade gage blocks. Use of the light-section microscope avoids the problem of an indicator marring the specimen surfaces. Specimens were typically ∿ 5.8 mm and 3.9 mm thick.

Tuff Targets

The tuff specimens presented several special problems, since the samples are ∿ 20% porous and the rock is hygroscopic. The measurements, construction, and storage were performed at atmospheric conditions after having determined that short (∿ 5 min) exposure to vacuum would almost completely dry the rock. Exposure to vacuum for at least a 10 min duration always proceeded the shots.

The requirement later in the program to simulate *in situ* conditions made it necessary to maintain a liquid environment about the porous tuff specimen for a period long enough to ensure saturation. To insure complete saturation, the specimen had to be submerged in water for approximately 48 hours (i.e. at least ∿ 95% of the water was absorbed within 48 hours; the final ∿ 5% took up to 2 weeks at atmospheric pressure). For the experiments the liquid enclosure had to also withstand an external vacuum in the target chamber. The basic target design will be described later as the stepped model with the addition of a cell cover plate and appropriate water seals.

After the target was epoxied in the mounting block, a ∿ 0.1 mm layer of epoxy was cast over the entire front surface of the target specimen and mounting block. The casting was made using shim-stock spacers between the casting fixture and the target block

surfaces. Thickness measurements made with the Zeiss light section microscope showed that the resulting epoxy surface was within 10^{-3} mm of being parallel with the target surface. Microscopic examination of epoxy coated specimens showed epoxy penetration to be less than 0.03 mm. The effect upon the velocity of a shock wave, initiated through the shim was shown by a computer hydrodynamic calculation to be less than a 0.1% retardation.

Target specimen saturation was then begun by evacuating the assembly and introducing deaireated water into the evacuated specimen cell. Without this procedure, capillary action forced trapped air toward the thin epoxy front surface shim causing the shim to release from the tuff specimen impact surface. The rear surface cell cover was epoxied in place with the target specimen in the wet condition. Fill tubes were provided on the cell through the cover plate.

Grout Targets

The tuff impedance-matching grout, $V44_D$, was rather plastic at room temperature and would deform about the pin caps under the light but continuous stress of the pin retaining spring. To limit the deformation as much as possible and maintain the target thickness as recorded optically, a brass shim was placed under the rear surface pin caps thus distributing the pressure over a larger area. The transit time measurements were corrected for the shim as described in Section III.

Alluvium Targets

The alluvium specimens were prepared in much the same manner as

described by Anderson, G. D. and A. L. Fahrenbruch[5], except that the pressed sample surfaces were not covered with aluminized mylar.

To avoid the effects of an unknown amount of water being absorbed from the air, sample preparation was carried out under controlled atmospheric conditions. The loose, finely particulate material was screened (No. 40 mesh) and placed overnight in a drying oven. Upon removal from the oven all samples were stored in a glove box set up to maintain an atmosphere of less than 1% absolute humidity. Specimens were exposed to room air for no longer than 5 minutes thereafter.

The alluvium was pressed into a steel ring with inside diameter of 15.2 mm and thickness was 5.1 mm. The front and rear surfaces of the ring were machined and lapped flat and parallel to the usual tolerances, and each specimen ring was precisely measured and weighed. The alluvium sample was then compacted into the ring at the desired specimen density. Tests conducted on several trial specimens showed that the surface of the compacted material had sufficient rigidity to not require a shim under the rear surface pin caps.

The front surface pins were placed in holes drilled through the ring so that the pins are aligned in a manner similar to that in the regular target construction. Finally, the ring assembly was epoxied to a modified target mounting block.

Stepped Target Design

Tests conducted during the early part of the research program used a different target design. Figure 10 illustrates this de-

sign. Originally, the tilt pins (stations 1 and A) were not in the plane of the impact surface; rather, they rested on two wings of the target of ∿ 0.76 mm thickness. The B and C pins were placed on steps of thickness 3.30 and 5.8 mm respectively. The pin guide fixture was about 4-5 mm above the target C step.

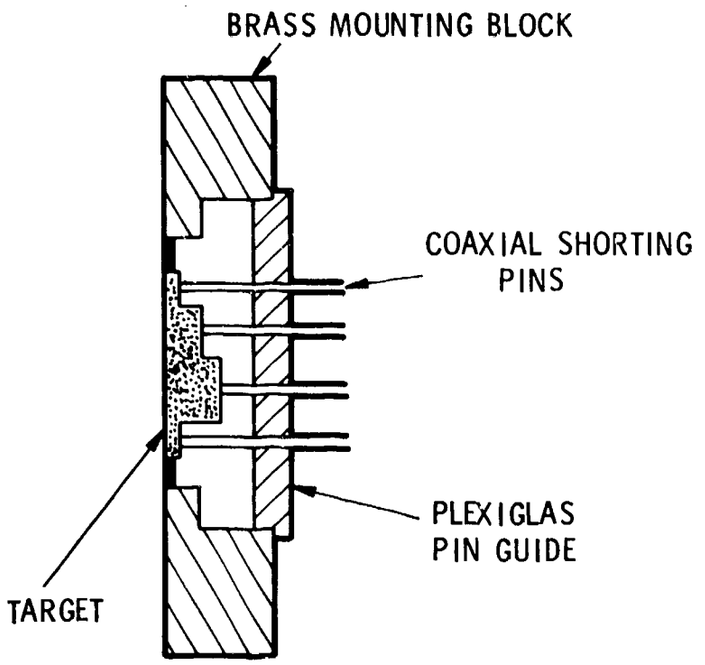

Figure 10 Early Equation of State Target Design (Step Target)

Shock wave velocities were measured through two different thicknesses of material. Thus, non-steady state wave behavior in the material could be measured, if present. This more complicated and time consuming target system was discontinued in favor of the system previously described when, within the resolution of the experiment, no significant differences in wave velocity were measured.

Machining of the stepped target configuration was difficult, and pin placement with the raised pin guide could allow the pin to slant or be displaced from the perpendicular to the target surface. In addition, higher tilt measuring accuracy could be gained by removing possible specimen material effects in the wings and increasing by about 5 mm the tilt measurement base line.

SECTION II

DATA ANALYSIS

Analysis of the experimental data obtained for the program was based upon the impedance match solution for the determination of particle velocity and pressure of the shock state achieved in the specimen during each test. The requisite information in this analysis is the shock wave velocity, the impact velocity, and the linear form of the hugoniot of the impactor material. A detailed analytical discussion of the approach is presented in the Appendix.

Shock Wave Velocity

The measurements relevant to shock wave velocity are the target thickness and the shock wave transit time interval. To determine as precisely as possible the shock wave transit time, refinements may be applied to the recorded time interval.

Two sources of refinement to the measurement are:

(i) Inclusion of the effects of shock wave tilt resulting from non-coplanar impact of the target and impactor surfaces.

(ii) Correction for the differences of closing times of coaxial pins with varying gaps, due to impactor-pin and target-pin interactions.

The coaxial shorting pin design includes a cap over the impact end of the pin which has a slightly recessed rear surface. The gap between the cap and the inner electrode is electrically insulating. When a large amplitude stress wave reaches the cap face, the cap is set into motion and the gap is assumed to be closed at a rate equal to the free-surface velocity of the cap material. Correction for shock transit through a rear surface shim is made by simply defining the pin cap thickness as the sum of the shim and measured pin cap thicknesses.

The system of analysis has been incorporated in a computer program SHOVEL - presented in the Appendix, and is permanently stored in a General Electric Company computer time-sharing service library.

Major sources of experimental error include unrecorded impact velocity, pin gap closure velocities and the impactor tilt. An unrecorded impact velocity results in an uncertainty of $\sim$ 4% in the specimen particle velocity but affects the shock velocity measurement insignificantly, i.e. < 0.1%. Pin cap closure velocity is subject to the errors of the assumption of $u_{\text{pin free surface}} = 2u_{\text{pin}}$. In practice, however, this assumption has a maximum effect on U_s of $\sim$ 0.1% since the pin closure time is on the order of 100 times smaller than the shock transit time.

The effect of impactor tilt on U_s can be quite large as seen by inspection of Equation A-18. However a measurement error of 100% results an uncertainty of U_s of only $\sim$ 2%. The system employed for tilt measurement for these experiments is accurate to within $\sim$ 0.0015 radians. The combined effect of these errors results in an uncertainty in U_s of between 0.2 to 0.5%, depending upon the target diameter and the shock wave transit time.

As has been shown, two values of shock velocity and hence two sets of values of particle velocity, pressure and specific volume are determined with each target in the four-pin configuration. The data presented in Section IV are shown as averages of the shock velocity and particle velocity between the B and C station measurements for each test whenever possible. The "internal" (or individual test) data scatter is listed and displayed graphically as error bars on all shots where averaging was possible. The internal scatter in most instances is outside the experimental systematic errors but in those cases where partial system failure occurred the error bars include the system error.

The linear form U_s (u_p) of the least squares analysis was employed to represent analytically the hugoniots of the materials tested in this program. Where the data suggest systematic deviations from linearity, the analytical form was considered to be represented by additional linear segments. Thus the reported hugoniot equations are followed by a designation of the range over which the least squares analysis was carried out. The standard errors (S.E.) are also listed to indicated the least mean square of the deviations of the dependent variable (U_s) from the computed linear fit.

SECTION III

EXPERIMENTAL RESULTS

Presented here are the results of the experiments and data analysis performed during the program. Although detailed interpretation of the data is beyond the scope of this work, where possible, comparisons of the results of other researchers which are considered to be of interest are made.

Impactor Materials Hugoniot Data

The hugoniot data for Fansteel-77 are listed in Table I. Indicated in the table are those shots performed under General Motors, NASA, and BRL sponsorship. The shot numbering indicates the laboratory at which the tests were performed: C, at GM Defense Research Laboratories, S, at Manufacturing Development, GM Technical Center. The seventeen shots listed establish with precision the Fansteel-77 hugoniot over the pressure range attainable in the rock experiments.

The physical properties of Fansteel-77, which is a powder metallurgy product, are presented in Table II. Microscopic examination reveals that the tungsten component is granular with the average grain diameter $\sim$ 1 μ. X-ray diffraction measurements show that the intragranular matrix is an alloy of $\sim$ 70% nickel with $\sim$ 30% copper.

TABLE I

HUGONIOT DATA FOR FANSTEEL-77

$V_o = 0.0588$ cm^3/gm
$\rho_o = 17.01 \pm 0.01$ gm/cm^3

Shot	Impactor Material	v Impact Velocity (km/sec)	U_s Shock Velocity (km/sec)	u_p Particle Velocity (km/sec)	P Pressure (Mb)	V/V_o Relative Volume	V Volume (cm^3/gm)	ρ Density (gm/cm^3)
S-23 □	FS	0.906	4.599	0.453	0.354	0.9015	0.0530	18.869
C-922	FS	1.478	4.978	0.740 ±0.016	0.627 ±0.016	0.8514 ±0.0039	0.0501 ±0.0002	19.980 ± 0.092
C-1161 o	FS	1.952	5.194	0.976	0.862	0.8121	0.0477	20.946
C-939	FS	2.152	5.336	1.076	0.977	0.7984	0.0469	21.306
C-1218 □	FS	2.689	5.661	1.344	1.294	0.7626	0.0448	22.306
C-921	FS	2.689	5.756	1.344	1.316	0.7665	0.0451	22.192
C-933	FS	2.774	5.786	1.387	1.365	0.7603	0.0447	22.373
S-21 □	FS	2.849	5.855	1.425	1.419	0.7566	0.0445	22.482
C-1155 o	FS	3.413	6.163	1.706	1.788	0.7232	0.0425	23.521
C-914 +	FS	3.548	6.221	1.774	1.877	0.7148	0.0420	23.796
C-940	FS	3.618	6.365	1.809	1.959	0.7158	0.0421	23.764
S-18 □	FS	3.648	6.412	1.824	1.989	0.7155	0.0421	23.772
C-931	FS	3.994	6.490	1.997	2.205	0.6923	0.0407	24.570
C-923	FS	4.657	6.939	2.329	2.749	0.6644	0.0391	25.604
C-1220 □	FS	4.809	7.082	2.405	2.897	0.6604	0.0388	25.757
C-1232 □	FS	6.646	8.239	3.323	4.529	0.6077	0.0357	24.990
C-962 +	FS	6.936	8.390	3.468	4.949	0.5867	0.0345	28.995

+ GM Sponsored o NASA □ BRL

TABLE II

CHEMICAL AND PHYSICAL PROPERTIES OF FANSTEEL-77

Chemical Properties

Element	Wt %
W	90 ± 1
Cu	3.8 ± 0.6
Ni	6.1 ± 0.2

Physical Properties

Ultimate Compressive Strength	176,000 psi
Ultimate Tensile Strength	98,000 psi(min)
% Elongation	2% (min)
Yield Strength (0.2% elong.)	85,000 psi(min)
Density	17.01 gm/cm^3
Sonic Velocity* Longitudinal	5.049 km/sec
Sonic Velocity* Shear	2.765 km/sec

Calculated Parameters

Bulk Sound Velocity	3.911 km/sec
Bulk Modulus	2.602 Mb
Bar Wave Velocity	4.432 km/sec
Young's Modulus	3.341 Mb
Poisson's Ratio	0.286
Rigidity Modulus	2.340 Mb
Lame's Parameter	1.042 Mb
Rayleigh Wave Velocity	2.628 km/sec

* Ultrasonic tests performed by R. Lingle, this Laboratory

MSL-68-15

The sonic velocity measurements were performed at Manufacturing Development by the pulse superposition technique. Using the manufacturers value of Poisson's ratio the bulk sound speed is 3.88 km/sec. The Poisson's ratio needed to bring into agreement the linear U_s-u_p hugoniot intercept of 4.00 ∿ km/sec for the present alloy is 0.31.

The hugoniot data for Fansteel-77 (with a measured density of 17.01 ± 0.01 gm/cm^3) in the U_s-u_p plane may be described by the linear equation:

$$U_s = 4.008 + 1.262\ u_p \text{ km/sec}, \quad 0.4 < u_p < 3.5 \text{ km/sec}$$

$$\text{S.E.}(U_s) = 0.036 \text{ km/sec}$$

Tests exhibiting less than 1% internal (B vs C Station) scatter in U_s were employed in the least squares analysis (7 tests). The effect of employing the additional twelve shots changes the slope by only 0.03%. The data are displayed along with the OFHC copper data in Figures 11 and 12.

OFHC copper (99.99% purity) was employed as the low and intermediate pressure standard (i.e. ∿ 0.1 to ∿ 1.0 Mb) in the hugoniot experiments on the rocks in the program. A number of other laboratories[6,7] have performed hugoniot tests for copper which are in generally quite good agreement with this laboratory. The hugoniot equation for the present data in the U_s-u_p plane is given by:

$$U_s = 3.960 + 1.464\ u_p \text{ km/sec}, \quad 1.7 < u_p < 4.7 \text{ km/sec}$$

$$\text{S.E.}(U_s) = 0.018 \text{ km/sec}$$

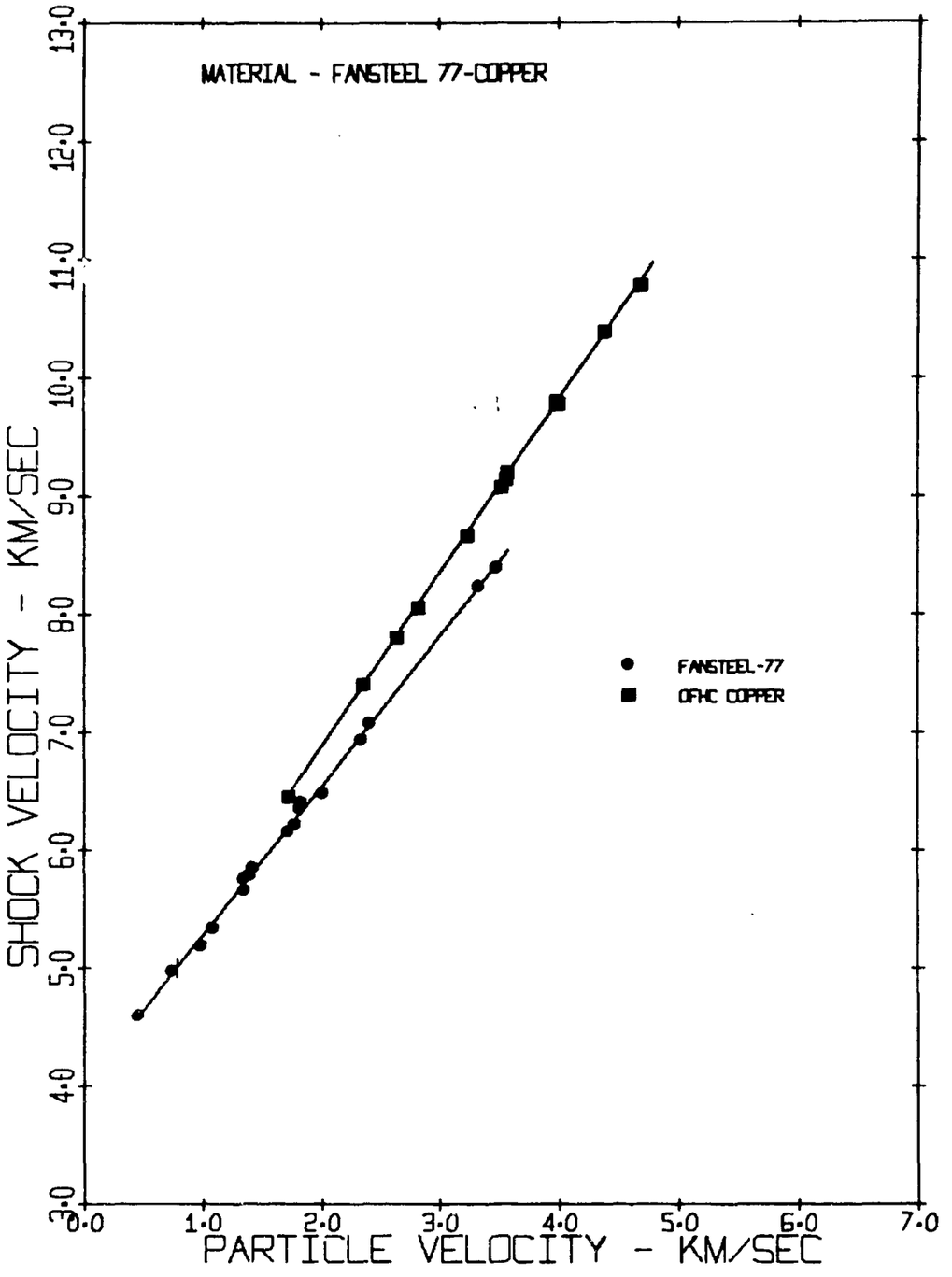

Figure 11 Shock Velocity vs Particle Velocity for Fansteel-77 and OFHC Copper

MSL-68-15

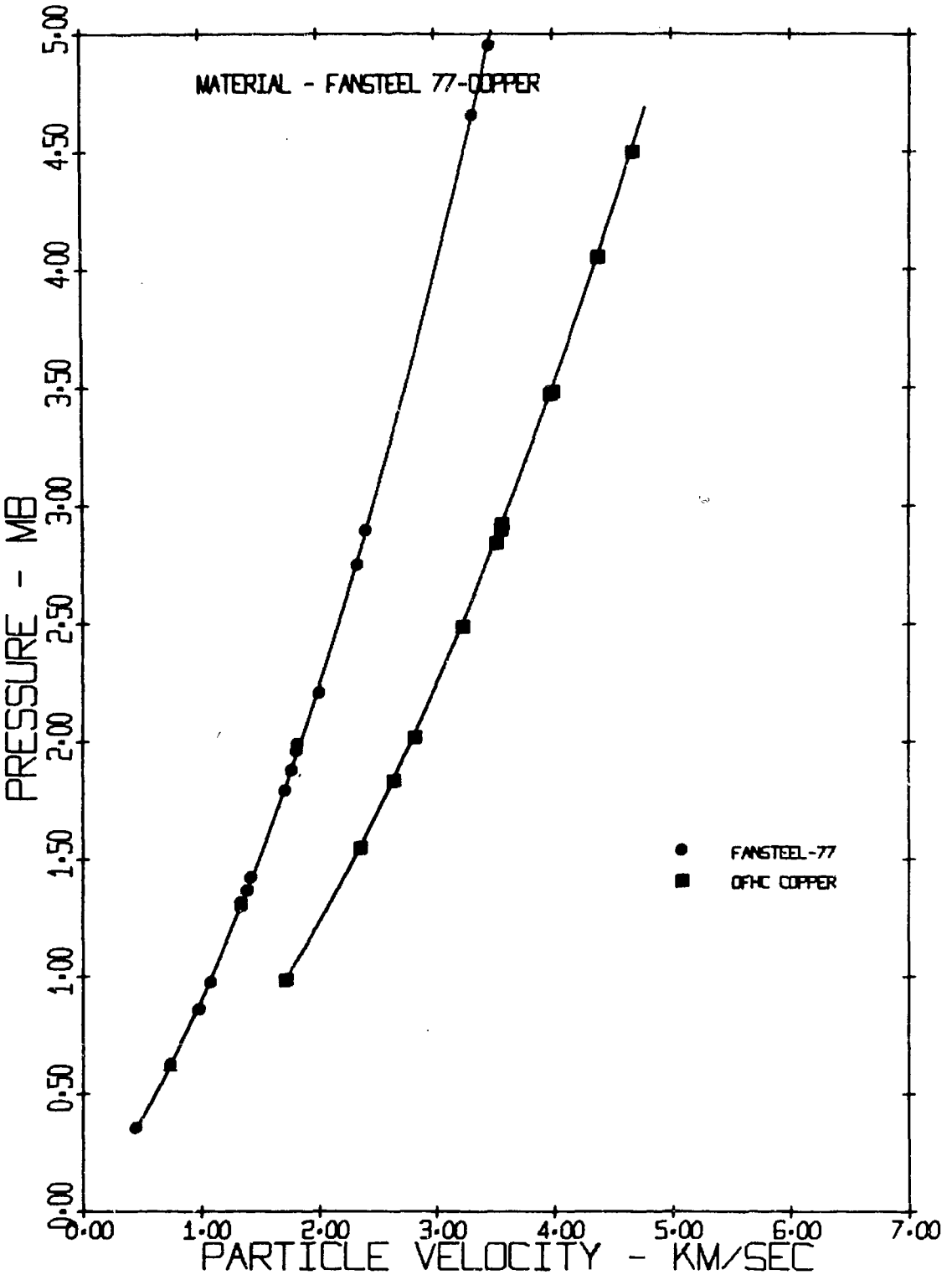

Figure 12 Pressure vs Particle Velocity for Fansteel-77 and OFHC Copper

All shots listed exhibited less than 2% B to C station scatter in U_s. The standard density employed was 8.930 gm/cm^3. Figure 12 illustrates that the shock hugoniot in pressure of copper is slightly more than half that of Fansteel-77. The hugoniot data are presented in Table III.

The third standard employed to achieve the lowest pressure data point in the saturated tuff experiments was 6061-T6 aluminum. The hugoniot of Al'tshuler[8] was employed.

$$U_s = 5.380 + 1.350\ u_p \text{ km/sec}$$

The impactor density was 2.72 gm/cm^3.

Climax Stock Granodiorite (Granite)

The physical and petrographic description of the Climax Stock Grandodiorite, "Granite", as well as the source of the samples is presented by Barnes.[9] A small sample of the original granite was tested independently,* and showed a dry effective porosity of 1.75%. The measured density for the target specimens for the hugoniot tests was 2.65 ± 0.01 gm/cm^3. The calculated bulk sound speed from reference[9] is in the range of 4.07 to 4.43 km/sec.

Granite was the first rock tested in the program, and the target design used was the stepped configuration.

The data presented in Table IV represent those tests which meet the requirements of low shock tilt and internal scatter. Figures 13 and 14 display the data in the U_s-u_p, and P-V planes

* Hornkohl Laboratories, Inc., Bakersfield, California

TABLE III

HUGONIOT DATA FOR OFHC COPPER

$V_o = 0.1120\ cm^3/gm$

$\rho_o = 8.980\ gm/cm^3$

Shot	Impactor Material	v Impact Velocity (km/sec)	U_s Shock Velocity (km/sec)	u_p Particle Velocity (km/sec)	P Pressure (Mb)	V/V_o Relative Volume	V Volume (cm^3/gm)	ρ Density (gm/cm^3)
C-1081 o	Cu	3.426	6.463	1.713	0.989	0.7350	0.0823	12.150
C-1240	FS	3.875	7.414	2.343	1.551	0.6840	0.0766	13.056
S-98	Al	7.929	7.815	2.631	1.836	0.6633	0.0743	13.462
S-15	FS	4.673	8.062	2.808	2.022	0.6517	0.0730	13.703
C-1082 o	Cu	6.434	8.669	3.217	2.490	0.6289	0.0704	14.199
S-76	Cu	7.018	9.076	3.509	2.843	0.6134	0.0687	14.559
C-963	Cu	7.097	9.149	3.549	2.900	0.6121	0.0685	14.589
C-1090 o	Cu	7.121	9.196	3.561	2.924	0.6128	0.0686	14.573
C-1249	FS	6.728	9.785	3.988	3.485	0.5924	0.0663	15.073
S-82	Cu	7.937	9.802	3.971	3.476	0.5949	0.0666	15.011
S-19	FS	7.405	10.390	4.368	4.053	0.5796	0.0649	15.407
S-161	FS	7.932	10.785	4.674	4.502	0.5666	0.0635	15.760

o Tests performed under contract NAS2-3427

TABLE IV

HUGONIOT DATA FOR CLIMAX STOCK GRANODIORITE (GRANITE)

$\rho_o = 2.65 \pm 0.01$ gm/cm^3

$V_o = 0.3774 \pm 0.0014$ cm^3/gm

Shot	U_s Shock Velocity (km/sec)	u_p Particle Velocity (km/sec)	P Pressure (Mb)	V Volume (cm^3/gm)
C-936	7.101(±0.096)	3.191(±0.010)	0.601(±0.010)	0.208(±0.002)
C-976	8.240(±0.020)	3.437(±0.002)	0.751(±0.002)	0.220
C-934	8.702(±0.020)	4.009(±0.080)	0.925(±0.020)	0.204(±0.003)
C-958	8.983(±0.076)	4.057(±0.081)	0.966(±0.027)	0.207(±0.002)
C-977	9.238(±0.110)	4.346(±0.012)	1.064(±0.016)	0.200(±0.001)
C-937	10.138(±0.006)	4.869(±0.097)	1.308(±0.027)	0.196(±0.003)
C-935	10.069(±0.129)	4.917(±0.014)	1.312(±0.021)	0.193(±0.002)
C-955	10.686 *	5.210	1.475	0.193
C-925	11.006 *	5.307(±0.106)	1.548(±0.031)	0.195(±0.003)
C-971	12.096 *	5.999	1.923	0.190

* Single pin data

MSL-68-15

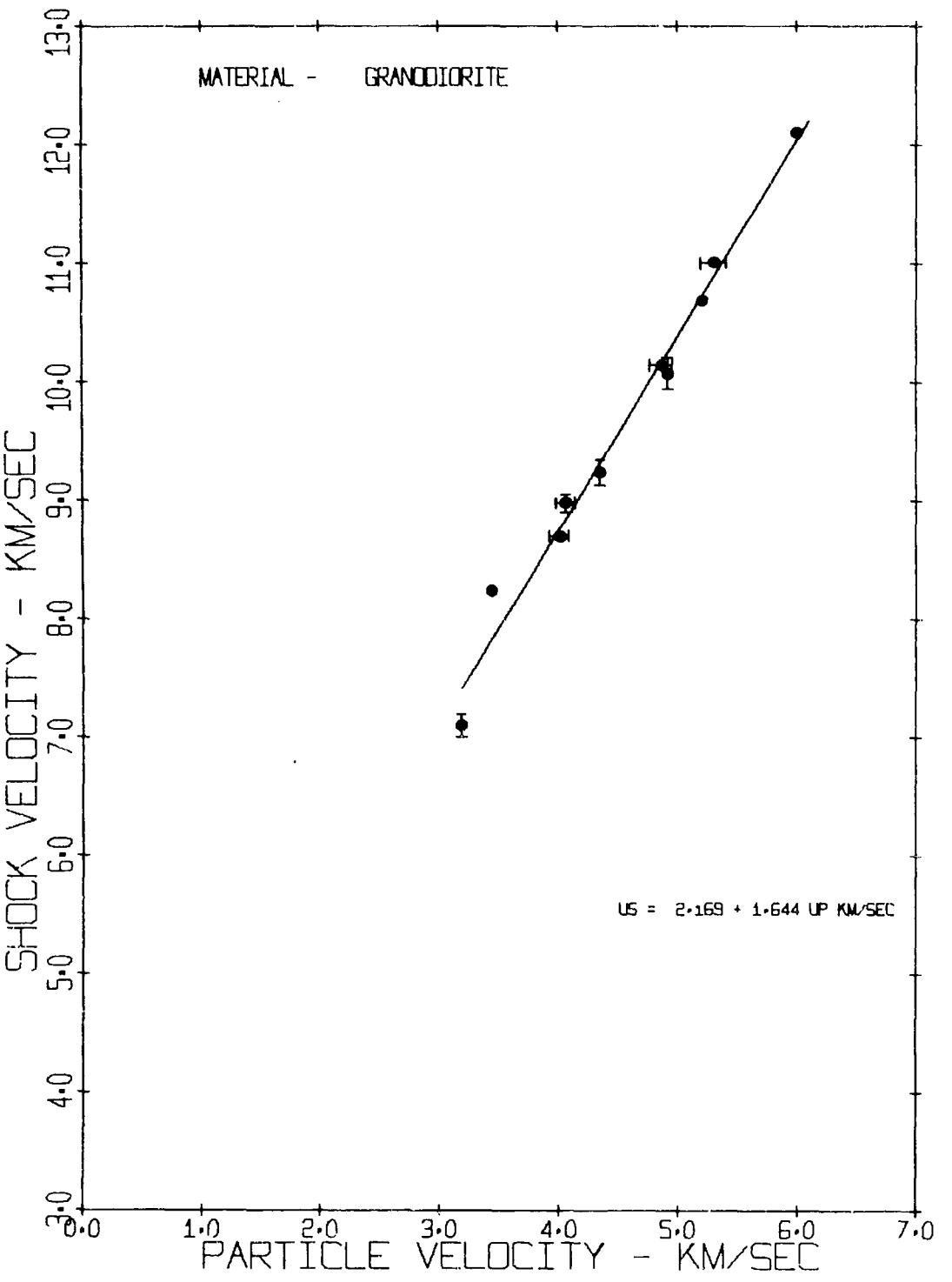

Figure 13 Shock Velocity vs Particle Velocity for Climax Stock Granodiorite

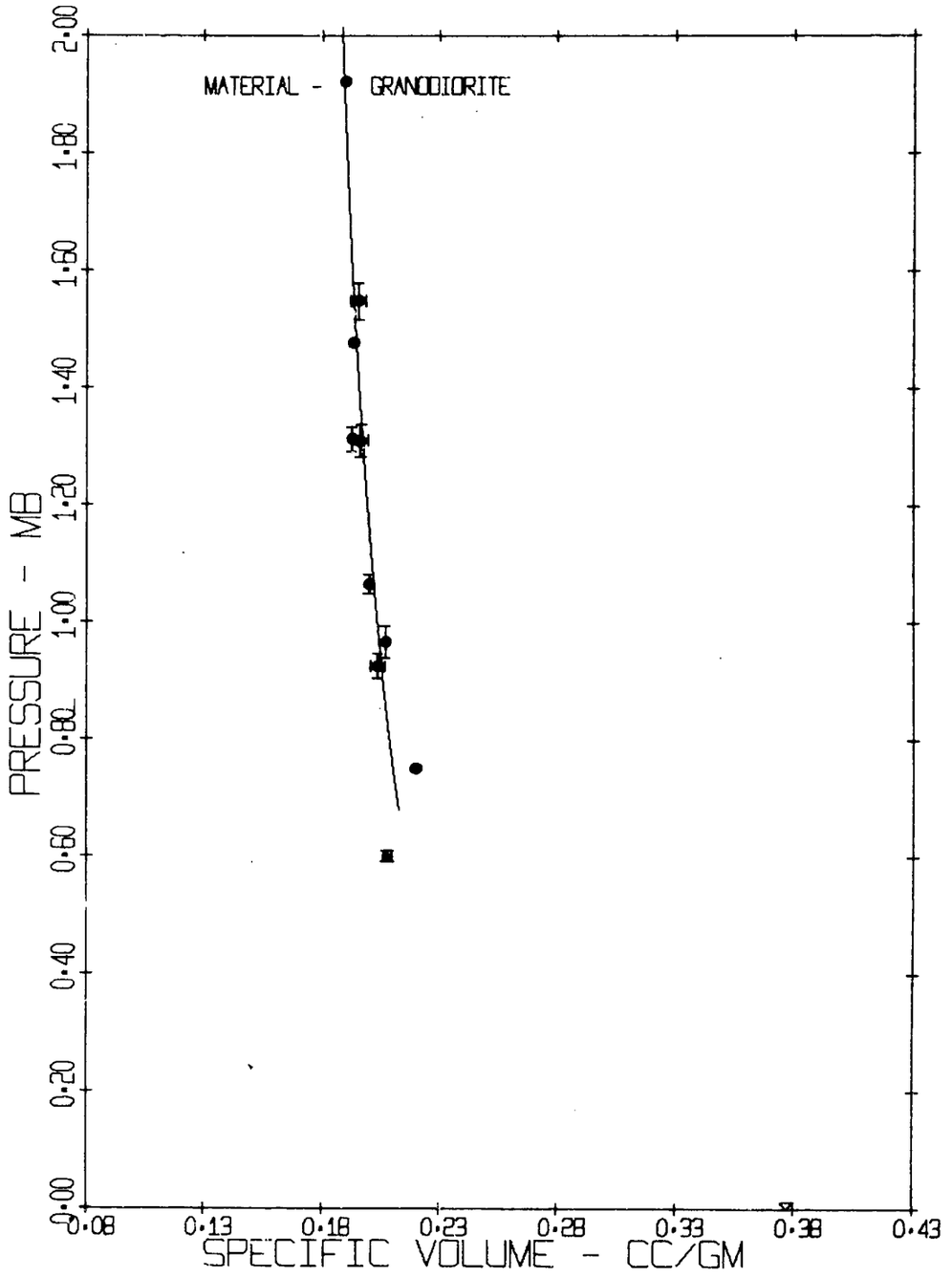

Figure 14 Pressure vs Specific Volume for Climax Stock Granodiorite

respectively. Points labeled single pin values are those shots employing only a single shock transit time pin. Error bars in the u_p axis represent the extremes of possible particle velocities induced by the impactor whose velocity was determined by measured gun firing parameters.

The linear hugoniot equation is given by:

$$U_s = 2.169 + 1.644\ u_p \text{ km/sec},\ 3.1 < u_p < 6.0 \text{ km/sec}$$

$$S.E.(U_s) = 0.190 \text{ km/sec for 10 points.}$$

Figure 15 is a comparison of the present results with the data of McQueen[10] (for Westerly, R.I. granite) and the LRL Compiler[11] for several NTS Area 15 granites. The hugoniot equation for the high density portion of McQueen's Westerly granite is:

$$U_s = 2.102 + 1.629\ u_p \text{ km/sec},\ 2.5 < u_p < 4.1 \text{ km/sec}$$

$$S.E.(U_s) = 0.052 \text{ km/sec for 8 points}$$

The least squares linear equation for the LRL Compiler data is given by:

$$U_s = 2.594 + 1.476\ u_p \text{ km/sec},\ 2.5 < u_p < 3.9 \text{ km/sec}$$

$$S.E.(U_s) = 0.056 \text{ km/sec for 4 data points.}$$

The large standard error of the GM data for this material is attributable to the many experimental problems encountered early in the program. The fact that the hugoniots of both LRL and McQueen compare very closely with the GM results, even for different granites, suggests the larger error does not significantly effect the results.

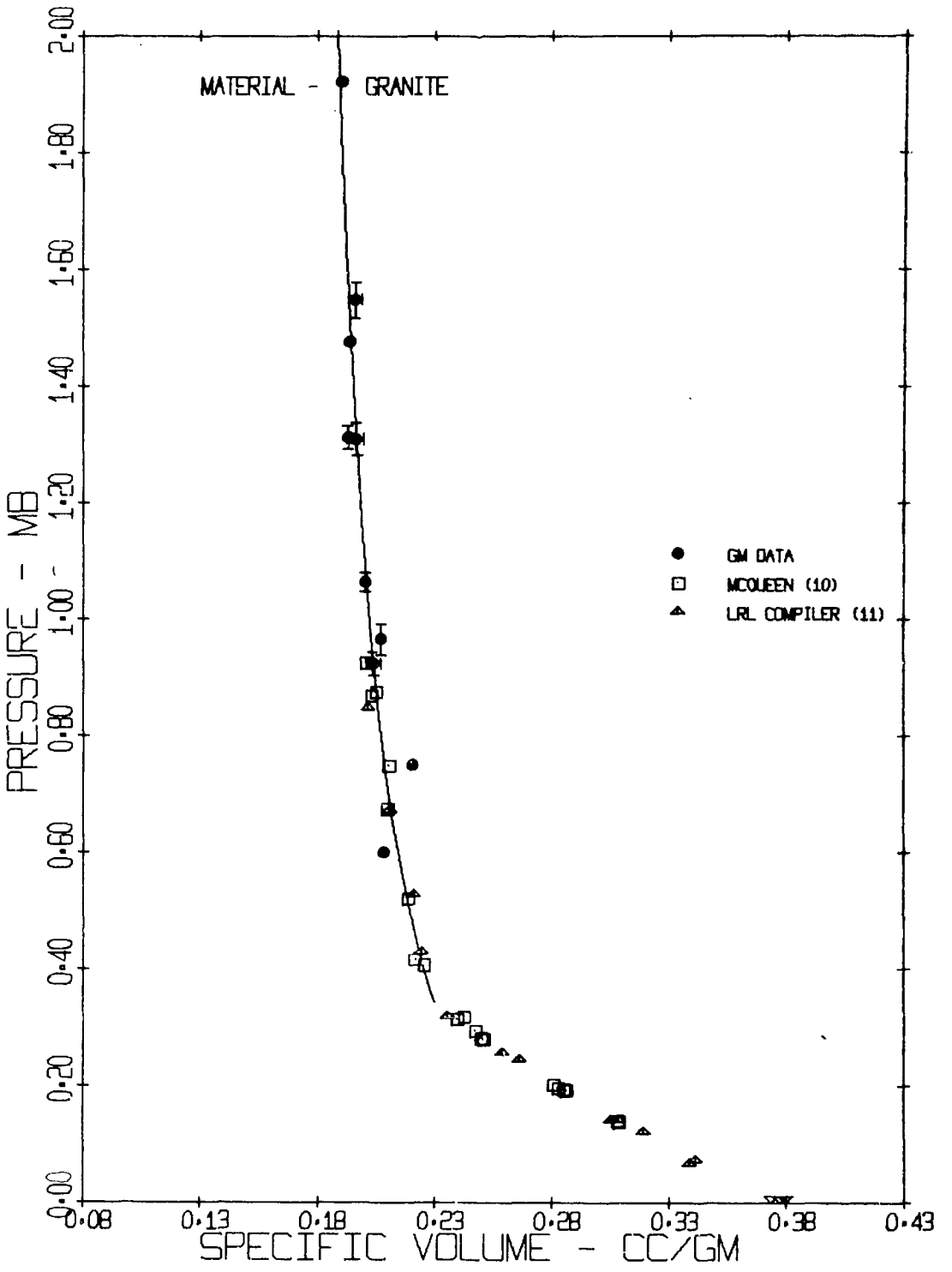

Figure 15 Pressure vs Specific Volume for Granites

A collection of all the granite high pressure phase data yields the following equation:

$$U_s = 1.994 + 1.673\ u_p \text{ km/sec},\ 2.5 < u_p < 6.0 \text{ km/sec}$$

$$S.E.(U_s) = 0.149 \text{ km/sec for 22 points.}$$

This combining of data appears reasonable for a general formulation of the high pressure "granite" hugoniot based on the initial densities and the mineral compositions shown below.

	GM	McQueen[10]	LRL Compiler[11]
Source	NTS Area 15	Westerly, R.I.	NTS Area 15
Ave. Density(gm/cm^3)	2.65	2.628	2.677
Composition (Wt %)			
Quartz	21-22%	27.5%	19.5%
Plagioclase	46-49%	31.4%	26.5%
Orthoclase	17-20%	35.4%	47.0%
Total Feldspar	63-69%	66.8%	73.5%

Although there were no tests performed in the lower phase regime, the following are the hugoniots obtained by McQueen and LRL respectively for this region:

$$U_s = 4.926 + 0.371\ u_p \text{ km/sec},\ 1.0 < u_p < 2.2 \text{ km/sec}$$

$$S.E.(U_s) = 0.019 \text{ km/sec for 11 points.}$$

$$U_s = 5.354 + 0.159\ u_p \text{ km/sec},\ 0.4 < u_p < 2.2 \text{ km/sec}$$

$$S.E.(U_s) = 0.134 \text{ km/sec for 9 points.}$$

Only the higher density of the two sets of LRL Compiler granite data are included here and in the figures. The granites compared here appear to exhibit similar hugoniots above the high density phase transition but appear to differ somewhat more below the transition.

Rainier Mesa Tuff (Vacuum dry)

The physical and petrographic descriptions for Rainier Mesa tuff are reported by Barnes.[9] The source of the samples is also given in this description.

The target configuration for the dry tuff and most of the water saturated tuff experiments was the stepped design. It was necessary to select target specimens having good uniformity and small granularity in the tilt pin steps.

Hugoniot data for the tuff initially in the vacuum dry condition are presented in Table V, and Figures 16 and 17. The linear form of the hugoniot is represented by the least squares equation:

$$U_s = 1.049 + 1.528\ u_p \text{ km/sec}, \quad 2.3 < u_p < 6.5 \text{ km/sec}$$

$$\text{S.E.}(U_s) = 0.086 \text{ km/sec for 8 data points.}$$

The initial density was 1.76 ± 0.02 gm/cm^3 as measured prior to the tests.

Comparison of the present data with selected results of other researchers is illustrated in Figure 18. Even though the specimens of Lombard,[12] Wiedermann,[13] Anderson,[14] and

TABLE V

HUGONIOT DATA FOR NTS RAINIER MESA TUFF (DRY)

$\rho_o = 1.76 \pm 0.02$ gm/cm^3
$V_o = 0.568 \pm 0.006$ cm^3/gm

Shot	U_s Shock Velocity (km/sec)	u_p Particle Velocity (km/sec)	P Pressure (Mb)	V Volume (cm^3/gm)
C-1030	4.763*	2.380	0.200	0.284
C-960	6.570(±0.101)	3.673(±0.073)	0.425(±0.015)	0.251(±0.002)
C-956	6.584(±0.010)	3.588	0.416	0.259
C-961	7.663(±0.038)	4.407(±0.004)	0.594(±0.004)	0.241(±0.002)
C-959	8.851(±0.020)	5.111(±0.007)	0.796(±0.003)	0.240
C-1028	9.490(±0.020)	5.444(±0.002)	0.909(±0.003)	0.242(±0.001)
C-597	9.849(±0.048)	5.819(±0.116)	1.009(±0.025)	0.233(±0.005)
C-972	11.035*	6.490(±0.130)	1.261(±0.026)	0.234(±0.007)

* Single Pin Value

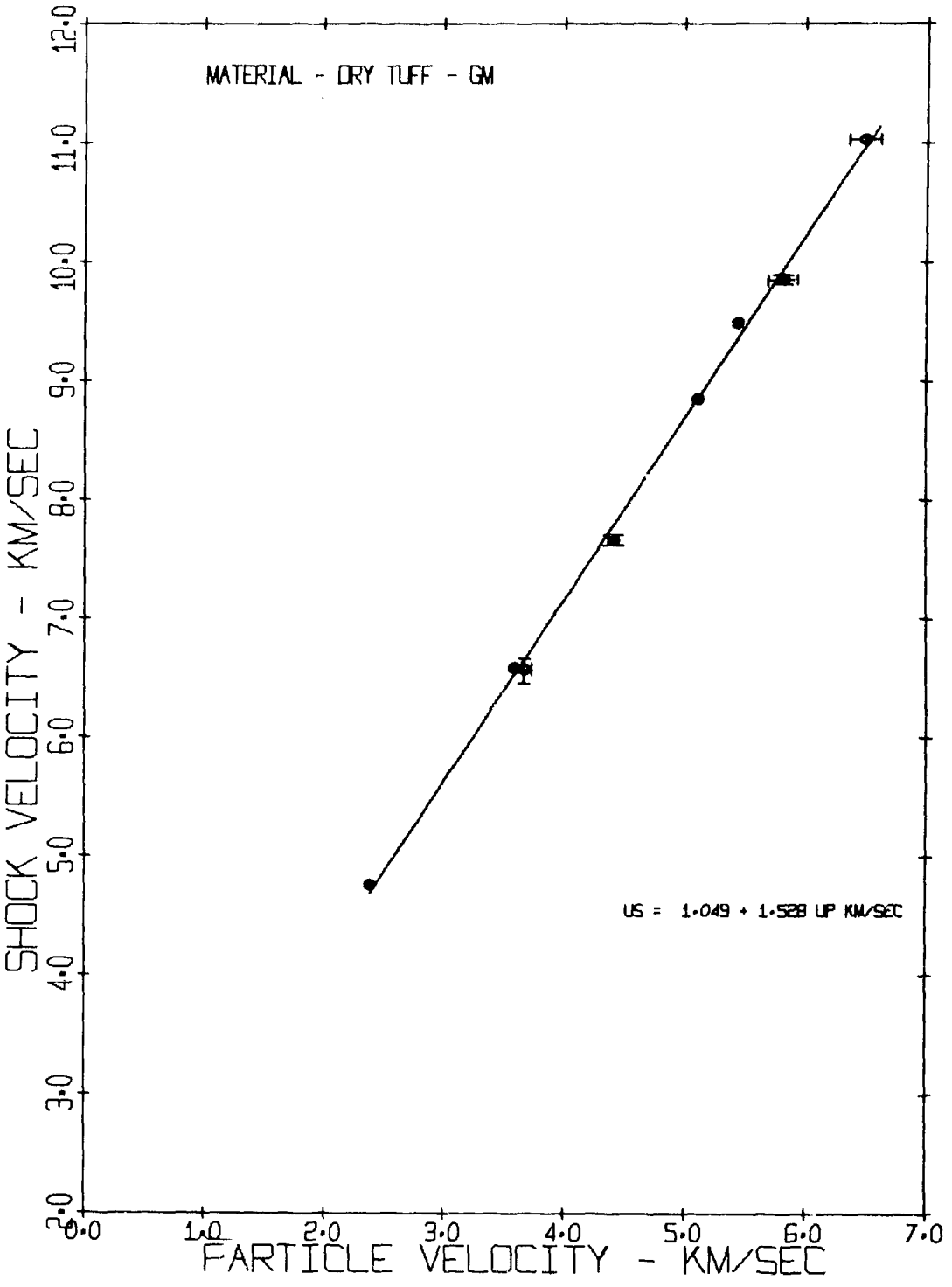

Figure 16 Shock Velocity vs Particle Velocity for Rainier Mesa Tuff (Dry)

MSL-68-15

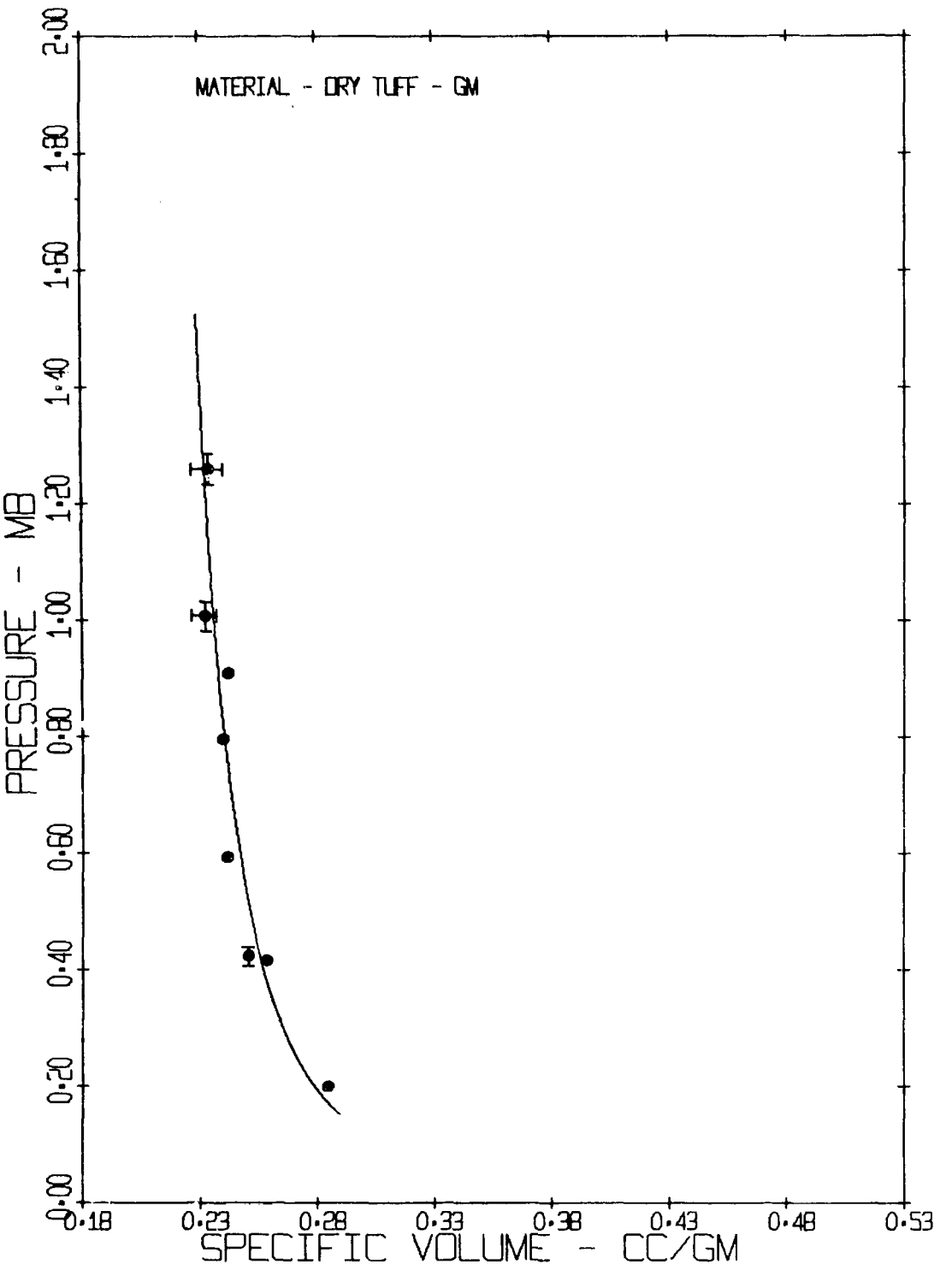

Figure 17 Pressure vs Specific Volume for Rainier Mesa Tuff (Dry)

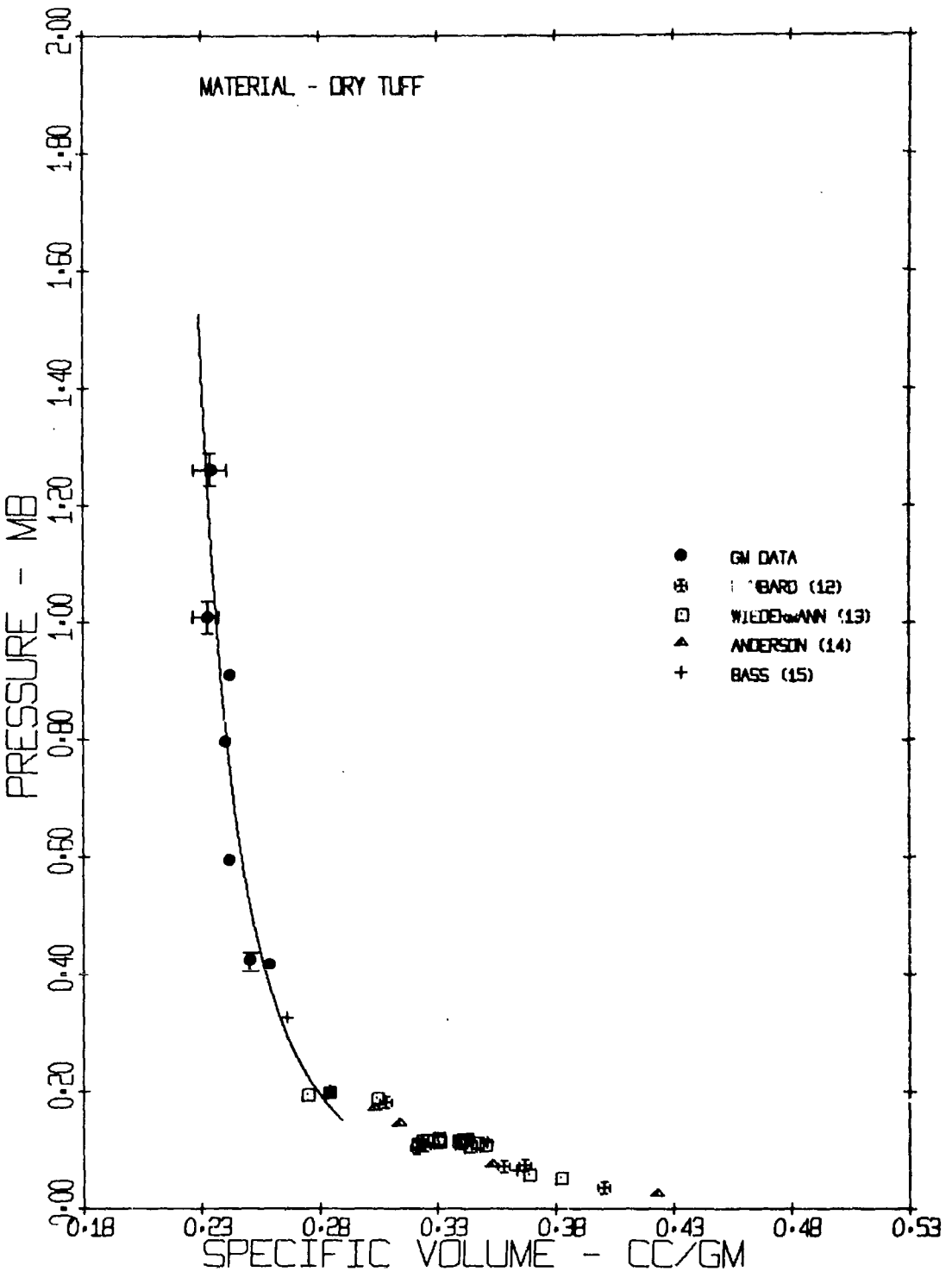

Figure 18 Pressure vs Specific Volume for Several Dry Tuffs

Bass[15] are reported to be from NTS Area 12, the Rainier Mesa area, there is considerable variability in the tuff's physical properties. The density and porosity of the comparison data were chosen to be in the ranges $\rho_o \sim 1.61$ to 1.80 gm/cm^3 and $\sim$ 20-30% respectively.

Nevertheless the data scatter is small as the figure displays and establishes a fairly well defined hugoniot when taken together.

A least squares fit to the selected and combined data of the low pressure regime is defined by the linear equation:

$$U_s = 1.371 + 1.431\ u_p \text{ km/sec}, \quad 0.7 < u_p < 2.5 \text{ km/sec}$$

$$S.E.(U_s) = 0.116 \text{ km/sec for 32 points.}$$

There is a slight disconinuity between the comparison data and the present linear fit to the higher pressure data. This break in the hugoniot shows up best in the P-V plane. Assuming that the data shown in Figure 18 (see also Figure 19) for the lower pressures are reliable and representative, a break appears to occur at $\sim$ 0.190 Mb and specific volume of 0.30 cm^3/gm. Using the average value of density ($\rho_{oAve} = 1.647$ gm/cm^3) and the slope of the linear fit to all the data, the following equation appears to describe a zone in P = P(V) which represents the range of the hugoniot states of the various tuffs up to a pressure of $\sim$ 0.19 Mb.

$$P = \frac{C_o^{\,2}\ (V_o - V)}{\left[V_o - 1.431\ (V_o - V)\right]^2}$$

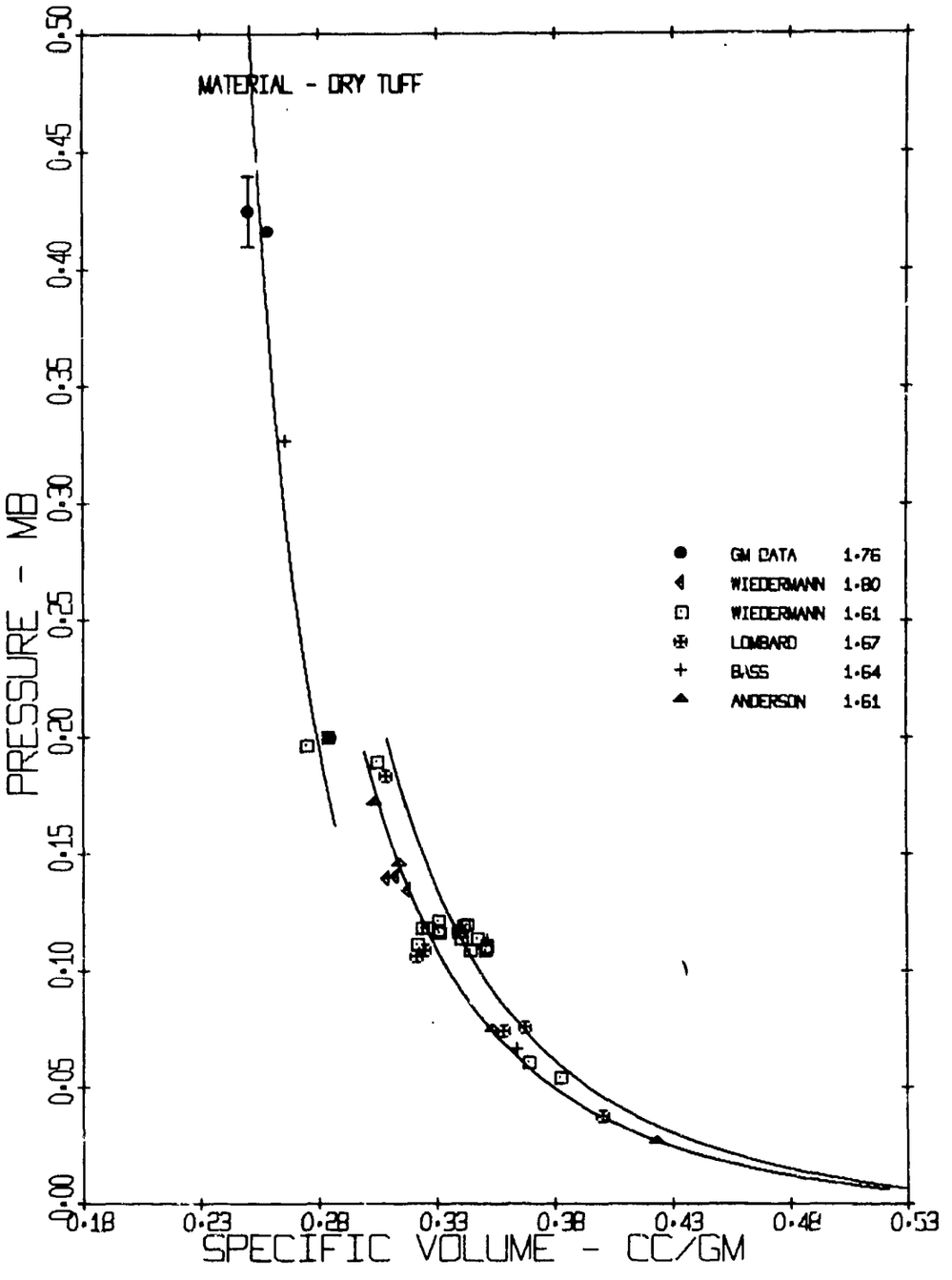

Figure 19 Pressure vs Specific Volume for Several Dry Tuffs Showing Low Pressure Regime

where V_o = 0.607 cm^3/gm, and C_o may range from 0.132 to 0.147 cm/μsec. The values of the initial densities of the various tuffs are included in the legend of Figure 19.

The evidence presented here for the existence of the phase change in the dry tuff is still subject to dispute, primarily because of the question of the reliability of the data in such varied polymineralic rock and of the mechanism which causes the spread in the shock velocity measurements. Unfortunately the lowest present experimental datum is either just above or at the discontinuity allowing no direct comparisons with the lower end of the hugoniot. The comparison made, however, between the several points reported by Lomard, Wiedermann, and Bass on either side of the suggested transition point appears to be in agreement.

Rainier Mesa Tuff (Water Saturated)

The design, construction and testing of the water saturated tuff targets is presented in Section III in detail.

Each target was checked for water leakage in vacuo prior to the actual hugoniot experiment. Several pin failures due to preshorting did occur; these are indicated in Table VI.

Figures 20 and 21 graphically present the data for saturated tuff. The measured initial density was 1.97 ± 0.02 gm/cm^3 for these specimens. The data are best represented by two line segments. The data are amenable to description by a linear segment given by:

TABLE VI

HUGONIOT DATA FOR NTS RAINIER MESA TUFF (WATER SATURATED)

$\rho_o = 1.97 \pm 0.02$ gm/cm^3

$V_o = 0.5076 \pm 0.005$ cm^3/gm

Shot	U_s Shock Velocity (km/sec)	u_p Particle Velocity (km/sec)	P Pressure (Mb)	V Volume (cm^3/gm)
C-1266	3.878*	1.003	0.077	0.376
C-1022	4.749*	1.401	0.131	0.358
C-1080	4.781(±0.011)	1.802	0.170	0.316(+0.001)
C-1069	5.105*	1.879	0.189	0.321
C-1031	5.012(±0.043)	1.934(±0.003)	0.191(±0.002)	0.312(±0.001)
C-1021	6.597(±0.070)	3.002(±0.008)	0.390(±0.005)	0.277(±0.001)
C-1067	6.904(±0.022)	3.328(±0.002)	0.453(±0.001)	0.263(±0.001)
C-1018	8.233(±0.002)	4.190(±0.084)	0.680(±0.013)	0.249(±0.005)
C-1026	9.341(±0.064)	4.748(±0.007)	0.874(±0.007)	0.250(±0.001)
C-1032	11.028*	5.883	1.278	0.237
C-1029	11.228*	6.019	1.331	0.236

*Single Pin Value

MSL-68-15

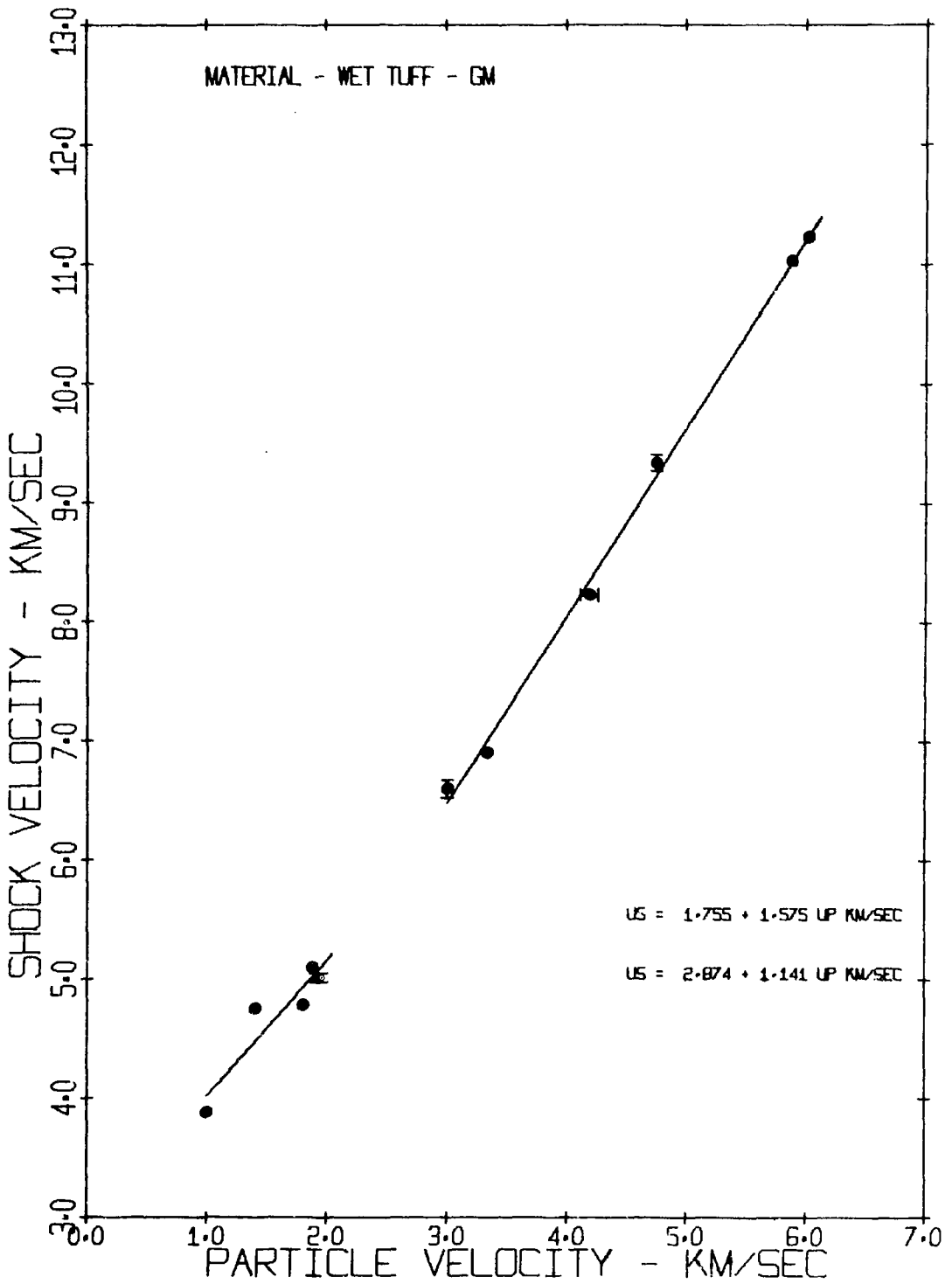

Figure 20 Shock Velocity vs Particle Velocity for Rainier Mesa Tuff (Wet)

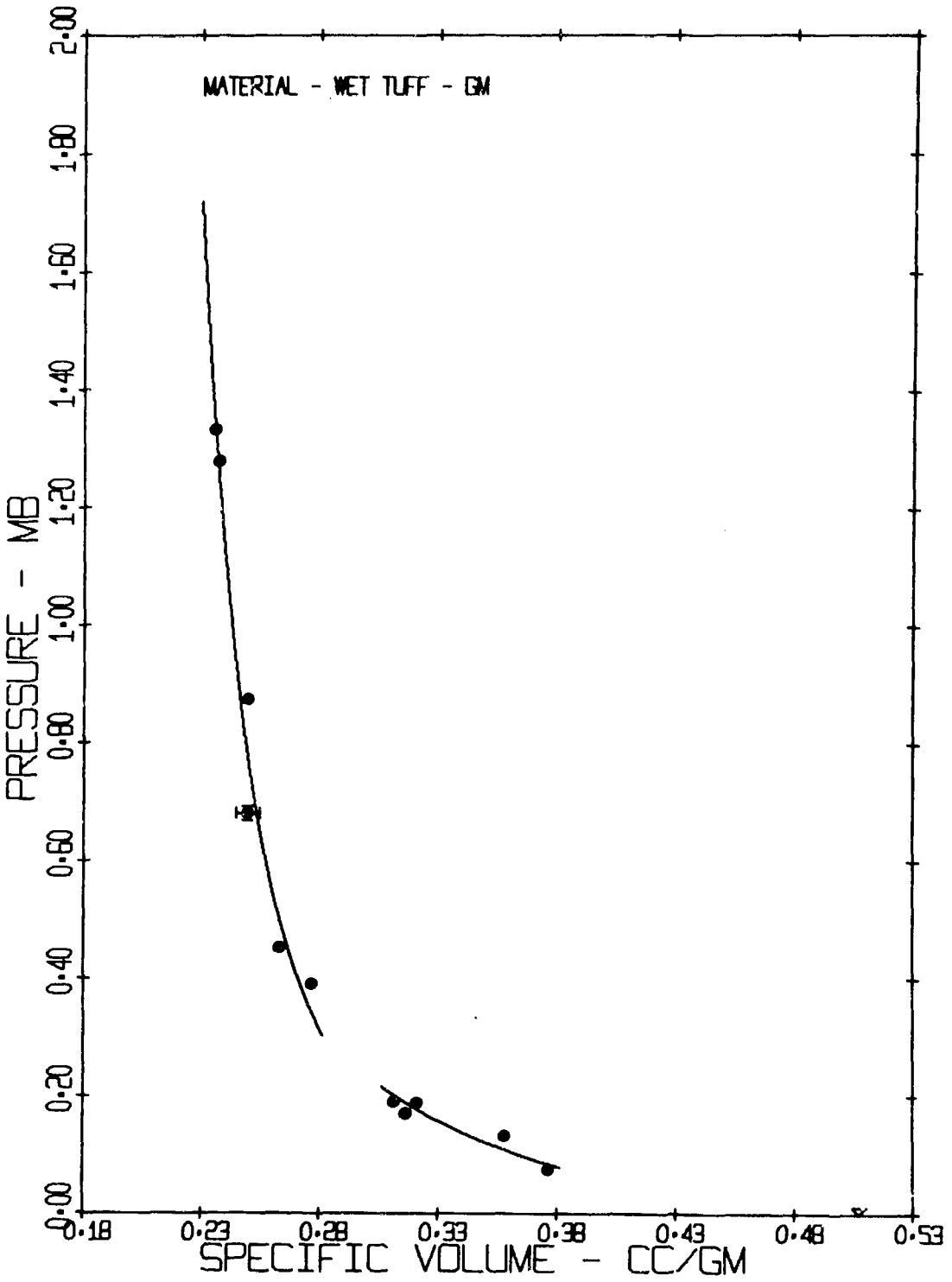

Figure 21 Pressure vs Specific Volume for Rainier Mesa Tuff (Wet)

$$U_s = 1.755 + 1.575\ u_p \text{ km/sec}, \quad 3.0 < u_p < 6.1 \text{ km/sec}$$

$$\text{S.E.}(U_s) = 0.089 \text{ km/sec for 6 points.}$$

The lower segment is much less well defined from the present data alone, but the linear form is presented for convenience as:

$$U_s = 2.874 + 1.141\ u_p \text{ km/sec}, \quad 1.0 < u_p < 2.0 \text{ km/sec}$$

$$\text{S.E.}(U_s) = 0.162 \text{ km/sec for 5 points.}$$

The reasons for the data scatter in the lower region are probably several. The two lowest pressure tests experienced a failure due to water preshorting of one of the two rear surface pins. Also at low shock stress and shock velocity, i.e. velocities below the sonic velocities of the basic minerals, it is expected that inhomogeneities of the specimens will effect wave propagation, as will specimen to specimen variations.

Shock wave arrival at a free surface in porous and granular rock materials has been observed to be irregular and non-planar.[16] With such few data available the representation cannot be considered to be an exact description. Based upon the obvious scatter of the data of other authors the velocities recorded are probably representative of the bulk material.

Figures 22 and 23 are comparison plots of the present data with those of other workers.[12,17,18,19] The least squares equations to all the data presented are given by:

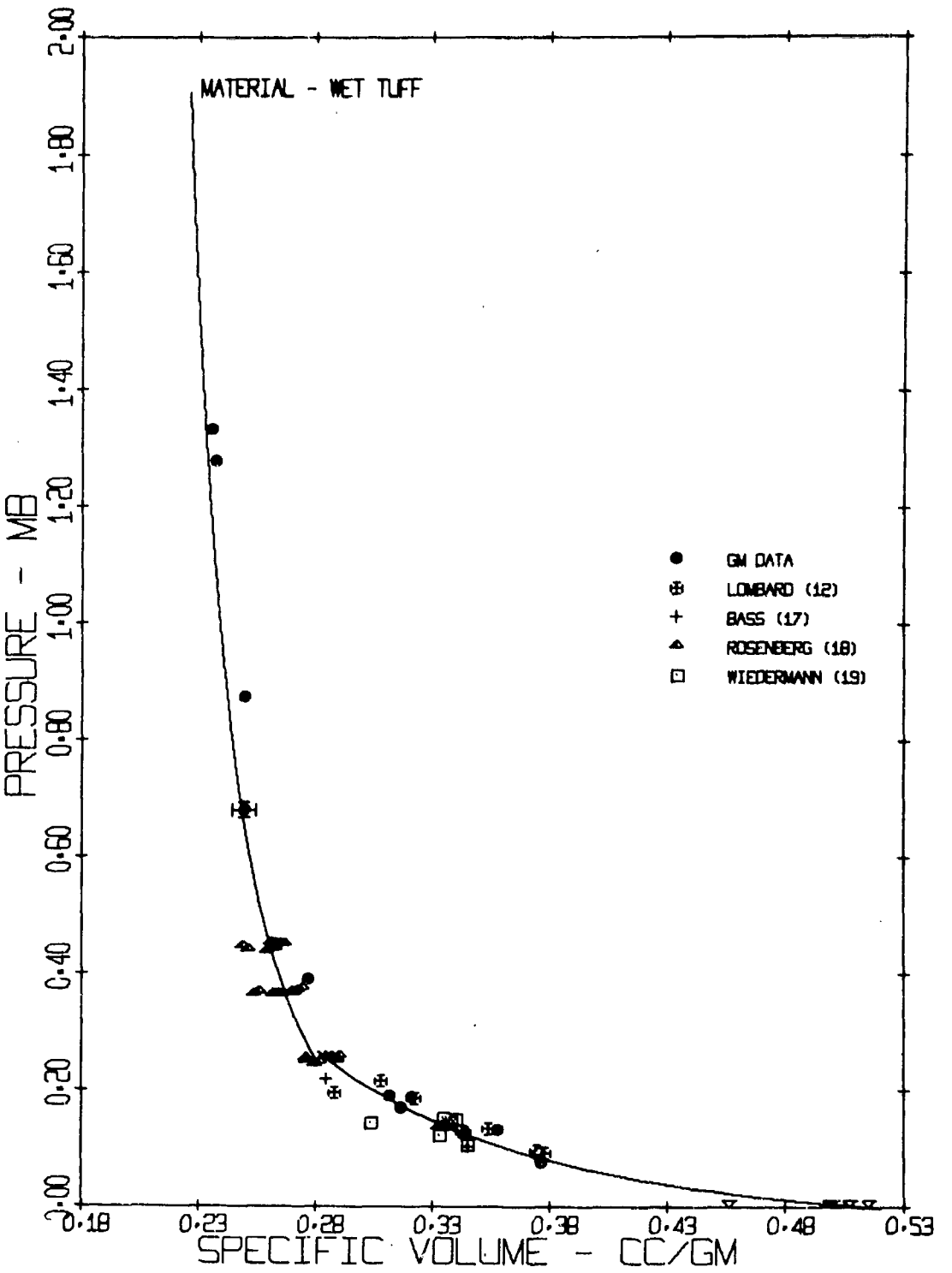

Figure 22 Pressure vs Specific Volume for Several Wet Tuffs

MSL-68-15

Upper regime

$U_s = 1.573 + 1.606\ u_p$ km/sec, $2.9 < u_p < 6.1$ km/sec

S.E.(U_s) = 0.141 km/sec for 26 points.

Lower regime

$U_s = 2.876 + 1.048$ km/sec, $1.0 < u_p < 2.4$ km/sec

S.E.(U_s) = 0.228 km/sec for 37 points.

The correlation of the data appears to be quite good, particularly because the highest data of Rosenberg[18] fall in very nicely with the lower end of the upper region described here. As in the dry tuff data, the problem of comparison is complicated by the differing initial densities and the general experimental scatter. The point of initiation of the high density phase appears from the comparison plots to occur between P ≃ 0.25 to 0.29 Mb and V ≃ 0.290 to 0.285 cm^3/gm. The data do not show a substantial volume decrease but merely exhibit a discontinuity in the slope of the hugoniot.

Figure 23 displays the low region as a zone bounded by lines representing the hugoniots parallel to the best least squares fit. The representation is given by:

$$P = \frac{C_o^2\ (V_o - V)}{\left[V_o - 1.048\ (V - V_o)\right]^2}$$

With C_o from 0.268 to 0.297 cm/μsec and V_o = 0.515 cm^3/gm. The initial densities for the various tuffs are presented in the legend in Figure 23.

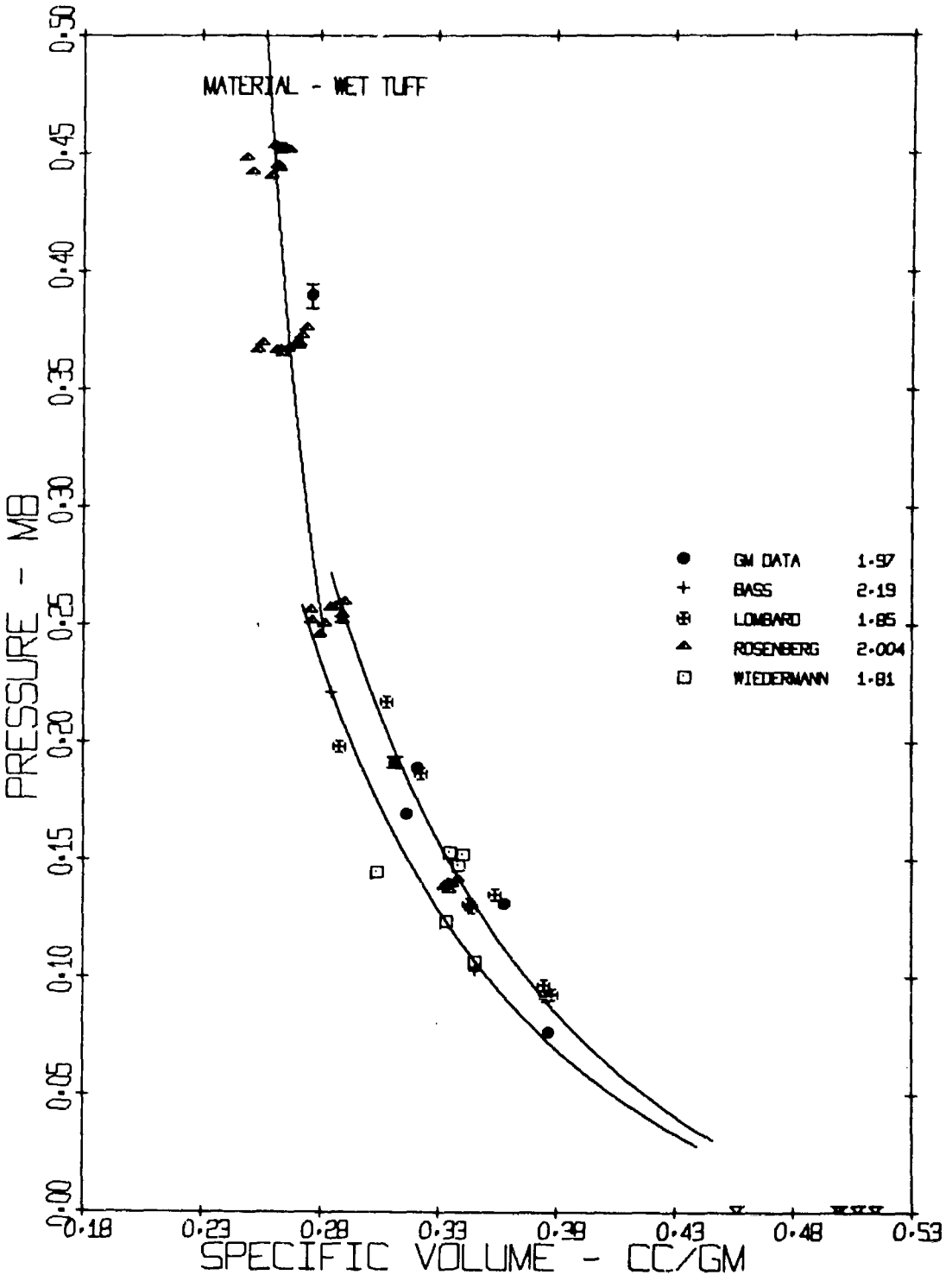

Figure 23 Pressure vs Specific Volume for Several Wet Tuffs Showing Low Pressure Regime

The evidence presented here and for dry tuff suggests a phase-transition to a higher density form of some component of the tuff. This component is most probably the silicate glass matrix of the tuff. The transition pressure corresponds well with the transition observed by Jones[20] for porous quartz (i.e a highly quartziferous sandstone) at ∿ 0.260 Mb.

Grouting Materials $V44_D$ and $V6_C$

The grouting material tested in the program was prepared by the Waterways Experimental Station (W.E.S.), Jackson, Mississippi. Grout $V44_D$ is employed as a hugoniot match for wet tuff. The following is a brief description of the material:

Ingredient	Wt %
Whitesides epoxy (Parts A and B)	54.6
Dolomite sand (passing No. 200 screen)	19.5
Bentonite (aquagel)	25.9

Details of preparation and sources of the ingredients may be obtained from James M. Polatty, Chief, Engineering Mechanics Branch, Concrete Division.

The sample received had a measured density of 1.45 ± 0.02 gm/cm^3, slightly lower than that measured by W.E.S. of 1.469 to 1.476 gm/cm^3 on a similar material.

The hugoniot data measured are listed in Table VII. Adjustments to the shock wave transit time interval were made for the 0.125 mm thick brass rear-surface shim. The time adjustment was performed using the impedance-match method described earlier and averaged only about 2% of the total time-interval.

TABLE VII

HUGONIOT DATA FOR GROUT $V44_D$

$\rho_o = 1.45 \pm 0.02$ gm/cm^3

$V_o = 0.690 \pm 0.009$ cm^3/gm

Shot	U_s Shock Velocity (km/sec)	u_p Particle Velocity (km/sec)	P Pressure (Mb)	V Volume (cm^3/gm)
C-1123	5.007(±0.075)	1.558(±0.004)	0.113(±0.002)	0.475(±0.003)
C-1125	5.688(±0.002)	2.064	0.170	0.439(+0.001)
C-1122	7.210(±0.060)	3.355(±0.004)	0.351(±0.003)	0.369(±0.002)
C-1133	8.617(±0.002)	4.385	0.548	0.339
C-1134	9.874(±0.095)	5.424(±0.109)	0.777(±0.023)	0.311(±0.004)
C-1136	10.318*	5.874(±0.118)	0.879(±0.018)	0.297(+0.008)
C-1153	11.772*	6.736(±0.135)	1.150(±0.023)	0.295(±0.008)

*Single Pin Value

Shown in Figures 24 and 25 are the data obtained and the data for three tests performed by W.E.S.*

A fit to the GM data is given by:

$$U_s = 2.998 + 1.275\ u_p \text{ km/sec}, \quad 1.5 < u_p < 6.7 \text{ km/sec}$$

$$\text{S.E.}(U_s) = 0.103 \text{ km/sec for 7 points.}$$

The W.E.S. fit is given by:

$$U_s = 2.68 + 1.53\ u_p \text{ km/sec}, \quad 1.0 < u_p < 2.1 \text{ km/sec}$$

$$\text{S.E.}(U_s) = 0.057 \text{ km/sec for 3 points.}$$

As can be seen in Figure 26, the hugoniot of the $V44_D$ grouting material lies significantly below the hugoniots of the dry and the saturated tuff. In the P-u_p plane, the grout is less stiff than the water saturated tuff and falls below the dry tuff hugoniot beginning at $\sim$ 0.3 Mb.

Figure 27 compares the hugoniot data for the W.E.S. granite matching grout $V6_C$ and the GM granite data.* The W.E.S. data are shown extrapolated to 2 Mb and are seen to match the granite reasonably well, within $\sim$ 6% in pressure at a given particle velocity.

* Private communication, Mr. W. R. Sullivan, Grouting and Engineering Physics Section, Concrete Division, Waterways Experimental Station, Jackson, Mississippi 39205.

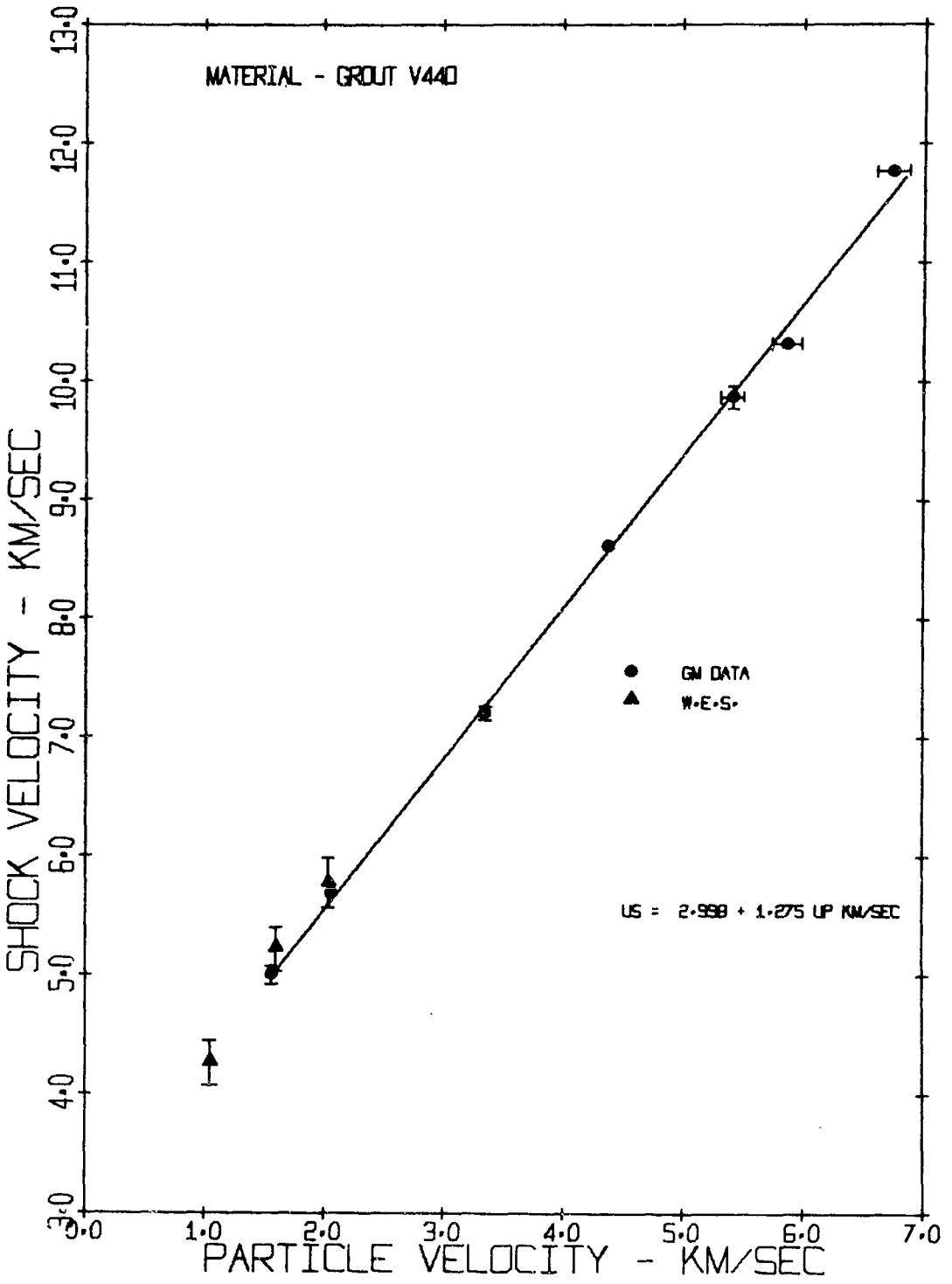

Figure 24 Shock Velocity vs Particle Velocity for Grouting Material $V44_D$

MSL-68-15

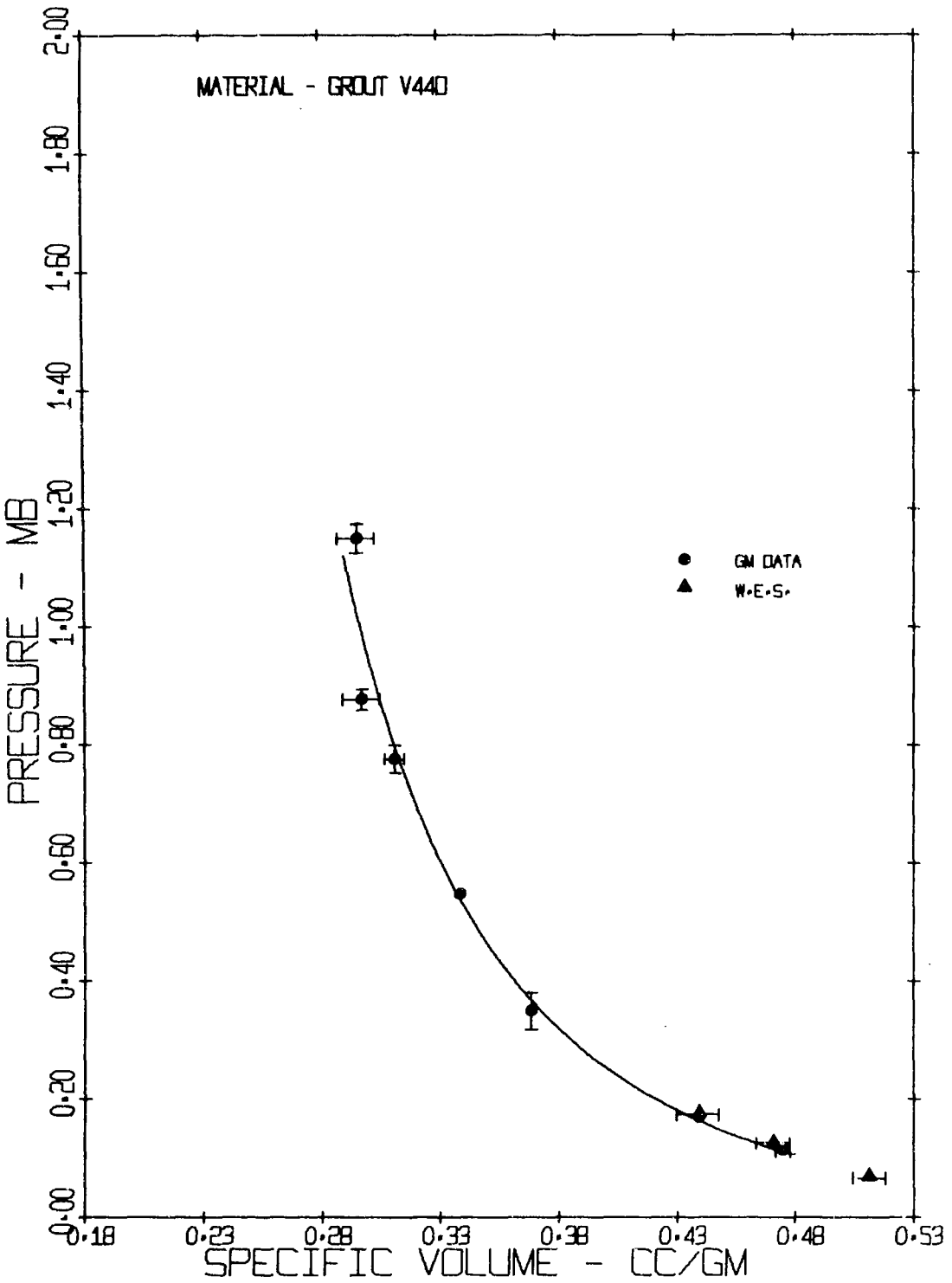

Figure 25 Pressure vs Specific Volume for Grouting Material $V44_D$

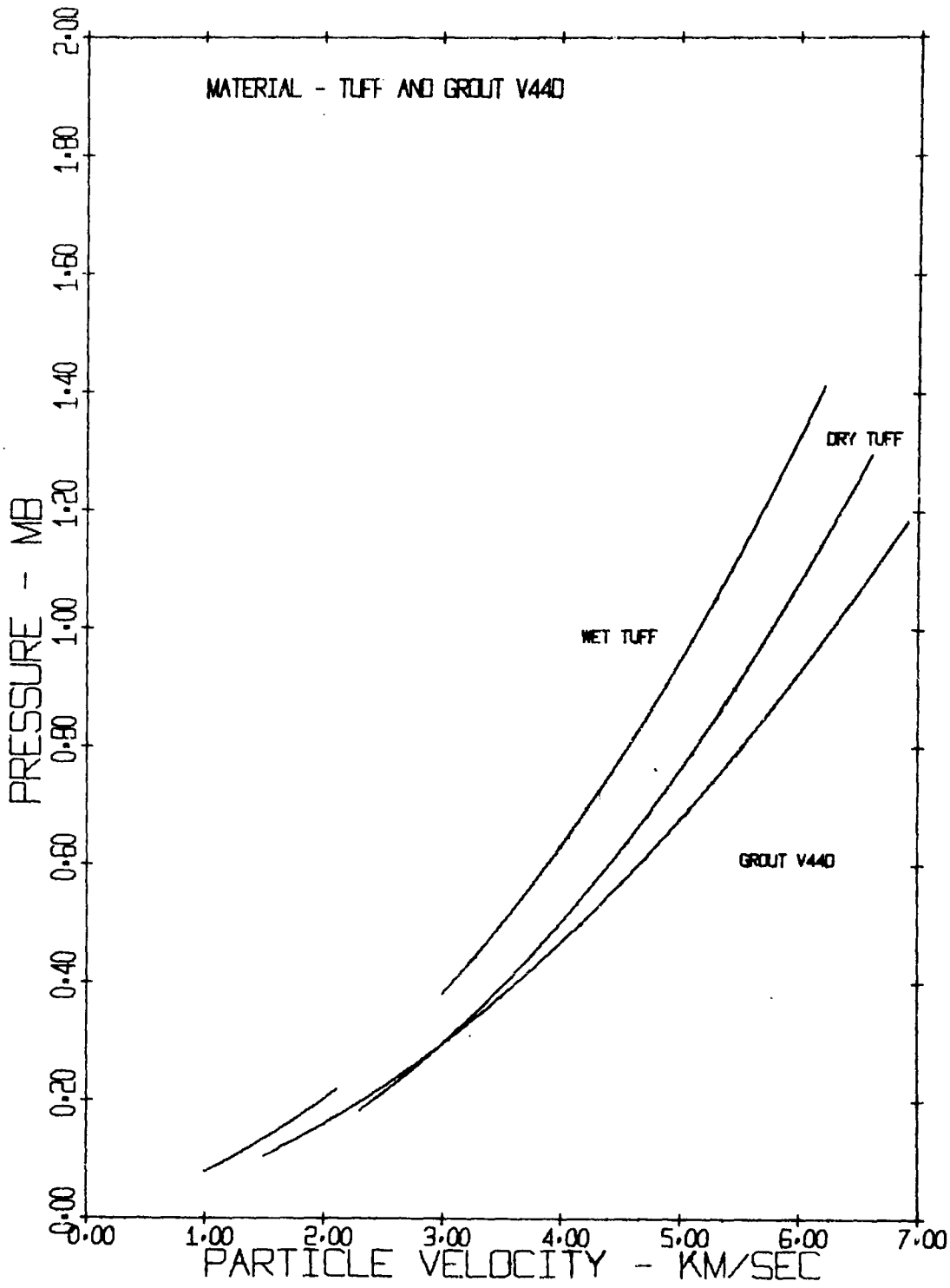

Figure 26 Pressure vs Particle Velocity for Rainier Mesa Tuff (Dry and Wet Conditions) and Grouting Material $V44_D$

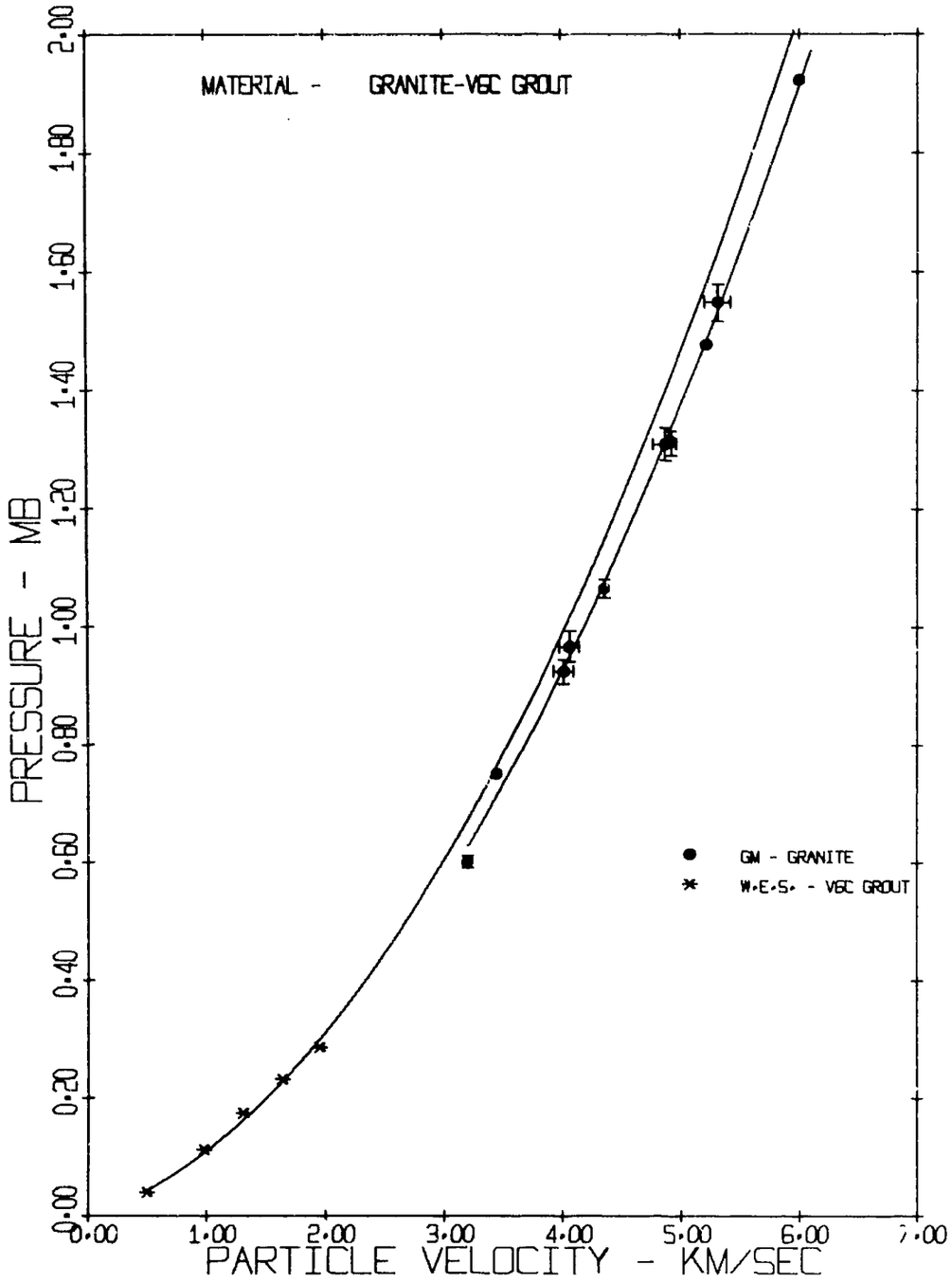

Figure 27 Pressure vs Particle Velocity for Climax Stock Granodiorite and $V6_C$ Grouting Material

Schistose Gneiss

A detailed petrographic analysis of the schistose gneiss tested during this program is at present unavailable. The following is a mineralogical description of the rock core used in the program.*

TABLE VIII

APPROXIMATE MINERALOGICAL COMPOSITION
OF SCHISTOSE GNEISS

Quartz	35%-33%
Plagioclase	22%-21%
Biotite	20%-15%
Muscovite	10%-15%
Clorite	7%
Garnet	5%
Magnetite and Pyrite	1%
Miscellaneous	Trace

"The rock core is a homogeneous, grey, dense, fresh, medium grained, quartz-biotite-plagioclase, gneiss. The mineral assemblage of quartz, plagioclase, biotite, muscovite, and minor garnet porphyroblasts, chlorite and accessory pyrite, magnetite, zircon, apatite and tourmaline as well as variation of grain size in the minerals would appear to indicate that these rocks are paragneisses, i.e., derived by regional metamorphism of pre-existing sediment."

* Petrographic Report No. 1M243-250, Department of the Army Corps of Engineers, South Atlantic Division, Division Materials Testing Laboratory, Marietta Georgia, sampled by Mr. Canning.

The hugoniot data are presented in Table IX. The initial density was 2.79 ± 0.02 gm/cm^3. Targets used were the rectangular design described earlier.

The hugoniot data are shown in Figures 28 and 29 and may be described by a least squares linear equation given by:

$$U_s = 2.376 + 1.604\ u_p \text{ km/sec}, \quad 2.5 < u_p < 6.1 \text{ km/sec}$$

$$\text{S.E.}(U_s) = 0.116 \text{ for 9 points.}$$

There appears to be a lower pressure phase below 0.3 Mb, but the two data points taken in this region are insufficient to determine an accurate hugoniot.

The data also exhibit a region of anomolous behavior in the pressure range of 0.9 to 1.2 Mb. The apparent discontinuity in this region accounts for the number of tests performed there. Without further experimentation, the cause for this behavior cannot be determined. If the data are analyzed without the two points falling below the line shown in the figures at a particle velocity of $\sim$ 4 km/sec (C-1085 and C-1086), the linear hugoniot of the high pressure phase is given by:

$$U_s = 2.363 + 1.611\ u_p \text{ km/sec}$$

where the standard error in U_s is reduced to 0.098 km/sec. Exclusion of these two shots results in a hugoniot displaced 0.6% lower in intercept and 0.4% upward in slope.

TABLE IX

HUGONIOT DATA FOR SCHISTOSE GNEISS

$\rho_o = 2.79 \pm 0.02$ gm/cm^3

$V_o = 0.358 \pm 0.003$ cm^3/gm

Shot	U_s Shock Velocity (km/sec)	u_p Particle Velocity (km/sec)	P Pressure (Mb)	V Volume (cm^3/gm)
C-1148	5.443*	0.704	0.107	0.312
C-1097	5.660(±0.005)	1.788	0.282(±0.001)	0.245
C-1083	6.590 †	2.554	0.470	0.220
C-1084	7.526*	3.182	0.668	0.207
C-1149	8.479(±0.020)	3.740(±0.002)	0.885(±0.002)	0.200(±0.001)
C-1085	8.643 †	4.019	0.969	0.192
C-1086	9.033(±0.003)	4.274	1.077(±0.001)	0.189
C-1068	9.266(±0.005)	4.331	1.120	0.191
C-1137	9.476(±0.028)	4.416(±0.003)	1.168(±0.004)	0.191(±0.001)
C-1150	10.940*	5.279(±0.106)	1.611(±0.033)	0.186(±0.004)
C-1151	12.172*	6.047	2.054	0.180

* Single Pin Value
† Double Pin Value

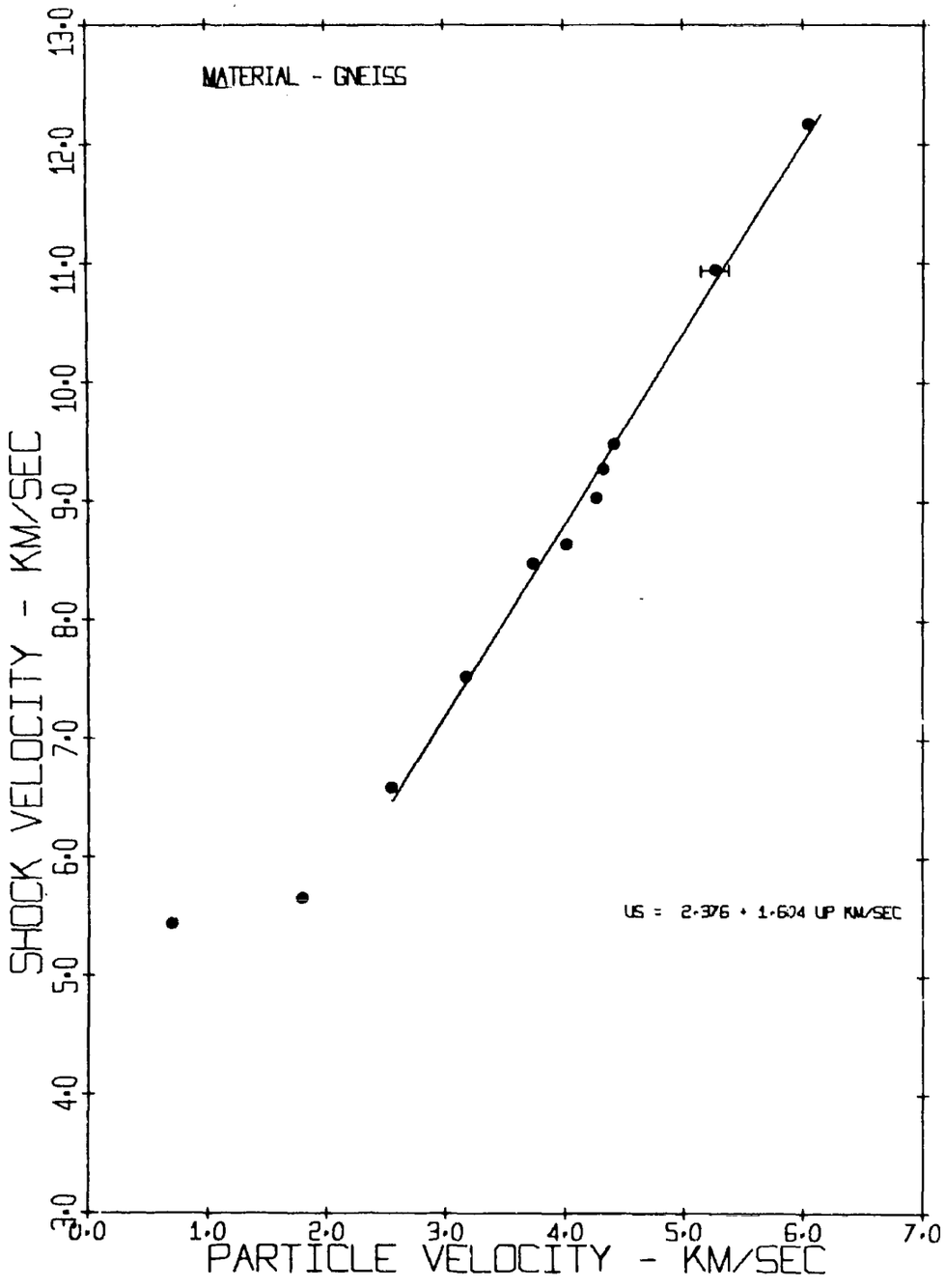

Figure 28 Shock Velocity vs Particle Velocity for Schistose Gneiss

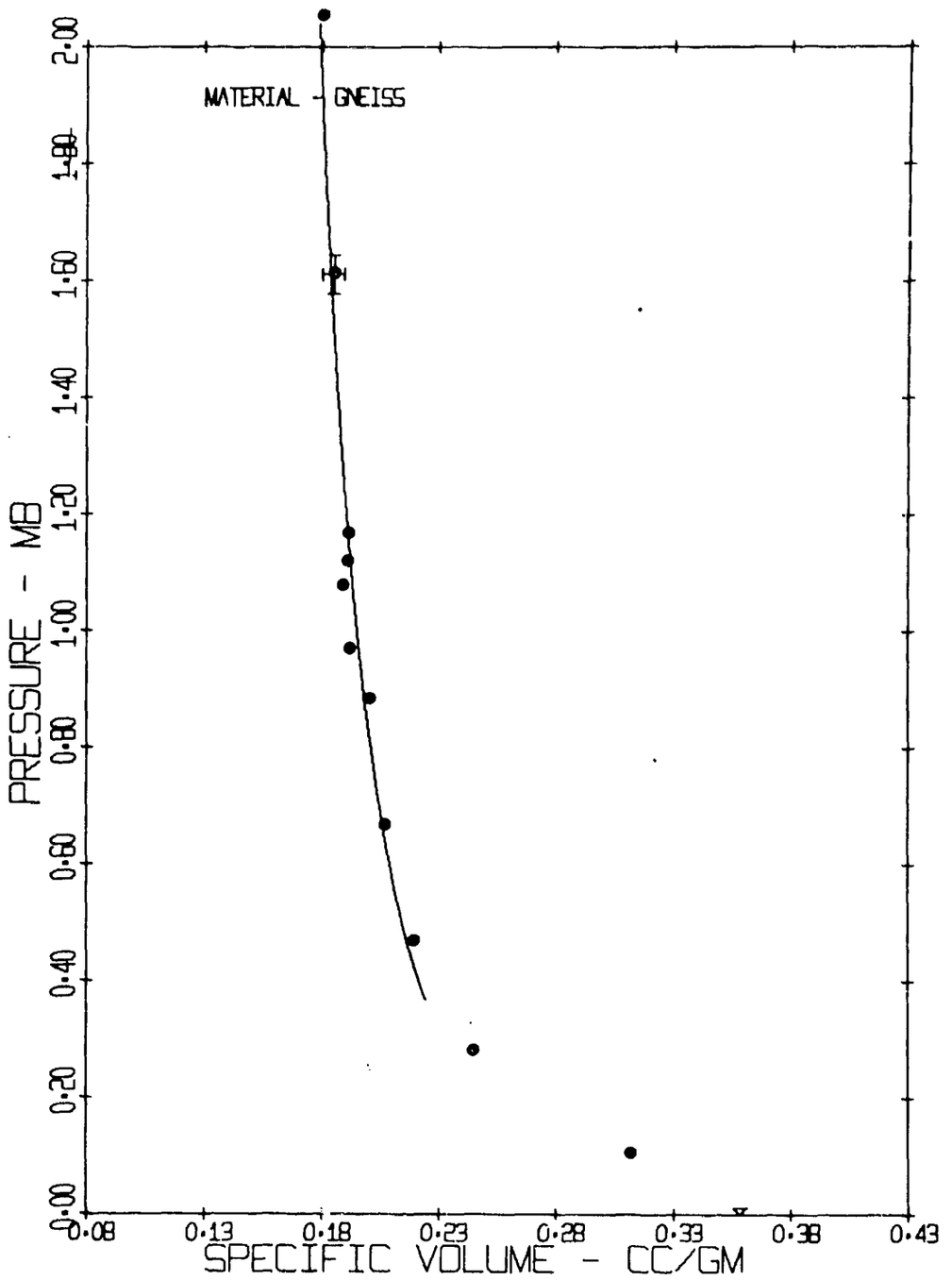

Figure 29 Pressure vs Specific Volume for Schistose Gneiss

Ferris Wheel Dolomite

The NTS Dolomite is characterized in Barnes.[9] A detailed chemical and mineralogical description is not available, but the rock probably consists of > 95% mineral dolomite, $CaMg(CO_3)_2$, based on an x-ray analysis of a megascopically similar sample of dolomite from the Banded Mountain area.* The density of the samples tested was 2.82 ± 0.01 gm/cm^3. The linear hugoniot fitted to the data in Table X is given by:

$$U_s = 5.196 + 1.191\ u_p \text{ km/sec}, \quad 2.6 < u_p < 5.4 \text{ km/sec}$$

$$S.E.(U_s) = 0.059 \text{ km/sec for 4 points.}$$

Figures 30 and 31 display the data in the U_s-u_p, and P-V planes. Also shown are four data points obtained by Lombard[12,21] for Area 12 dolomites of comparable initial density, i.e. $\rho_o \simeq 2.84$ and 2.815 gm/cm^3. The linear hugoniot reported for these points is given by:

$$U_s = 5.626 + 1.016\ u_p \text{ km/sec}$$

$$S.E.(U_s) = 0.048 \text{ km/sec for 5 points.}$$

A linear fit to the GM and Lombard data is given by:

$$U_s = 5.441 + 1.124\ u_p \text{ km/sec}, \quad 0.5 < u_p < 5.4 \text{ km/sec}$$

$$S.E.(U_s) = 0.098 \text{ km/sec for 9 points.}$$

* Private communications, H. Barnes, USGS, Denver, Colorado.

TABLE X

HUGONIOT DATA FOR NTS FERRIS WHEEL DOLOMITE

$\rho_o = 2.820 \pm 0.005$ gm/cm^3

$V_o = 0.3546 \pm 0.0006$ cm^3/gm

Shot	U_s Shock Velocity (km/sec)	u_p Particle Velocity (km/sec)	P Pressure (Mb)	V Volume (cm^3/gm)
C-1002	8.413(±0.027)	2.653(±0.002)	0.629(±0.003)	0.243
C-1004	9.600(±0.013)	3.731(±0.075)	1.010(±0.022)	0.217(±0.003)
C-1003	10.045(±0.007)	4.134(±0.083)	1.171(±0.024)	0.209(±0.003)
C-1005	11.581(±0.051)	5.312(±0.106)	1.735(±0.042)	0.192(±0.003)

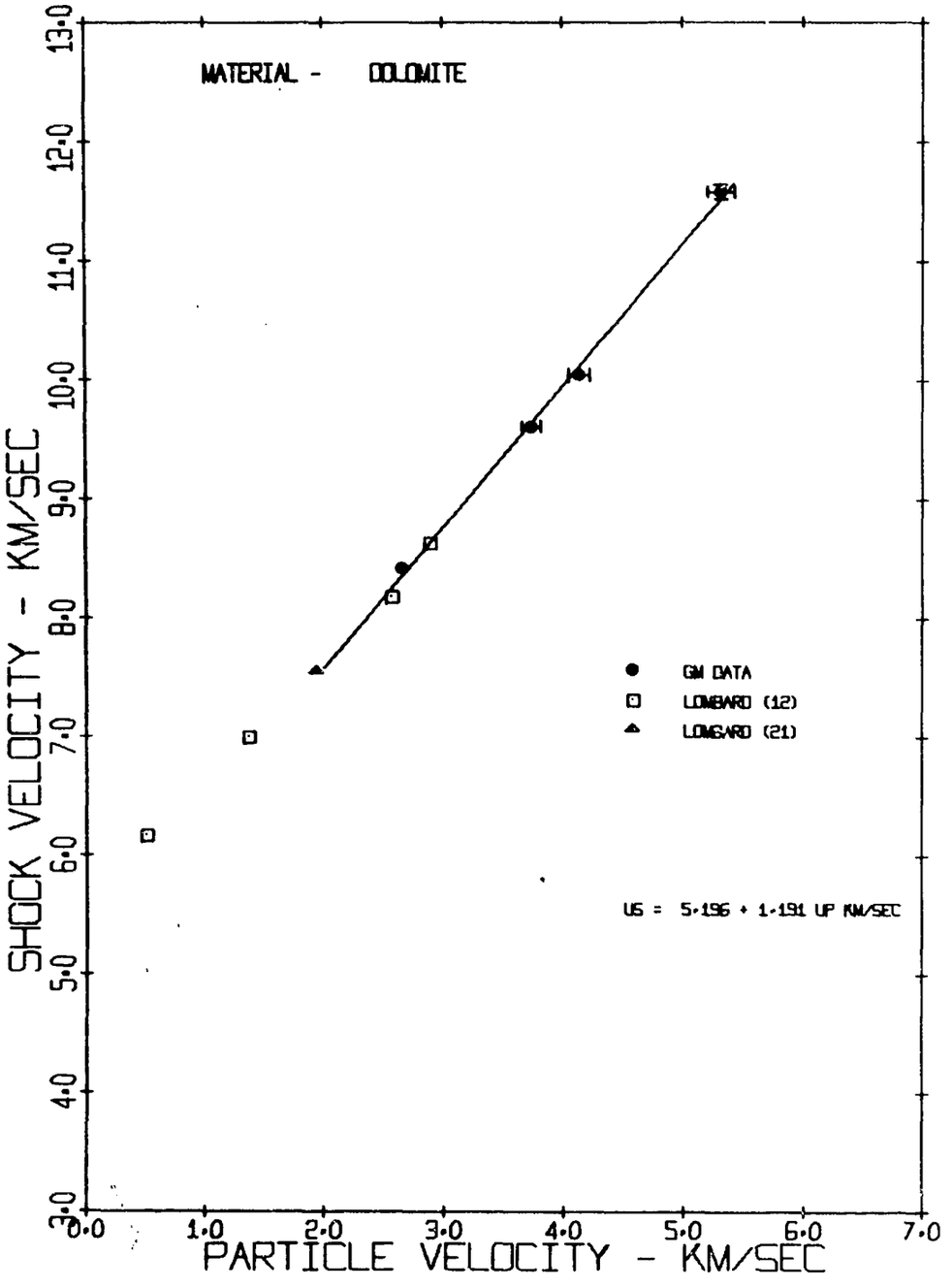

Figure 30 Shock Velocity vs Particle Velocity for Several NTS Area 12 Dolomites

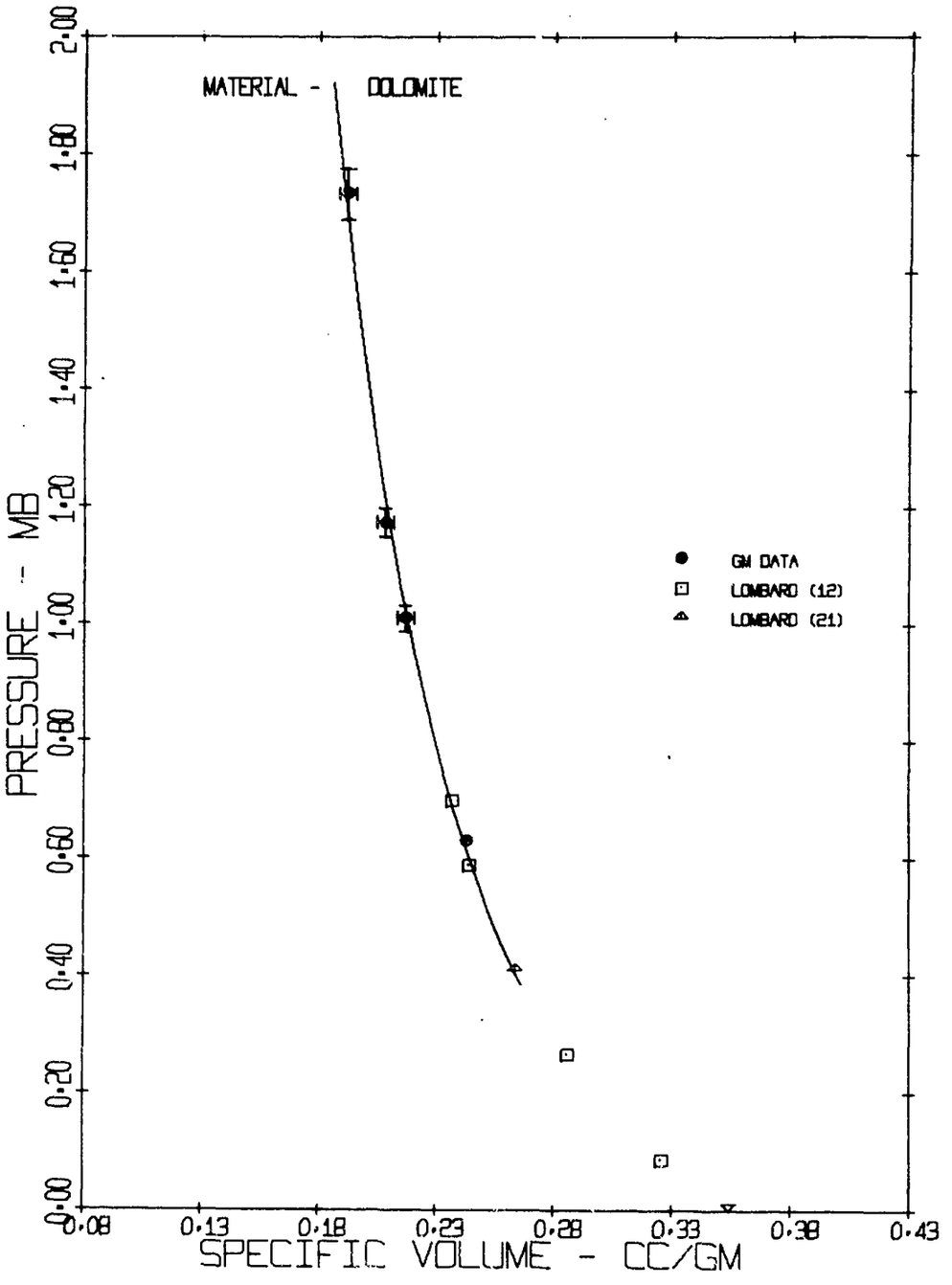

Figure 31 Pressure vs Specific Volume for Several NTS Area 12 Dolomites

Banded Mountain Limestone

A petrographic description of Banded Mountain limestone is included in Barnes.[9] The specimens are essentially pure calcite, 96 - 98% $CaCO_3$ (calculated) with initial densities of 2.702 ± 0.004 gm/cm^3. The linear least squares fit to the data listed in Table XI is given by:

$$U_s = 4.047 + 1.391\ u_p \text{ km/sec}, \quad 1.0 < u_p < 4.4 \text{ km/sec}$$

$$\text{S.E.}(U_s) = 0.085 \text{ km/sec for 6 points.}$$

Figures 32 and 33 display the present data in the U_s-u_p and P-V planes respectively. Included in Figure 32 are the data of Dremin[22] for a marble of initial density of 2.70 gm/cm^3 and the data of Bass[15] for a NTS limestone of density 2.66 gm/cm. The break in the data of Dremin indicate that a phase change occurs in the marble near 0.150 Mb; just below the lowest GM data point. The lowest point of Bass's NTS limestone hugoniot data falls below a linear extrapolation of the higher pressure data of GM and Dremin as well as his own. This point is probably in a low density phase regime similar to that reported by Dremin, and unobserved by the present work. Evidence presented here suggests that only the top four data of Bass's limestone hugoniot are in the high pressure phase regime and we have chosen to include them in a least squares analysis for comparison. The linear form of the least squares analysis of the combined data in the high pressure regime is given by:

$U_s = 4.080 + 1.386\ u_p$, $1.0 < u_p < 4.4$ km/sec

S.E.(U_s) = 0.075 km/sec for 10 points.

The combined analysis differs from the GM data by only 0.8% in intercept and 0.4% in slope.

TABLE XI

HUGONIOT DATA FOR NTS BANDED MOUNTAIN LIMESTONE

$\rho_o = 2.702 \pm 0.004$ gm/cm^3
$V_o = 0.3701 \pm 0.0006$ cm^3/gm

Shot	U_s Shock Velocity (km/sec)	u_p Particle Velocity (km/sec)	P Pressure (Mb)	V Volume (cm^3/gm)
C-1231	5.491*	1.029	0.153	0.301
C-1221	6.820(±0.013)	1.979	0.365	0.263
C-1250	8.519*	3.246	0.747	0.229
C-1222	9.436(±0.024)	3.918(±0.003)	0.999(±0.003)	0.216(±0.001)
C-1227	9.884*	4.264	1.138	0.211
C-1223	10.318(±0.036)	4.388(±0.088)	1.223(±0.029)	0.213(±0.003)

* Single Pin Value

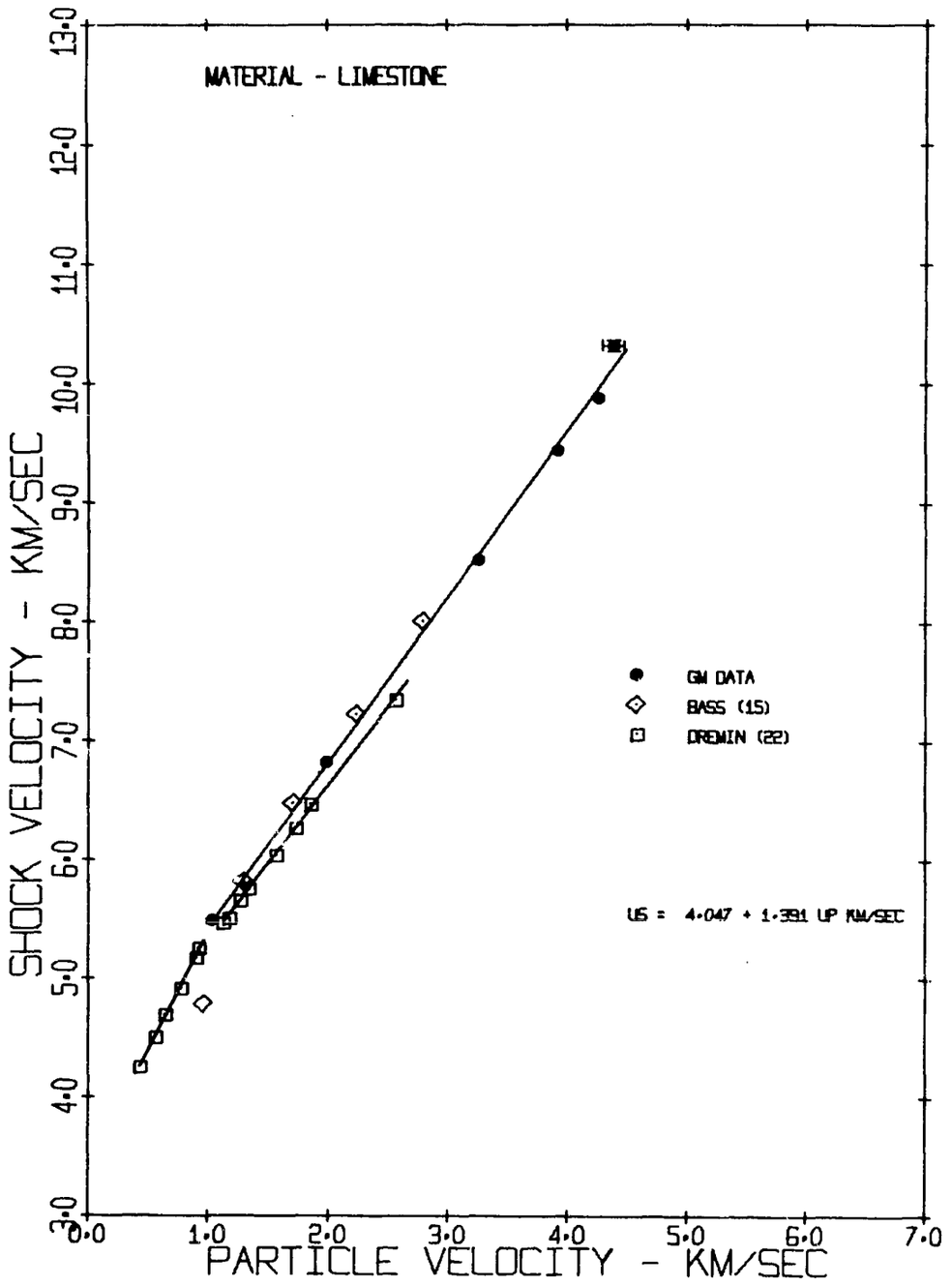

Figure 32 Shock Velocity vs Particle Velocity for Two NTS Limestones

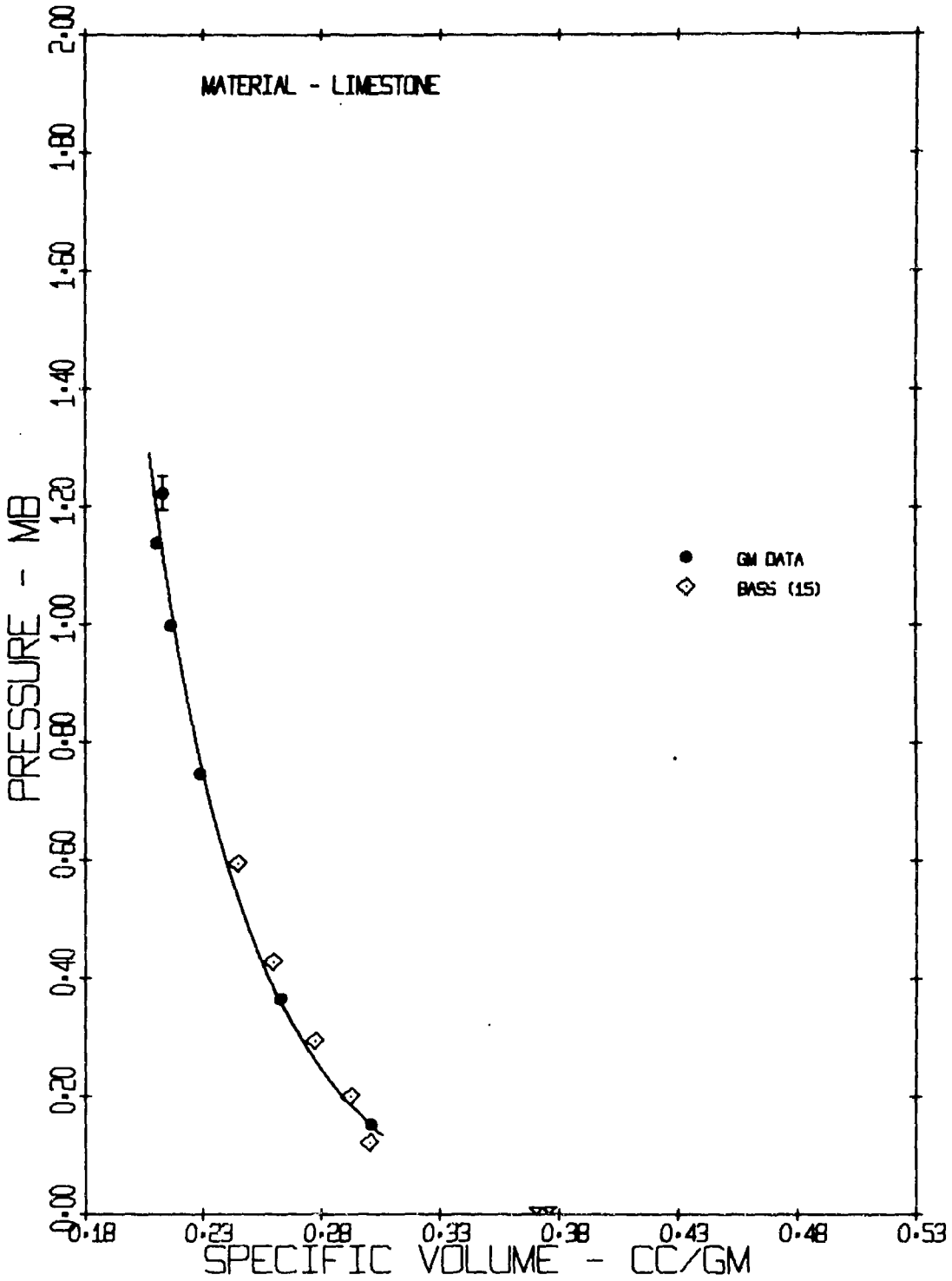

Figure 33 Pressure vs Specific Volume for Two NTS Limestones

Nevada Desert Alluvium

A chemical and physical description of the Nevada desert alluvium is given in Barnes.[9] The data are presented in Table XII and Figures 34 and 35. Probably due to the extreme fineness and homogeneity of the specimens, the recorded shock velocities show remarkably little internal scatter (less than 1% average). The compaction density averaged 1.54 ± 0.02 gm/cm^3 for these tests and corresponded to the low density material of Anderson[5] and McQueen[23] (ρ_o = 1.55 and 1.54 gm/cm^3 respectively).

The hugoniot data shown in Figure 34 does not appear amenable to description by a single simple equation. At least two line segments are necessary for a linear description. The high pressure region may be described by:

$$U_s = 0.363 + 1.533\ u_p \text{ km/sec},\quad 2.4 < u_p < 6.1 \text{ km/sec}$$

$$\text{S.E.}(U_s) = 0.132 \text{ km/sec for 7 points.}$$

The two lowest data are not considered adequate in themselves to define the lower hugoniot and no line or equation is given. In Figures 36 and 37 the data of McQueen and Anderson are compared and combined with the present results. Again the data suggest a two regime hugoniot structure. The high pressure regime hugoniot is given by:

$$U_s = 0.683 + 1.544\ u_p \text{ km/sec},\quad 2.3 < u_p < 6.1 \text{ km/sec}$$

$$\text{S.E.}(U_s) = 0.214 \text{ km/sec for 25 points.}$$

TABLE XII

HUGONIOT DATA FOR NTS NEVADA DESERT ALLUVIUM

$\rho_o = 1.54 \pm 0.02$ gm/cm^3

$V_o = 0.649 \pm 0.008$ cm^3/gm

Shot	U_s Shock Velocity (km/sec)	u_p Particle Velocity (km/sec)	P Pressure (Mb)	V Volume (cm^3/gm)
S-33	2.339(±0.003)	1.055	0.038	0.357
S-40	3.173(±0.019)	1.543	0.075(±0.001)	0.334(±0.002)
S-35	4.034(±0.057)	2.401(±0.004)	0.149(±0.003)	0.263(±0.005)
S-36	4.991 †	2.999	0.231	0.259
S-42	6.491(±0.036)	3.913(±0.003)	0.391(±0.003)	0.258(±0.002)
S-41	6.710(±0.022)	4.068(±0.002)	0.420(±0.002)	0.256(±0.001)
S-37	6.653(±0.005)	4.298	0.441	0.229
S-38	8.377(±0.024)	5.231(±0.003)	0.675(±0.002)	0.244(±0.001)
S-39	9.675(±0.024)	6.036(±0.002)	0.899(±0.003)	0.244(±0.001)

† Double Pin Value

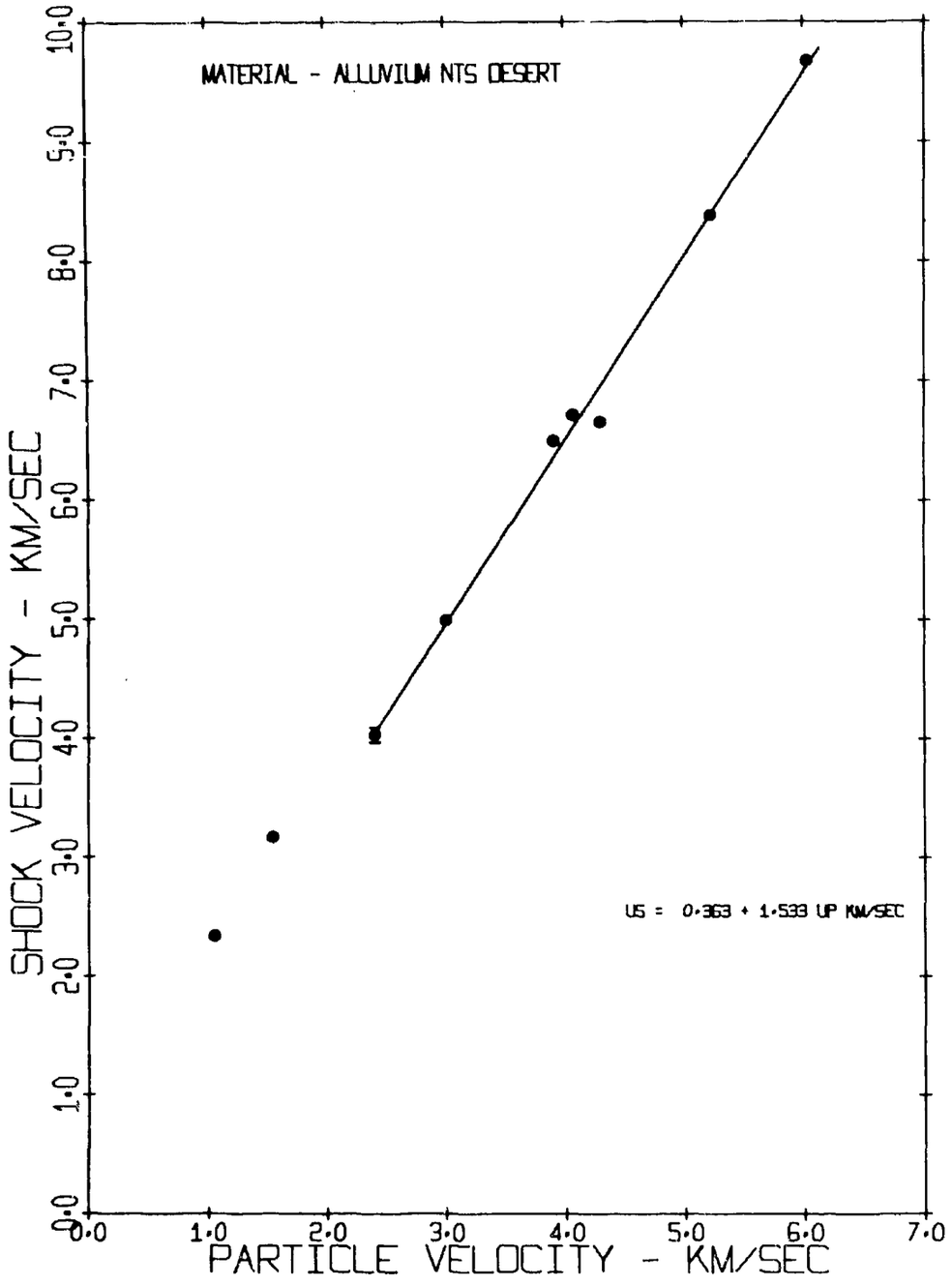

Figure 34 Shock Velocity vs Particle Velocity for NTS Desert Alluvium

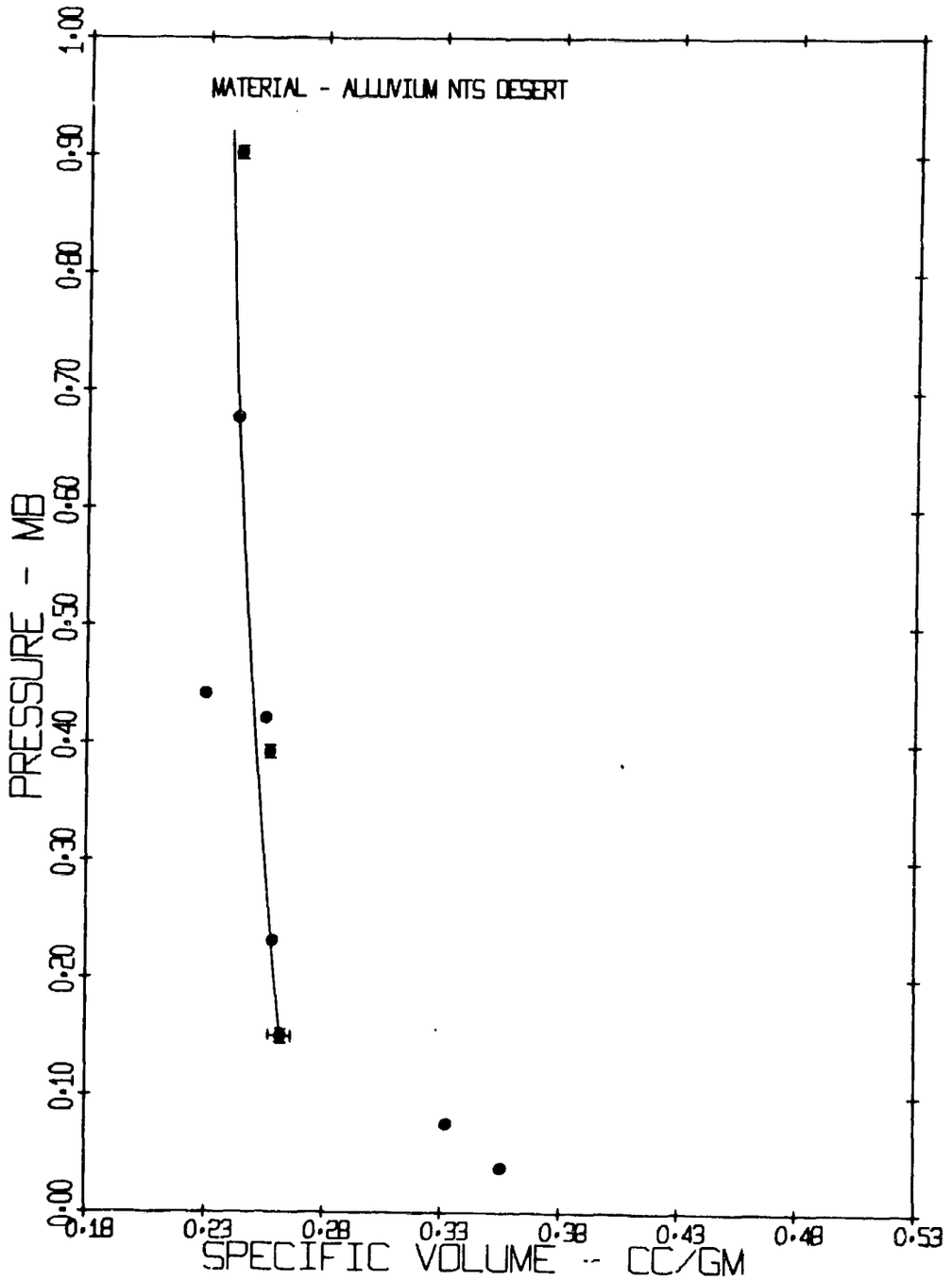

Figure 35 Pressure vs Specific Volume for NTS Desert Alluvium

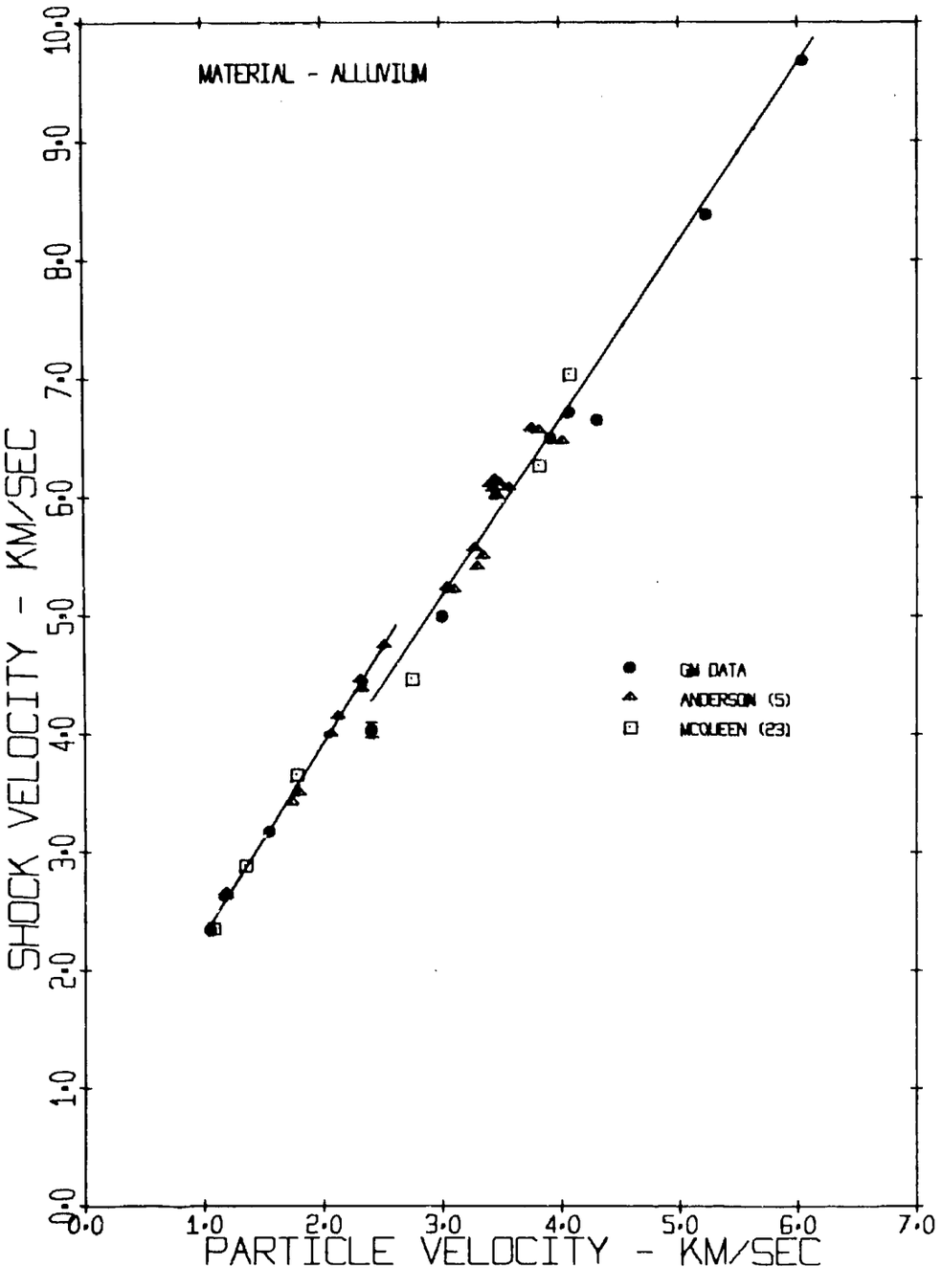

Figure 36 Shock Velocity us Particle Velocity for Several NTS Alluvia

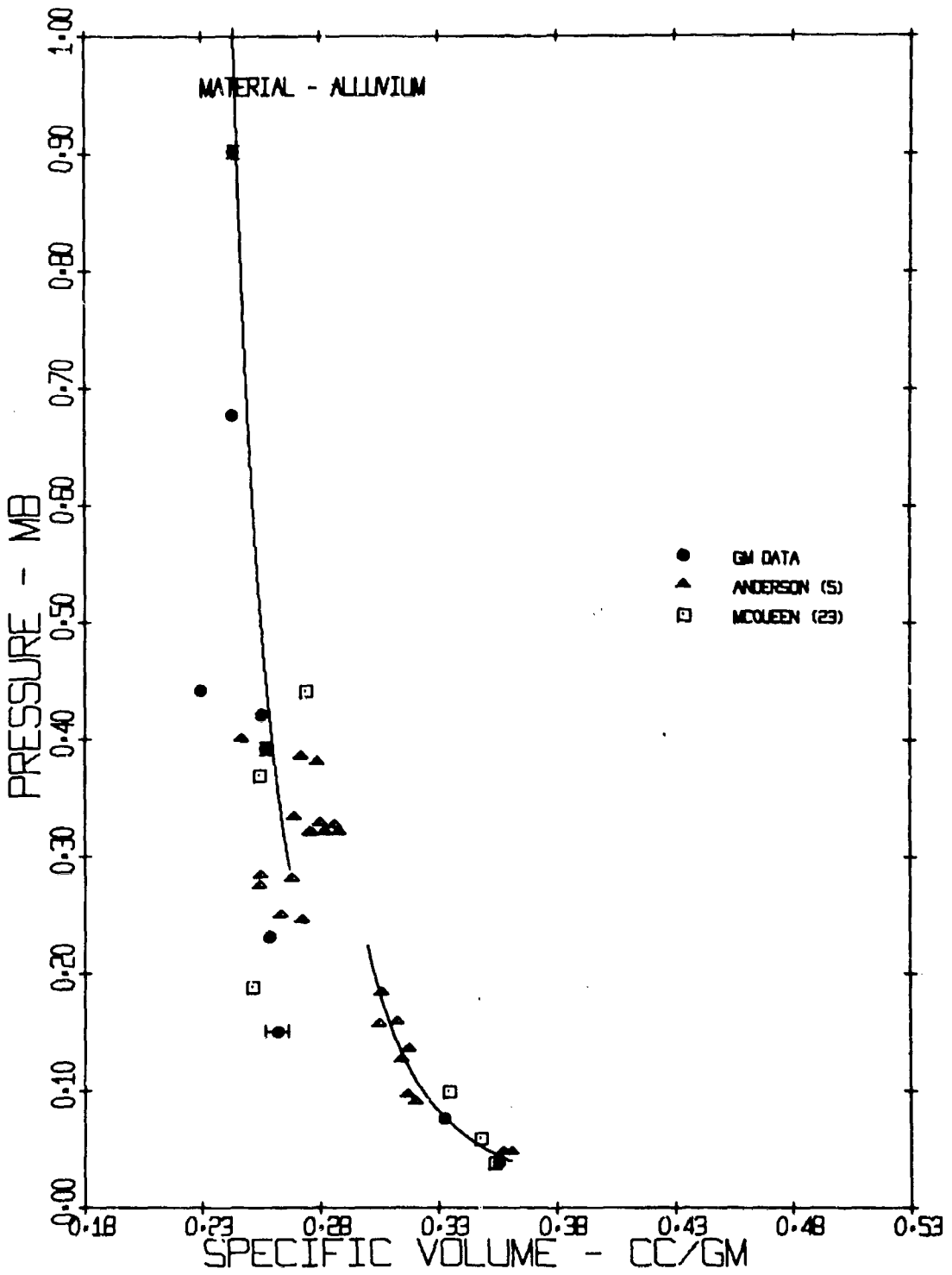

Figure 37 Pressure vs Specific Volume for Several NTS Alluvia

The lower regime may be described by:

$$U_s = 0.682 + 1.618\ u_p \text{ km/sec},\ 1.0 < u_p < 2.6 \text{ km/sec}$$

$$S.E.(U_s) = 0.055 \text{ km/sec for 14 points.}$$

The combined data for the upper regime compares with the GM data by raising the slope by $\sim$ 0.7% and the intercept by 0.3 km/sec, both small effects.

The combined data presents a complicated picture of the transition from the lower to the upper regime. Anderson's data suggests that the low regime extends to at least 0.190 Mb and yet a shot reported here implies the minimum of the upper regime is lower than 0.145 Mb. Whether or not it is possible to account for this discrepancy on the basis of specimen composition or experimental technique cannot be decided at present. The chemical compositions of ours and Anderson's samples are nearly identical, but the mineralogy of the two may vary somewhat more.

The constituent most likely undergoing the observed transition between 0.145 and 0.190 Mb is the quartz component which amounts to $\sim$ 53% in the initial state. The large volume scatter in the pressure range of 0.20 to 0.40 Mb makes an analysis of the trend of the hugoniot extremely difficult. With just the present data, the P-V hugoniot appears to be nearly vertical and at higher pressures may even show volume expansion due to shock heating.

It is likely that above 0.40 Mb the quartz component is completely converted to stishovite, but below 0.40 Mb, it is

difficult to determine whether or not the quartz component passes through a mixed phase regime. An additional complication is introduced by the ∿ 36% porosity of the initial sample.

SECTION IV

CONCLUSIONS

The experimental results of the determination of the hugoniot equations of state for several Nevada Test Site rocks are summarized in Table XIII. The present work has extended the ranges of hugoniot equation of state data for a granite, wet and dry volcanic tuff, dolomite, limestone and desert alluvium from the Nevada Test Site. A hugoniot was determined for a schistose gneiss and the hugoniots of Fansteel-77 and OFHC copper were confirmed. In addition, the range of hugoniot data for volcanic tuff impedance matching grouting material was extended. In general, the present results are in good agreement with data of other researchers. When possible a least squares fit has been included in the comparison data for each reference as well as in combination with the present results.

TABLE XIII HUGONIOT DATA SUMMARY

Material	Initial Density ρ_o (gm/cm^3)	C_o (km/sec)	S	Standard Error (km/sec)	Pressure Range (Mb)	Number of Points	References	Comments
IMPACTOR STANDARDS								
1. Fansteel-77	17.01	4.008	1.262	0.036	0.3->5.0	7	General Motors	All data with internal scatter <1%
2. OFHC Copper	8.93	3.960	1.464	0.018	1.0-4.5	12	General Motors	All data with internal scatter <2%
GEOLOGICAL MATERIALS								
1.(a) NTS Granodiorite	2.65	2.169	1.644	0.190	0.6-1.9	10	General Motors	High pressure regime
(b) Granite (Westerly, R.I.)	2.63	2.102	1.629	0.030	0.4-0.9	8	McQueen[10]	High pressure regime
(c) Granite (Area 15, NTS)	2.677*	2.594	1.476	.052	0.4-0.8	4	LRL Complier[11]	High pressure regime
(d) Combined Granite Data	2.648*	1.994	1.673	.149	0.4-1.9	22	Selected data of GM, (10) and (11)	High pressure regime, combined data

* Averaged values employed for the analysis.

TABLE XIII HUGONIOT DATA SUMMARY (Continued)

	Material	Initial Density ρ_o (gm/cm^3)	C_o (km/sec)	S	Standard Error (km/sec)	Pressure Range (Mb)	Number of Points	References	Comments
(e)	Granite (Westerly, R.I.)	2.63	4.926	0.371	0.030	0.14-0.31	11	McQueen[10]	Low pressure regime
(f)	Granite (Area 15, NTS)	2.677*	5.354	0.159	0.127	0.06-0.32	9	LRL Complier[11]	Low pressure regime
2. (a)	Rainier Mesa Tuff Dry	1.76	1.049	1.528	0.086	0.2-1.3	8	General Motors	High pressure regime
(b)	Tuff (NTS) Dry	1.61*	1.262	1.419	0.011	0.03-0.17	4	Anderson[14]	Low pressure regime
(c)	Tuff (NTS) Dry	1.67*	1.417	1.412	0.093	0.04-0.18	6	Lombard[12]	Low pressure regime
(d)	Tuff (NTS) Dry	1.61	1.395	1.406	0.092	0.05-0.19	17	Wiedermann[13]	Low pressure regime
(e)	Combined Tuff Data (Dry)	1.647*	1.371	1.431	0.116	0.03-0.19	32	Selected Data of (12), (13), (14) and (15)	Low pressure regime included by $1.32 < C_o < 1.47$ km/sec
3. (a)	Rainier Mesa Tuff Wet	1.97	1.755	1.575	0.089	0.39-1.33	6	General Motors	High pressure regime
(b)	Tuff (NTS) Wet	2.004*	2.000	1.464	0.148	0.36-0.46	20	Rosenberg[18]	High pressure regime
(c)	Combined Tuff Data (Wet)	1.99*	1.573	1.606	0.141	0.36-1.33	26	Selected data of GM and (18)	High pressure regime

* Averaged values employed for the analysis.

TABLE XIII HUGONIOT DATA SUMMARY (Continued)

Material	Initial Density ρ_o (gm/cm^3)	C_o (km/sec)	S	Standard Error (km/sec)	Pressure Range (Mb)	Number of Points	References	Comments
(d) Rainier Mesa Tuff Wet	1.97	2.874	1.141	0.162	0.08-0.19	5	General Motors	Low pressure regime
(e) Tuff (NTS) Wet	2.004*	3.089	0.993	0.088	0.14-0.26	15	Rosenberg[18]	Low pressure regime
(f) Tuff (NTS) Wet	1.81*	2.029	1.346	0.205	0.11-0.15	6	Wiedermann[19]	Low pressure regime
(g) Tuff (NTS) Wet	1.85*	2.910	0.965	0.133	0.09-0.22	9	Lombard[12]	Low pressure regime
(h) Combined Tuff Data (Wet)	1.942*	2.876	1.048	0.228	0.07-0.26	37	Selected data of GM, (12), (17), (18) and (19)	Low pressure regime included by 2.68 $<C_o<$ 2.98 km/sec
4.(a) Grout $V44_d$	1.45	2.998	1.275	0.103	0.11-1.15	7	General Motors	
(b) Grout $V44_d$	1.473*	2.68	1.53	0.057	0.07-0.17	3	Waterways Experimental Station	Impedence match for wet tuff
(c) Grout $V6_c$	2.686*	2.414	1.703	0.228	0.04-0.290	5	Waterways Experimental Station	Impedence match for granite
5. Schistose Gneiss	2.79	2.376	1.604	0.116	0.47-2.05	9	General Motors	High pressure regime
6.(a) Ferris Wheel Dolomite	2.82	5.196	1.191	0.059	0.63-1.74	4	General Motors	
(b) Dolomite (NTS-Area 12)	2.82*	5.626	1.016	0.048	0.08-0.70	5	Lombard[12],[21]	
(c) Combined Dolomite Data	2.815*	5.441	1.124	0.098	0.08-1.74	7	Selected data from GM, (12) and (21)	

* Averaged values employed for the analysis.

TABLE XIII HUGONIOT DATA SUMMARY (Continued)

	Material	Initial Density ρ_o (gm/cm^3)	C_o (km/sec)	S	Standard Error (km/sec)	Pressure Range (Mb)	Number of Points	References	Comments
7. (a)	Banded Mountain Limestone	2.702	4.047	1.391	0.085	0.15-1.22	6	General Motors	High pressure regime
(b)	Limestone (NTS)	2.66	3.977	1.452	0.026	0.20-0.60	4	Bass[15]	High pressure regime
(c)	Combined Limestone Data	2.69*	4.080	1.386	0.075	0.15-1.22	10	Selected data from GM and [15]	High pressure regime
8. (a)	Nevada Desert Alluvium	1.54	0.363	1.533	0.132	0.15-0.90	7	General Motors	High pressure regime
(b)	Alluvium	1.54	-0.640	1.855	0.124	0.18-0.045	3	McQueen[23]	High pressure regime
(c)	Alluvium	1.556*	0.397	1.604	0.184	0.24-0.41	15	Anderson[5]	High pressure regime
(d)	Combined Alluvium Data	1.544*	0.683	1.496	0.214	0.15-0.90	25	Selected data from GM, [5] and [23]	High pressure regime
(e)	Alluvium	1.54	0.390	1.850	0.016	0.043-0.10	3	McQueen[23]	Low pressure regime
(f)	Alluvium	1.556*	0.736	1.588	0.048	0.04-0.19	9	Anderson[5]	Low pressure regime
(g)	Combined Alluvium Data	1.544*	0.682	1.618	0.055	0.03-0.19	14	Selected data from GM, [5] and [23]	Low pressure regime

* Averaged values employed for the analysis.

ACKNOWLEDGEMENTS

The authors wish to express their appreciation for the assistance given them during the course of this program to B. Barrett and his gun crew at GM DRL in Santa Barbara, California. For the work performed at GM Manufacturing Development, Warren, Michigan, our thanks go to A. R. McMillan, D. S. Chapin, J. W. Thomlinson, J. M. Paavola, J. M. Hessell, H. Reynolds, C. W. Woodcock, and R. Lingle. We also acknowledge our gratitude to Dr. C. J. Maiden, Assistant Manager, Process Engineering for his encouragement during the course of the program.

REFERENCES

1. Jones, A. H., et. al., "Measurement of Very-High-Pressure Properties of Materials Using a Light-Gas Gun", International Conference on High-Pressure Research, LeCreusot, Saone et Loire, France, August 1965.

2. Walsh, J. M., et. al., Phys. Rev., 108, 196 (1957).

3. Curtis, J. S., An Accelerated Reservoir Light-Gas Gun, NASA TND-1144, 1962.

4. Lingle, R. and A. H. Jones, Triggering System at the Muzzle of an Accelerating-Reservoir Light-Gas Gun, TR65-65, GM Defense Research Laboratories, Santa Barbara, Calif., September 1965.

5. Anderson, G. D. and A. L. Fahrenbruch, Part 3, Investigation of Equation of State of Porous Material, WL-TRD-64-59, Contract AF-29(601)-6024, August 1964.

6. McQueen, R. G., et. al., "The Determination of New Standards for Shock Wave Equation-of-State Work", High Dynamic Pressure, September 1957, Paris.

7. Al'tshuler, L. V., et. al., Soviet Physics JETP, 34, 614 (1958).

8. Al'tshuler, L. V., et. al., Soviet Physics JETP, 11, 573 (1960).

9. Barnes, H., Geologic Description of Selected Rock Samples from the Nevada Test Site, Technical Letter: NTS-185, June 21, 1967.

10. McQueen, R. G., et. al., Jr. Geophys. Res., 72, 4999 (1967).

11. LRL Compiler - Compedium of shock Wave Data, ed. M. Van Thiel, UCRL-50108 (2 Vols.), Lawrence Radiation Laboratory, University of California, Livermore, California (1966).

12. Lombard, D. B., The Hugoniot Equation of State of Rocks, UCRL-6311, February 1961.

13. Wiedermann, A. H. and O. E. Curth, Shock Unloading Characteristics of Crushable Rocks, WL-TDR-64-52, Contract AF29(601)-6007, June 1964.

14. Anderson, D. C., and F. B. Porzel, Close-In Time-of-Arrive Measurements for Yield of Underground Rainier Shot, WT-1495, December, 1959.

15. Bass, R. C., Additional Hugoniot Data for Geologic Materials, SC-RR-66-548, Sandia Corporation, October 1966.

16. Ahrens, T. J. and V. G. Gregson, Jr., Jr. Geophys Res., 69, 22, 4839 (1964).

17. Bass, R. C. et. al., Hugoniot Data for Some Geologic Materials, SC-4903 (RR), Sandia Corporation, June 1963.

18. Rosenberg, J. T., et. al., Dynamic Properties of Rocks, DASA 2112, Contract DASA-01-67-C-0017, July 1968.

19. Wiedermann, A. H. and O. E. Curth, Shock Unloading Characteristics of Porous Geological Materials, AFWL-TR-66-118, Contract AF 29(601)-6699, January 1967.

20. Jones, A. H., et. al., Material Properties Measurements for Selected Materials, Contract NASZ-3427, National Aeronautics and Space Administration Ames Research Center, Moffett Field, California, April 1968.

21. Lombard, D. B., Rock Equations of State, University of California, Lawrence Radiation Laboratory Memorandum UOPK 63-2, January 1963.

22. Dremin, A. N. and G. A. Adadurov, Proc. (Dokl.) Acad. Sci., USSR, 128, 261-269 (1959).

23. McQueen, R. G. and B. P. Marsh, Equation of State of Nevada Alluvium, GMX-6-491, Los Alamos Scientific Laboratory, 1962.

BLANK PAGE

APPENDIX

DATA ANALYSIS PROCEDURES FOR THE DETERMINATION OF HUGONIOT STATES FROM SHOCK WAVE DATA

INTRODUCTION

The following is a detailed description of the data analysis method employed for the determination of hugoniot state data derived from the experimental system described in the main body of this report. The first part of this appendix presents the equations and assumptions employed in the analysis and the second part describes a computer routine written to perform the calculations.

Experiment Analysis

Figure A-1 illustrates the system schematically with the following nomenclature:

v = impact velocity	cm/μsec
b = pin cap thickness	cm
g = pin gap	cm
h = target thickness	cm
x = pin position on line 1-A	cm
θ = impactor tilt	radians
D = shock velocity in target	cm/μsec

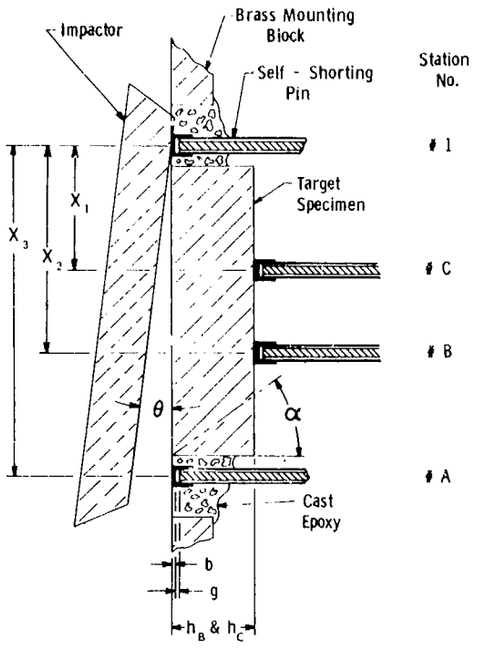

Figure A-1 Schematic of Equation of State Studies Target

Two cases of pin correction are necessary; the first involves the "start" pins 1 and A which are struck by the impactor directly. The second case involves the rear surface pins B and C, which receive the shock transmitted by the target material; and thus have closing velocities different from pins 1 and A.

The times to pin closure are given by:

$$t_1 = \frac{b_1}{U_{spin}} + \frac{g_1}{2\,u_{pin}} \qquad \text{(A-1)}$$

$$t_A = \frac{X_3 \tan\theta}{v} + \frac{b_A}{U_{spin}} + \frac{g_A}{2\,u_{pin}} \qquad \text{(A-2)}$$

$$t_B = \frac{(X_2 - h_B \tan\frac{D}{V}\theta)\ \tan\theta}{v} + \frac{h_B}{D}\sec(\frac{D}{V}\theta) + \frac{b_B}{U_{spt}} + \frac{g_B}{2\,u_{pt}} \qquad \text{(A-3)}$$

$$t_C = \frac{(X_3 - h_C \tan\frac{D}{V}\theta)\ \tan\theta}{v} + \frac{h_C}{D}\sec(\frac{D}{V}\theta) + \frac{b_C}{U_{spt}} + \frac{g_C}{2\,u_{pt}} \qquad \text{(A-4)}$$

where subscripts 1, A, B, C refer to pin locations, and

U_{spin} = pin cap shock velocity induced by impactor

u_{pin} = pin cap partical velocity induced by impactor

u_{spt} = pin cap shock velocity induced by target

u_{pt} = pin cap particle velocity induced by target

U_{spin} and u_{pin} are evaluated by the impedance match solution for the direct impact of the projectile material into the pin material. The particle velocity derived from this analysis is:

$$\frac{B - \sqrt{B^2 - 4AC}}{2A} \qquad \text{(A-5)}$$

where $A = \rho_{op}S_p - \rho_{opin}S_{pin}$ (A-6)

$$B = \rho_{op}C_{op} + \rho_{opin}C_{pin} + 2\rho_{op}C_{op}v$$

$$C = \rho_{op}v(C_{op} + S_p v)$$

and $U_{spin} = C_{pin} + S_{pin}u_{pin}$ (A-7)

the impactor hugoniot being given by:

$$U_{sp} = C_{op} + S_p u_p \qquad \text{(A-8)}$$

For the pin gap velocity correction of the wave interaction between the specimen and the rear surface pins on the impedance match solution is employed again. Although the equations are similar to those already derived, the hugoniot state of the specimen must first be estimated and then determined by iteration.

The first approximation of the shock velocity is found by the following procedure: Subtracting Equation (A-6) from Equation (A-7) we obtain

$$\tan \Theta = \frac{v}{X_3} \left[(t_A - t_1) - \frac{b_A - b_1}{U_{spin}} - \frac{g_A - g_1}{2\, u_{pin}} \right] \qquad \text{A-9}$$

Neglecting several small corrections, the approximate shock velocity in the target at Station B is given by

$$D'_B = h_B \Big/ \left[(t_B - t_1) - \frac{X_2}{v} \tan \Theta + \frac{b_1}{U_{spin}} + \frac{g_1}{2\, u_{pin}} \right] \qquad \text{(A-10)}$$

The particle velocity, u', at this shock velocity is given by Equation (A-5), where:

$$A = \rho_{op} S_p$$

$$B = \rho_{op} C_{op} + \rho_{ot} D' + 2\rho_{op} S_p v \qquad \text{(A-11)}$$

$$C = \rho_{op} v (C_{op} + S_p v)$$

The first approximation of the shock pressure is given by:

$$P' = \rho_{ot} D' u' \qquad \text{(A-12)}$$

The approximate shock and particle velocities thus obtained are used in the more exact solution for shock velocity given by Equation (A-13). The results may be iterated several times until the desired convergence is reached. With the convergence test set at 0.01% only two iterations are required.

$$U_{s_B} = h_B \sec \frac{D}{v}\theta \Bigg/ \left[(t_B - t_1) - \frac{\tan\theta \left[X_2 - h_B \tan\left(\frac{D}{v}\theta\right)\right]}{v} + \frac{b_1}{U_{spin}} + \frac{g_B}{2\,u_{pin}} - \frac{b_B}{U_{spt}} - \frac{g_B}{2\,u_{pt}} \right] \qquad \text{(A-13)}$$

The particle velocity, u_p is calculated by Equation (A-5) with:

$$A = \rho_{op} S_p$$

$$B = \rho_{op} C_{op} + \rho_{ot} U_s + 2\rho_{op} S_p v \qquad \text{(A-14)}$$

$$C = \rho_{op} v (C_{op} + S_p v)$$

Pressure is calculated from

$$P = \rho_{ot} U_s u_p \qquad \text{(A-15)}$$

where it is assumed that $P_o = 0$

The procedure is then applied to analyze the data from pins 1, A and C, A, 1, and B, and A, 1 and C using the appropriate values of g, h, b, and X.

Shim transit time corrections were made by adjusting the value of b, the pin cap thickness, to include the thickness of the shim. Since both shim and pin cap were brass, no significant difference in shock impedance exists across the shim-cap interface.

The procedure described above is a refinement upon the simplest form of average velocity determination (i.e. distance/time) where the time term is corrected for impactor tilt. The above refinement results in an average effect on U_s of $\sim$ 0.2% compared with the simplest form. The overall effect on a shot basis has been found for metals such as copper and Fansteel-77 to reduce data scatter about a linear form of the hugoniot in U_s-u_p.

Data Analysis Program - SHOVEL

The computer program described below is written in Mark I Fortran for use on the General Electric Timesharing Computer Service. This Fortran is very similar to Fortran IV used on most computers and provides some convenience for adapting to teletype I/O.

The program has two sections and one subroutine. The first portion of the program is merely an operator convenience to convert all input data into the required units and formats. The latter portion calculates the shock velocity at each station. The subroutine COMPUT is in the form of the quadratic solution that results in a meaningful value of u_p.

Definition of Terms

The terms presented below are in the following order:

1. Values required as input
2. Intermediate terms
3. Output values

1. INPUT TERMS

TERM	NAME	UNITS
Shot No.	SHOT	I
D	RUN	
Impactor Material	MATLP(2)	H
Target Material	MATLT(2)	H
Impactor C_o	CZERO	km/sec
Impactor S_p	SP	
Impactor ρ_o	RP	gm/cm^3
Target ρ_o	RT	gm/cm^3
Pin 1-B time	DTB	μsec
Pin 1-C	DTC	μsec
Pin 1 height	H1	in.
Pin A height	HA	in.
Pin B height	HB	in.
Pin C height	HC	in.
Pin 1 gap	G1	in.
Pin A gap	GA	in.
Pin B gap	GB	in.
Pin C gap	GC	in.
Pin 1-C Spacing	X1	in.
Pin 1-B Spacing	X2	in.
Pin 1-A Spacing	X3	in.
D	H2	
D	H3	
Polaroid target fiducial spacing	M2	cts.
Impactor to Window #1 Ref. Spacing	L1	cts.
Impactor to Window #2 Ref. Spacing	L2	cts.
X-ray Flash Time Interval	TSI1	μsec.
X-ray #1 to Pin C Time Interval	TSI2	μsec.
Front Surface Shim Thickness (If Used)	SHIM	in.
Tilt Time Interval	TILT	μsec.
Approximate Slope of Target Hugoniot (S=1.5 if zero)	S	
Pin Combination	COMBO	H
Computer Run No.	RUNS	I

I - Integer, D - Dummy, H - Holorith Field

2. COMPUTED TERMS

TERM	NAME	UNITS
X-ray 1 Scale Factor	F1	in/ct
X-ray 2 Scale Factor	F2	in/ct
Window Fiducial Spacing	D	in
Impact Velocity	W	ft/sec
Impact Velocity	W1	ft/sec
Impact Velocity	V	cm/μsec
D	USTAR	
Pin and ρ_o	RPIN	gm/cm^3
Pin Material Hugoniot Slope	SPIN	
Pin Material C_o	CØPIN	km/sec
Pin Cap Thickness	B1	in
Specific Volume (initial)	SVOLØ	cm^3/gm
Quadratic Solution Term	A	
Quadratic Solution Term	B	
Quadratic Solution Term	C	
Particle Velocity of Pin Cap	UPIN	cm/μsec
Shock Velocity of Pin Cap	USPIN	cm/μsec
Impactor Tilt	THETA	radians
First Approximation U_s (B Station)	USB1	cm/μsec
First Approximation u_p	UB1	cm/μsec
First Approximation P	PB1	Mb
First Approximation ρ_1	RT1	gm/cm^3
First Approximation Sound Velocity	C2	cm/μsec
Particle Velocity Induced by Target	UPT	cm/μsec
Shock Velocity Induced by Target	USPT	cm/μsec
Shock Wave Tilt in Target	THET1	radians

3. OUTPUT TERMS

B Shock Velocity	USB	km/sec
B Particle Velocity	UB	km/sec
B Pressure	PB	Mb
B Relative Volume	VOL	
Specific Volume	SVOL	cm^3/gm

The term labeling is essentially identical for the "C" station calculations with the output being:

C Shock Velocity	USC	km/sec
C Particle Velocity	UC	km/sec
C Pressure	PC	Mb
C Relative Volume	VOL1	
C Specific Volume	SVOL1	cm^3/gm

The "D" station calculation employs the C station approximate velocity and corrects for the time interval difference between B and C. The output terms are:

Shock Velocity	US	km/sec
Particle Velocity	U	km/sec
Pressure	P	Mb
Relative Volume	VOL2	
Specific Volume	SVOL2	cm^3/gm

Additional output terms:

D Station Calculation of Shock Tilt	THET3	Radians
Calculated Impactor Tilt Time Interval	TILT1	μsec
% Difference of (B-C)/C Shock Velocities	DIFF	%

The Mark II Time Sharing System allows chaining of programs and SHOVEL is continued as SHOVEN and an external file INFORM is used as the data source. Up to seven files may be linked and called in process.

MSL-68-15

SHOVEL

```
100  COMMON U,A,B,C
110 REAL DIMENSION MATLP(2), MATLT(2)
120 INTEGER SHOT,RUN,COMBO,RUNS
130C
140 200 READ(1,40)SHOT,RUN,MATLP(1),MATLP(2),MATLT(1),MATLT(2)
150 READ(1)CZERO,SP,RP,RT,DTB,DTC,H1,HA,HB,HC,G1,GA,GB,GC,X1,X2,X3,
160 +H2,H3,M2,L1,L2,TSI1,TSI2,SHIM,TILT,S
170C
180 40 FORMAT(5X,I5,I2,4A
190C
200 PRINT,"ENTER PIN COMBINATION (1 START = 1, A START = A) AND RUN NO."
210 INPUT 30, COMBO,RUNS
220C
230 30 FORMAT(2A1)
240C
250CMPTV COMPUTE TILT AND VELOCITY
252 PRINT 61,CZERO,SP,RT,RP,DTB,DTC,HB,HC,G1,GA,GB,GC,X1,X2,X3,
254 +TILT,S
256 61 FORMAT(////6F5.3,2F7.5,4F6.4//5F6.4///)
260C
270 IF(L1)46,48,46
280 46 F1=.4756E-03;F2=.4771E-03;D=11.9951
290 IF(L2)41,42,41
300 41 D1=(L1*F1+L2*F2+D)/12.0
310 VEL1=(D1/TSI1)*1.0E+06
320  42 D2=(L1*F1+D+M2*F2+.9537+SHIM)/12.0
330 VEL2=(D2/(TSI2-DTC))*1.0E+06
340 IF(L2)43,44,43
350 44 GO TO 45
360 43 W=VEL1;W1=VEL2
370 GO TO 49
380 45 W=VEL2;W1=0.0
390 GO TO 49
400  48 READ(1)W
410 W1=0.0
420C
430CTC CONVERT INPUT TO CGS
440C
450 49 V=(W/3.281)*1.0E+02
460 CZERO=CZERO*1.0E+05;USTAR=USTAR*1.0E+05
470 DTB=DTB*1.0E-06;DTC=DTC*1.0E-06;TILT=TILT*1.0E-06
480 H1=H1*2.54;HA=HA*2.54;HB=HB*2.54;;HC=HC*2.54
490 RPIN =8.41;SPIN=1.42;C0PIN=3.8E+05;B1=5.08E-03
500 G1=G1*2.54;GA=GA*2.54;GB=GB*2.54;GC=GC*2.54
510 X1=X1*2.54;X2=X2*2.54;X3=X3*2.54
520 THET3=0.0;SVOL0=1.0/RT;SVOL=0.0;SVOL1=0.0
530C
540CSV COMPUTE SHOCK VELOCITY
550C
560 IF (DTB)1,,11,1000
```

SHOVEL CONTINUED

```
570 11 UB=0.0;PB=0.0;USB=0.0;VOL=0.0
580 GO TO 5
590C
600 1000 B=RP*CZERO+RPIN*C0PIN+2*RP*SP*V
610 A=RP*SP-RPIN*SPIN;C=RP*V*(CZERO+SP*V)
620 CALL COMPUT
630  UPIN=U;USPIN=C0PIN+SPIN*UPIN
640 THETA=(V/X3)*(TILT-(GA-G1)/(2*UPIN))
650 USB1=(HB-H1)/(DTB-X2*THETA/V)
660 1001 B=RP*CZERO+RT*USB1+2*RP*SP*V;A=RP*SP
670 C=RP*V*(CZERO+SP*V)
680 CALL COMPUT
690 UB1=U;PB1=RT*USB1*UB1
700 RT1=(RT*USB1)/(USB1-UB1)
710 C2=USB1*SQRT(.49+((USB1-UB1)/USB1)**2)
720 IF(S)50,50,51
730 50 S=1.5
740 51 B=RPIN*C0PIN+RT1*C2+2*RT1*S*UB1;A=S*RT1-SPIN*RPIN
750 C=S*RT1*UB1**2+RT1*C2*UB1+PB1
760 CALL COMPUT
770 UPT=U; USPT=C0PIN +SPIN*UPT
780 THET1=(USB1/V)*THETA
790 DELT1=DTB-THETA*(X2-(HB-H1)*THET1)/V
800 DELT1=DELT1+B1/USPIN+G1/(2*UPIN)-B1/USPT-GB/(2*UPT)
810 USB=(HB-H1)*SQRT(THET1**2+1)/DELT1
820 3 IF(.0001-(ABS((USB-USB1)/USB)))1002,1003,1003
830 1002 USB1=USB
840 GO TO 1001
850 1003 B=RP*CZERO+RT*USB+2*RP*SP*V;A=RP*SP;C=RP*V*(CZERO+SP*V)
860 CALL COMPUT
870 UB=U;PB=RT*USB*UB;VOL=1-UB/USB
880 SVOL0=1.0/RT;SVOL=VOL/RT
890C
900 5 IF(DTC)6,6,7
910 6 USC=0.0;UC=0.0;PC=0.0;VOL1=0.0;TILT=TILT*1.0E+06;US=0.0;U=0.0
920 TILT1=0.0;USB=USB*1.0E-05;UB=UB*1.0E-05;PB=PB*1.0E-12
930 P=0.0;VOL2=0.0
940 SVOL1=0.0;SVOL2=0.0;DIFF=0.0
950 GO TO 2
960C
970 7 B=RP*CZERO+RPIN*C0PIN+2*RP*SP*V
980 A=RP*SP-RPIN*SPIN;C=RP*V*(CZERO+SP*V)
990 CALL COMPUT
1000 UPIN=U;USPIN=C0PIN+SPIN*UPIN
1010 THETA=(V/X3)*(TILT-(GA-G1)/(2*UPIN))
1020 USC1=(HC-H1)/(DTC-X1*THETA/V)
1030 1004 B=RP*CZERO+RT*USC1+2*RP*SP*V;A=RP*SP
1040 C=RP*V*(CZERO+SP*V)
1050 CALL COMPUT
1060 UC1=U;PC1=RT*USC1*UC1
```

SHOVEL CONTINUED

```
1070 RT2=(RT*USC1)/(USC1-UC1)
1080 C3=USC1*SQRT(.49+((USC1-UC1)/USC1)**2)
1090 B=RPIN*C0PIN+RT2*C3+2*RT2*S*UC1;A=S*RT2-SPIN*RPIN
1100 C=S*RT2*UC1**2+RT2*C3*UC1+PC1
1110 CALL COMPUT
1120 UPT1=U; USPT1=C0PIN+SPIN*UPT1
1130 THET2=(USC1/V)*THETA
1140 DELT2=DTC-THETA*(X1-(HC-H1)*THET2)/V
1150 DELT2=DELT2+B1/USPIN+G1/(2*UPIN)-B1/USPT1-GC/(2*UPT1)
1160 USC=(HC-H1)*SQRT(THET2**2+1)/DELT2
1170 4 IF(.0001-(ABS((USC-USC1)/USC)))1005,1006,1006
1180 1005 USC1=USC
1190 GO TO 1004
1200 1006 B=RP*CZERO+RT*USC+2*RP*SP*V;A=RP*SP;C=RP*V*(CZERO+SP*V)
1210 CALL COMPUT
1220 UC=U;PC=RT*USC*UC; VOL1=1-UC/USC
1230 UB=UB*1.0E-5;USB=USB*1.0E-05;PB=PB*1.0E-12
1240 UC=UC*1.0E-05;USC=USC*1.0E-05;PC=PC*1.0E-12
1250 DELT=(DELT1-DELT2)*1.0E+06
1260 TILT=TILT*1.0E+06
1270 TILT1=(DTB-DTC)*X3/(X2-X1)*1.0E+06
1280 DIFF=0.0;SVOL1=VOL1/RT
1290C
1300C
1310 IF(DTB)70,70,21
1320 70 TILT1=0.0;U=0.0;US=0.0;P=0.0;VOL2=0.0
1330 GO TO 2
1340 21 US1=(HC-H1)/DTC
1350 B=RP*CZERO+RT*US1+2*RP*SP*V;A=RP*SP
1360 C=RP*V*(CZERO+SP*V)
1370 CALL COMPUT
1380 U1=U;P1=RT*US1*U1
1390 1007 RT3=(RT*US1)/(US1-U1)
1400 C4=US1*SQRT(.49+((US1-U1)/US1)**2)
1410 IF(S)22,22,23
1420 22 S=1.5
1430 23 B=RPIN*C0PIN+RT3*C4+2*RT3*S*U1;A=S*RT3-SPIN*RPIN
1440 C=S*RT3*U1**2+RT3*C4*U1+P1
1450 CALL COMPUT
1460 UPT=U;USPT=C0PIN+SPIN*UPT
1470 DTILT=DTB-(HB-H1)/US1+B1/USPIN+G1/(2*UPIN)-B1/USPT-GB/(2*UPT)
1480 THET3=V*DTILT/X2
1490 SHTIM=DTC-THET3*(X1-(HC-H1)*US1*THET3/V)/V+B1/USPIN+G1/(2*UPIN)
1500 +-B1/USPT-GC/(2.*UPT)
1510   US=(HC-H1)*SQRT(1.0+(US1*THET3/V)**2)/SHTIM
1520 B=RP*CZERO+RT*US+2*RP*SP*V;A=RP*SP
1530 C=RP*V*(CZERO+SP*V)
1540 CALL COMPUT
1550 U=U;P=RT*US*U
1560 IF(.0001-(ABS((US-US1)/US)))1008,1009,1009
```

SHOVEL CONTINUED

```
1570 1008 US1=US;U1=U;P1=P
1580 GO TO1007
1590 1009 VOL2=1-U/US;U=U*1.0E-05;US=US*1.0E-05;P=P*1.0E-12
1600 SVOL1=VOL1/RT;SVOL2=VOL2/RT
1610 DIFF=(ABS((USB-US)/USC))*100.0
1620 $USE SHOVEN
```

SHOVEN

```
1700C  OUTPUT STATEMENTS FOR SHOVEL
1710C
1720 2 PRINT 60,SHOT,RUNS,COMBO,MATLT(1),MATLT(2),MATLP(1),MATLP(2),
1730 +RT,RP,SVOL0,W,THET3,V,TILT,W1,TILT1,DIFF,
1740 +USB,UB,PB,VOL,SVOL,USC,UC,PC,VOL1,SVOL1,US,U,P,VOL2,SVOL2
1750C
1760C  OUTPUT FORMAT
1770C
1780 60 FORMAT(////////10X,9HSHOT NO. ,I5,10X,8HRUN NO. ,A1//
1790 +10X,17HPIN COMBINATION: ,A1,1X,7H- START,//
1800 +5X,14HTARGET MATL.- ,2A6,
1810 +4X,13HPROJ. MATL.- ,2A6//8X,9HDENSITY- ,F6.3,1X,5HGM/CC,8X,
1820 +9HDENSITY- ,F6.3,1X,5HGM/CC//8X,8HVOLUME- ,F6.4,1X,5HCC/GM,
1830 +/////5X,18HPROJECTILE VEL. = ,E12.5,
1840 +1X,6HFT/SEC,4X,13HSHOCK TILT = ,F9.6//23X,E12.5,1X,6HCM/SEC,
1850 +4X,13HTILT MEAS. = ,F9.6//23X,E12.5,1X,6HFT/SEC,4X,
1860 +13HTILT CALC. = ,F9.6///5X,21HSHOCK VEL. SCATTER = ,F7.3,1X,1H#,
1870 +/////2X,4HSTA.4X,10HSHOCK VEL. 4X,10HPART. VEL. 7X,8HPRESSURE
1880 +4X,4HV/V05X,6HVOLUME//10X,6HKM/SEC,8X,6HKM/SEC,11X,8HMEGABARS,
1890 +13X,5HCC/GM////
1900 +2X,1HB,6X,F8.4,6X,F8.4,8X,F10.6,1X,F9.5,1X,F8.5//
1910 +2X,1HC,6X,F8.4,6X,F8.4,8X,F10.6,1X,F9.5,1X,F8.5//
1920 +2X,1HD,6X,F8.4,6X,F8.4,8X,F10.6,1X,F9.5,1X,F8.5//////)
1930 GO TO 200
1940 END
1950 SUBROUTINE COMPUT
1960 COMMON U,A,B,C
1970 U=(B-SQRT(B**2-4*A*C))/(2*A)
1980 RETURN
1990 END
2000 $FILE INFORM
```

UNCLASSIFIED
Security Classification

DOCUMENT CONTROL DATA - R&D
(Security classification of title, body of abstract and indexing annotation must be entered when the overall report is classified)

1 ORIGINATING ACTIVITY *(Corporate author)* Manufacturing Development, General Motors Corporation, G.M. Tech. Center, Warren, Michigan 48090

2a REPORT SECURITY CLASSIFICATION: UNCLASSIFIED

2b GROUP:

3. REPORT TITLE
High Pressure Hugoniot Measurements for Several Nevada Test Site Rocks

4. DESCRIPTIVE NOTES *(Type of report and inclusive dates)*
Final Report

5 AUTHOR(S) *(Last name, first name, initial)*
Shipman, F. H., Isbell, W. M., Jones, A. H.

6. REPORT DATE	7a TOTAL NO OF PAGES	7b. NO OF REFS
1969, March	107	23

8a. CONTRACT OR GRANT NO.	9a. ORIGINATOR'S REPORT NUMBER(S)
Contract No. DA-49-146-XZ-429	Manufacturing Development General Motors Corporation Report MSL-68-15
b. PROJECT NO. NWER Subtask SB047	
c.	9b OTHER REPORT NO(S) *(Any other numbers that may be assigned this report)* DASA-2214
d.	

10 AVAILABILITY/LIMITATION NOTICES
"Each transmittal of this document outside the agencies of the U.S. Government must have prior approval of the Director, Defense Atomic Support Agency, Washington, D. C. 20305."

11. SUPPLEMENTARY NOTES	12. SPONSORING MILITARY ACTIVITY
	Director Defense Atomic Support Agency Washington, D.C. 20305

13 ABSTRACT

The hugoniot equations of state have been determined experimentally for the materials over the following pressure ranges: Fansteel-77 (0.3 to 5.0 Mb), OFHC copper (1.0 to 4.5 Mb), NTS Climax Stock granodiorite (0.6 to 1.9 Mb), NTS Rainier Mesa tuff - vacuum dry - (0.2 to 1.3 Mb), NTS Rainier Mesa tuff - > 95% water saturated - (0.08 to 1,33 Mb), $V44_D$ grouting material (0.11 to 1.15 Mb), schistose gneiss (0.47 to 2.5 Mb), NTS Ferris Wheel dolomite (0.63 to 1.74 Mb), NTS Banded Mountain limestone (0.15 to 1.22 Mb), NTS desert alluvium (0.15 to 0.90 Mb). Where possible, comparisons are made to previous hugoniot measurements by other workers.

DD FORM 1 JAN 64 1473

UNCLASSIFIED
Security Classification

14. KEY WORDS	LINK A		LINK B		LINK C	
	ROLE	WT	ROLE	WT	ROLE	WT
Hugoniot Equation of State High Pressure Rocks Nevada Test Site						

INSTRUCTIONS

1. ORIGINATING ACTIVITY: Enter the name and address of the contractor, subcontractor, grantee, Department of Defense activity or other organization *(corporate author)* issuing the report.

2a. REPORT SECURITY CLASSIFICATION: Enter the overall security classification of the report. Indicate whether "Restricted Data" is included. Marking is to be in accordance with appropriate security regulations.

2b. GROUP: Automatic downgrading is specified in DoD Directive 5200.10 and Armed Forces Industrial Manual. Enter the group number. Also, when applicable, show that optional markings have been used for Group 3 and Group 4 as authorized.

3. REPORT TITLE: Enter the complete report title in all capital letters. Titles in all cases should be unclassified. If a meaningful title cannot be selected without classification, show title classification in all capitals in parenthesis immediately following the title.

4. DESCRIPTIVE NOTES: If appropriate, enter the type of report, e.g., interim, progress, summary, annual, or final. Give the inclusive dates when a specific reporting period is covered.

5. AUTHOR(S): Enter the name(s) of author(s) as shown on or in the report. Enter last name, first name, middle initial. If military, show rank and branch of service. The name of the principal author is an absolute minimum requirement.

6. REPORT DATE: Enter the date of the report as day, month, year; or month, year. If more than one date appears on the report, use date of publication.

7a. TOTAL NUMBER OF PAGES: The total page count should follow normal pagination procedures, i.e., enter the number of pages containing information.

7b. NUMBER OF REFERENCES: Enter the total number of references cited in the report.

8a. CONTRACT OR GRANT NUMBER: If appropriate, enter the applicable number of the contract or grant under which the report was written.

8b, 8c, & 8d. PROJECT NUMBER: Enter the appropriate military department identification, such as project number, subproject number, system numbers, task number, etc.

9a. ORIGINATOR'S REPORT NUMBER(S): Enter the official report number by which the document will be identified and controlled by the originating activity. This number must be unique to this report.

9b. OTHER REPORT NUMBER(S): If the report has been assigned any other report numbers *(either by the originator or by the sponsor)*, also enter this number(s).

10. AVAILABILITY/LIMITATION NOTICES: Enter any limitations on further dissemination of the report, other than those imposed by security classification, using standard statements such as:

(1) "Qualified requesters may obtain copies of this report from DDC."

(2) "Foreign announcement and dissemination of this report by DDC is not authorized."

(3) "U. S. Government agencies may obtain copies of this report directly from DDC. Other qualified DDC users shall request through _____."

(4) "U. S. military agencies may obtain copies of this report directly from DDC. Other qualified users shall request through _____."

(5) "All distribution of this report is controlled. Qualified DDC users shall request through _____."

If the report has been furnished to the Office of Technical Services, Department of Commerce, for sale to the public, indicate this fact and enter the price, if known.

11. SUPPLEMENTARY NOTES: Use for additional explanatory notes.

12. SPONSORING MILITARY ACTIVITY. Enter the name of the departmental project office or laboratory sponsoring *(paying for)* the research and development. Include address.

13. ABSTRACT: Enter an abstract giving a brief and factual summary of the document indicative of the report, even though it may also appear elsewhere in the body of the technical report. If additional space is required, a continuation sheet shall be attached.

It is highly desirable that the abstract of classified reports be unclassified. Each paragraph of the abstract shall end with an indication of the military security classification of the information in the paragraph, represented as *(TS), (S), (C), or (U)*

There is no limitation on the length of the abstract. However, the suggested length is from 150 to 225 words.

14. KEY WORDS: Key words are technically meaningful terms or short phrases that characterize a report and may be used as index entries for cataloging the report. Key words must be selected so that no security classification is required. Identifiers, such as equipment model designation, trade name, military project code name, geographic location, may be used as key words but will be followed by an indication of technical context. The assignment of links, rules, and weights is optional.

Defense Threat Reduction Agency
45045 Aviation Drive
Dulles, VA 20166-7517

CPWC/TRC May 6, 1999

MEMORANDUM FOR DEFENSE TECHNICAL INFORMATION CENTER
ATTN: OCQ/MR WILLIAM BUSH

SUBJECT: DOCUMENT REVIEW

The Defense Threat Reduction Agency's Security Office has reviewed and declassified or assigned a new distribution statement:

- AFSWP-1069, **AD-341090,** STATEMENT A ~~A~~ waiting for reply
- DASA-1151, AD-227900, STATEMENT A
- DASA-1355-1, **AD-336443**, STATEMENT A OK
- DASA-1298, AD-285252, STATEMENT A
- DASA-1290, AD-444208, STATEMENT A
- DASA-1271, AD-276892, STATEMENT A
- DASA-1279, AD-281597, STATEMENT A
- DASA-1237, AD-272653, STATEMENT A
- DASA-1246, AD-279670, STATEMENT A
- DASA-1245, AD-419911, STATEMENT A
- DASA-1242, AD-279671, STATEMENT A
- DASA-1256, AD-280809, STATEMENT A
- DASA-1221, AD-243886, STATEMENT A ~~FAD~~
- DASA-1390, **AD-340311**, STATEMENT A
- ~~DASA-1283, AD-717097~~, STATEMENT A OK
- DASA-1285-5, AD-443589, STATEMENT A
- DASA-1714, AD-473132, STATEMENT A
- DASA-2214, AD-854912, STATEMENT A
- DASA-2627, AD-514934, STATEMENT A
- DASA-2651, AD-514615, STATEMENT A
- ~~DASA-2536, AD-876697, STATEMENT A~~
- DASA-2722T-V3, AD-518506, STATEMENT A
- DNA-3042F, AD-525631, STATEMENT A
- DNA-2821Z-1, AD-522555, STATEMENT A

If you have any questions, please call me at 703-325-1034.

Ardith Jarrett

ARDITH JARRETT
Chief, Technical Resource Center